UNIVERSITY OF TRENTO

International PhD Program in Biomolecular Sciences

Department of Cellular, Computational and Integrative Biology – CIBIO

34 Cycle

Isolation and validation of novel monoclonal antibodies targeting the tumor microenvironment for the selective delivery of cytokines payloads

Dr. Roberto De Luca

Philochem AG

Prof. Guido Grandi

University of Trento

Ph.D. Thesis of

Lisa NADAL

Philochem AG & University of Trento

Academic Year 2020-2021

To the ones who have always been there

Table of contents

1. Summary

Cancer immunotherapy has revolutionized the field of oncology by giving the possibility to ligands (e.g., antibodies) to selectively target tumor antigens and accumulate at the site of the disease while sparing normal tissues. During the past years, the number of patient eligible for immune-based cancer treatments has seen an exponential increase as these therapies are becoming first line treatment for many cancer indications.

A promising anticancer strategy consists in the targeted delivery of bioactive compounds (e.g., cytokines) to the tumor microenvironment with high-affinity ligands specific for tumor-associated antigens. This approach improves the efficacy of the drug by reducing related side effects and increasing the therapeutic index of the payload. Currently, antibodies represent one of the most successful class of ligands used for this purpose as they can be generated against virtually any antigen. Many methodologies have been described for the generation and isolation of antibodies with high antigen-binding specificity. Among these, phage display technology has emerged as a powerful and versatile tool for the *in vitro* discovery of antibodies and peptides. Since it was invented in mid 1980s, phage-display has paved the way to the generation of more than 70 phage–derived monoclonal antibodies (mAbs) that entered clinical studies, and 14 of which have been approved in the market.

Cytokines are proteins capable of modulating the activity of the immune system and some cytokine-products have gained marketing authorization for the treatment of cancer. In order to increase the therapeutic index of cytokine payloads, the generation of fusion proteins with tumor-homing antibodies has been proposed. These so-called "immunocytokine" products constitute a class of "armed" antibody products, in which a tumor-targeting immunoglobulin is fused with a cytokine.

In this thesis, we present the generation and characterization of antibodies specific for two tumor microenvironment-associated antigens: Tenascin C and Fibroblast Activation Protein. Both antigens are undetectable in healthy tissues but abundantly expressed in the tumor stroma.

In the first part of the thesis, we have isolated antibodies specific for the spliced domain D of Tenascin C from the synthetic phage library "ETH2Gold". Antibodies were affinity matured randomizing key residues of CDR1 of heavy and light chains. The highest affinity clone, R6N, was characterized *in vitro* and *in vivo* showing selective accumulation at the tumor site in mouse models of cancer. An immunocytokine featuring IL12 as payload has been generated and its therapeutic activity evaluated in tumor bearing mice. R6N-IL12 exhibited potent antitumor activity in immunodeficient mice bearing SKRC52 renal cell carcinoma, as well as in immunocompetent mice bearing SMA-497 glioma.

In the second part of this thesis, a monoclonal antibody has been isolated against Fibroblast Activation Protein. After affinity maturation of the CDR2 of heavy and light chains of the parental antibody C5, the selected 7NP2 antibody showed improved affinity and excellent tumor targeting properties in SKRC52-hFAP tumor bearing mice. When fused to IL12, 7NP2 was able to induce tumor growth retardation and tumor remission in mouse models of cancer.

Collectively, in this thesis we have isolated and validated two monoclonal antibodies selective for tumor microenvironment-associated antigens. Both antibodies when fused to IL12 induced tumor growth retardation and remission in immunodeficient and immunocompetent mouse models providing a rationale for possible future applications of R6N and 7NP2 antibodies for the treatment of cancer patients.

2. Introduction

2.1 Cancer

According to estimates from the World Health Organization in 2019, cancer is the first leading cause of death before 70 years in most of the countries in the world. In 2020, worldwide, 10 million cancer deaths were estimated with 19.3 million newly reported cases[1]. The most frequent cancer in women and men is lung and bronchus cancer; breast cancer is the predominant in women whereas prostate cancer is the fifth cancer death leading cause in men. Other type of common cancers are liver, stomach, cervix and skin malignancies[2].

Cancer cannot be considered as a simple and unique disease. It develops as results of biological, chemical or physical damage of the genetic code which lead to aberrant and uncontrollable growth of proliferative cells due to uncorrected cell mitosis[3]. Cancer cells grow and divide invading normal tissue and spreading throughout the body as consequence of an accumulation of abnormalities in different cell regulatory systems. The behavior of cancer cells is far from the one of the normal counterparts; this reason a major problem in treating cancer is controlling metastasis that could interfere with body function essential to sustain life[4].

Typically, the neoplastic bodies are induced, after recognition, to cell death with FAS-L pathway[5]. This early recognition is referred as "immune surveillance" as Lewis Thomas and Frank MacFarlane Burnet formulated in 1950s[6]. This hypothesis is based on tumor growth and divided in three crucial steps: elimination, equilibrium, and escape phase. During the elimination phase, the immune system recognizes and destroys potential tumor cells. The equilibrium phase follows if the elimination of cancer cells was not successful: cells can be subjected to mutations which help them to survive to the Darwinian selection pressure of the immune system[7]. This process, known under the name of "cancer immunoediting", describes the tumor-sculpting actions of the immune system able to shape the properties of the tumor cells that are surviving[8]. The escape phase is the final step of the tumor growth process: many surviving tumor variants elude the immune system and grow in a totally uncontrolled manner evolving in malignant tissues. The uncontrolled formation and proliferation of cancer cells opens the way not only to the invasion

of healthy organs but also to the formation of new generation cells able to resist to anticancer treatments[9].

Six functional capabilities ("Hallmark of cancer") were identified in 2000 by Douglas Hanahan and Robert Weinberg and are considered prerequisites for the distinction between normal and malignant cells: (i) unlimited proliferation, (ii) replicative immortality, (iii) evasion of apoptosis, (iv) insensitivity of anti-growth signals, (v) sustained angiogenesis and (vi) tissue invasion[10].

A better and profound understanding of the disease led to the addition of other four characteristics in 2011: genome instability (vii), sustained inflammation (viii), evasion of immune destruction (ix) and reprogramming of cellular metabolism (**Figure 2.1**)[11].

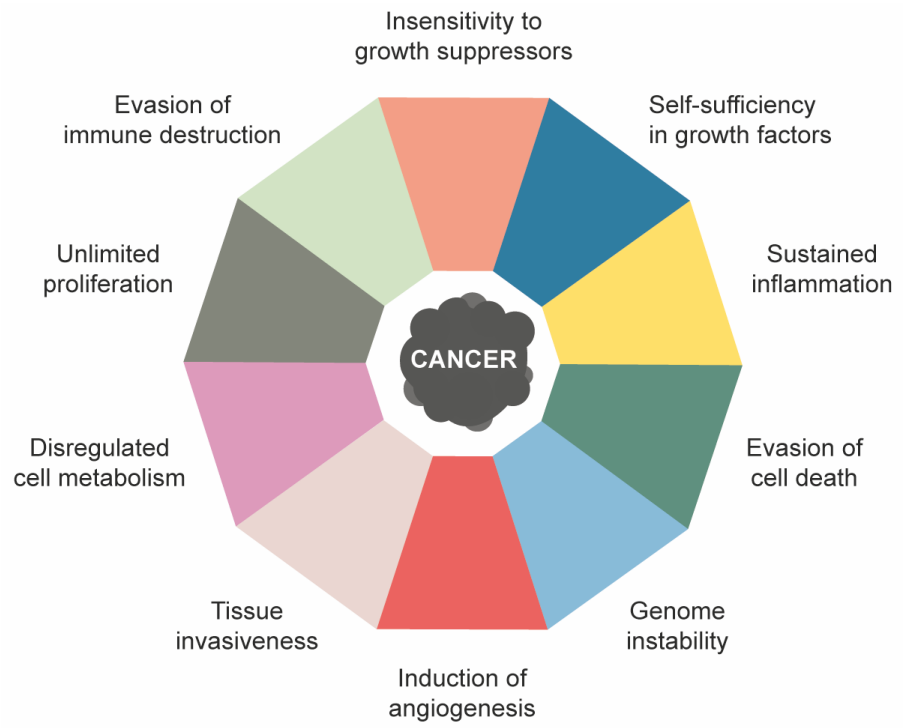

Figure 2.1 The hallmarks of cancer are features that distinguish malignant from healthy cells. They were identified by Douglas Hanahan and Robert Weinberg. Adapted from (11).

The understanding of cancer progression supported the development of more effective treatment. Surgical removal of tumor masses together with radiotherapy and chemotherapy have been efficacious cancer treatments especially when the disease is localized and when used in combination[12]. Since not all the neoplastic

masses are easily accessible for surgery or develop in metastasis difficult to reach, radiotherapy is an alternative used as cancer treatment or adjuvant. Unfortunately, radiation therapy becomes more complicated once the tumor has metastasized[13].

Chemotherapy has been one of the most important treatment modalities in oncology, particularly in advance disease state when the tumor has disseminated into the whole body[14].

It refers to the intravenous administration of cytotoxic agents or kinase inhibitors capable of killing cells interfering with the fundamental molecular mechanisms of cell proliferation and survival (e.g. DNA replication and transcription, formation and/or protein biosynthesis, signaling cascades). The treatment of cancer with chemicals started in 1940s when nitrogen mustard has been administered as first chemical agent acting through the alkylation of the DNA. In 1970s the introduction of cisplatin in the treatment of solid tumors has been considered a milestone in modern chemotherapy[15,16]. Chemotherapy has brought important benefits in curing patients with lymphomas, leukemia and testicular cancer[16–18]. However, the impossibility for chemotherapy drugs to discriminate between normal and cancer cell selectively localizing to the site of the tumor proved the limitation of this approach. PET scans of patient injected with radiolabelled cytotoxic drugs showed poor tumor to organ bioavailability causing substantial toxicity and preventing potential dose escalation (**Figure 2.2**)[19]. Moreover, even if chemotherapeutic agents have shown long-lasting complete remission for some types of metastatic cancer, many patients do not respond to the treatments[20].

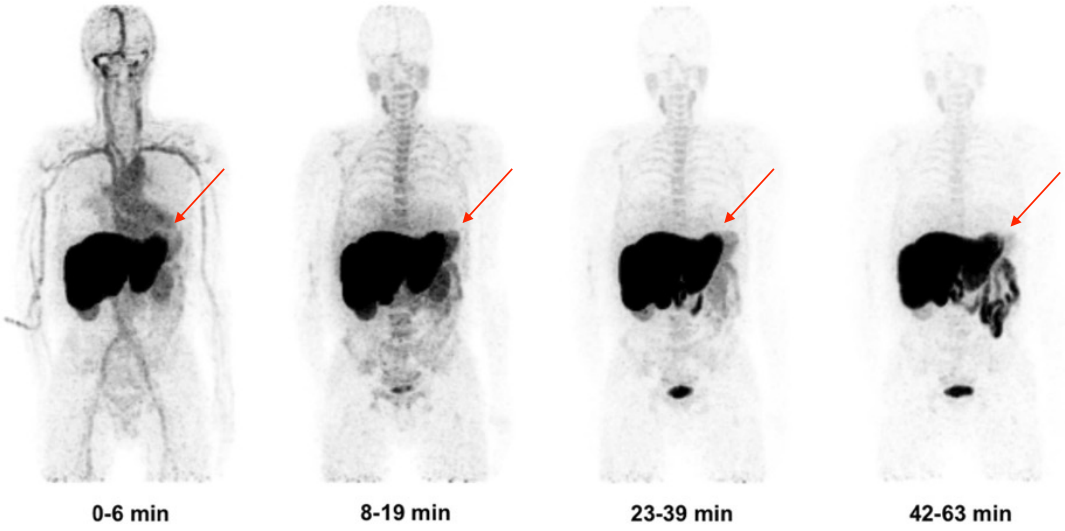

Figure 2.2: Whole body PET scans at various time points of a patient with mesothelioma (a tumor of the pleura), treated with [11^{C}]docetaxel. The images show no preferential uptake of the drug at the site of disease (thoracic area, red arrow). Adapted from (19).

The necessity of selective targeting for cancer therapy was recognized already 100 years ago when Paul Ehrlich proposed the concept of magic bullets ("Zauberkugeln") suggesting that the immune system can prevent tumors[21]. Together with concepts already described as "immune surveillance" and "cancer immunoediting", there was indeed a better understanding of how the immune system plays a dual role in the tumor progression, protecting the host and promoting tumor development. From these theories, cancer immunotherapy started to develop, and it is now considered the "fifth pillar" of cancer therapy alongside surgery, cytotoxic chemotherapy, radiation and targeted therapy[22].

William Coley is considered the "grandfather" of cancer immunotherapy. In early 1900s, after reading about a case of a cancer patient who went complete tumor remission after a postoperative infection, he used heat-inactivated bacterial preparation named "Coley's Toxin" to purposely infect one of his patients with advanced tumors[23]. The toxin was strikingly active in renal carcinoma and sarcoma leading to durable complete response in 50% of the patient even though the toxin was subsequently not effective in other solid tumors[24]. In the 1980's, Steve Rosenberg, a researcher working at the National Cancer Institute (NCI), was able to induce long lasting cancer remission of various solid tumors administering large

amount of a recombinant preparations of a pro-inflammatory cytokine, Interleukin 2 (IL2). This treatment was, however, highly toxic, and as for Coley's toxin, effective only in a limited portion of the treated patients (e.g., patients with sarcoma or renal cancer)[25].

The development of more selective anti-cancer agents relies on the use of tumor-homing molecules. The use of antibodies as therapeutic agents has grown steadily since mid-1990s due to the advantages offered from these molecules to selectively target tumor antigens and accumulate at the site of the disease while sparing normal tissues[26]. Thanks to the profound studies on immune systems mechanism to fight cancer, it was possible to develop checkpoint inhibitors antibodies capable of "release the brakes" of immune cells fighting cancer. A first scientific milestone coincided with the identification of T-lymphocyte antigen 4 (CTLA-4) as a main regulator of T cell activity: CTLA-4 inhibits the function of T lymphocytes by competing with CD28 for binding to certain co-stimulatory proteins (e.g., CD80, CD86)[27]. In 1996 James Allison and colleagues had shown that inhibition of CTLA-4 with a monoclonal antibody (e.g., Ipilimumab) in patients could lead to a long-term survival for a small proportion of patients with metastatic melanoma[27]. The field of cancer immunotherapy was then further revolutionized with the targeting of Programmed cell death protein-1 (PD-1), a surface marker of T cells, with cognate antibody products (Nivolumab and Pembrolizumab). A T-cell based response against hematological malignancies and solid tumors was indeed possible by blocking the PD-1/PD-1 ligand (PD/L-1)[28].

Another strategy that has been explored in the past decades is the coupling of cytokines with antibodies selective for specific tumor associated antigens. Cytokines are small immunoregulatory proteins secreted by various cell types (e.g. leukocytes, endothelial cells, fibroblasts and stromal cells) which act as messenger of the immune system[29]. They have the ability to induce functional changes in tissues increasing vascular permeability or body temperature, activating or inhibiting the immune system[30]. They play an important role in fighting cancer cells, overcoming the inhibitory micro-environment created by malignancies[31]. Side effects often prevent an effective use of cytokines, as seen by Rosenberg and colleagues, which have been fused to antibodies to improve their therapeutic index protein capitalizing on the targeting properties of antibody[32,33].

The next paragraph of this thesis will examine in detail the previously described aspects of immunotherapy.

2.2 Antibodies

2.2.1 Natural occurring antibodies

Antibodies, also called immunoglobulins (Ig), are a class of large Y-shaped glycoprotein produced by differentiated B cells in response to infection or immunization to antigens of foreign origin. Immunoglobulins exist in two different forms: a membrane-bound form on the surface of B cells, serving as B-cell receptor (BCR), and a soluble secreted form by terminally differentiated B cells, known as plasma cells[34].

The capability of binding specifically to a particular antigen renders antibodies extremely important during adaptive immune system response. Each antibody molecule has a unique structure that allows its binding to the cognate antigen, but all antibodies share the same overall structure. They are 150 kDa proteins bonded by non-covalent interaction and disulfide bridges, composed of two identical set of heavy and light chains which are linked to each other by interchain disulfide bonds. Heavy and light chains are composed of variable (V) and constant (C) regions. The domains responsible for the binding specificity of each molecule are the variable ones, V_H and V_L, which are at the N-termini of the chains. These variable domains are composed by three complementarity-determining regions (CDRs), essential for the binding with the target epitope. Figure **2.3** depicts the molecular structure of Ig which consists of a Fab portion (antigen binding fragment), and an Fc portion, which play key role in recruiting effector cells and initiating processes such as the complement cascade[35]. The Fab portion is the one constituted by V_H and V_L together with the first constant domain of the heavy and light chain. Two Fabs are attached to the rest of the constant domains of the heavy chain by a flexible amino acid stretch called "hinge region" generating two matching antigen-binding site. In human, two families of light chains are found: lambda (λ) and kappa (κ), with a frequency of 40% and 60%, respectively[34]. The affinity of an antibody to its target depends on cumulative non-covalent interactions. The strength of these interactions is referred as a constant of dissociation (K_D). Since the antibody consists of two identical arms, it can potentially bind to two identical antigens: the complex formed from two simultaneous binding events is referred as avidity[36].

The humoral immune response to infection or foreign antigens starts with the production of antibodies by B-cells that recognize the cognate antigen via BCR with an interaction which is unique for each B-cell. The presence of ~10^{11} different B-cells conveys immune protection from virtually any antigen. The diversity observed in the CDRs loops is based on random gene rearrangement known as V, D and J recombination[37]. The variable heavy chain (up to 46 functional genes) with a variable light chain (up to 38 functional genes) are the first to be rearranged; once the complex is formed somatic recombination of the V, D and J gene domain ensures random rearrangement[37]. To create even further variability, the imprecise joining process of the variable domains is carried by a transferase enzyme that inserts additional nucleotides at the extremities of the V and J DNA strands and afterwards a final ligation step generates the complete V-region exon.

Five Ig isotypes are found in humans, defined by their heavy chain constant region: IgM, IgG, IgA, IgE and IgD, subclasses that determine the functional properties of the antibody. Upon activation, B-cells produce IgM and IgD[38]. IgM are pentameric structure capable of activating the complement system, but not the NK-FcRg mediated killing[39]. Furthermore, they have a half-life in serum of 10 days and have poor diffusion into extravascular sites. Immunoglobulin D (IgD) is the rarest of the five classes (0.2% of serum antibodies) whose exact function and role is yet to be confirmed[40].

A process called class switching is the responsible for the expression of the other isotypes: external stimuli, such as cytokine present where the B-cell is located, induce another DNA recombinant process leading to the generation of IgA, IgE or IgG. Immunoglobulin A is the most abundant in mucosal tissue and in breast milk. There are two subclasses of secretory IgA, IgA1 and IgA2, which form both monomeric and dimeric structures. The major function of IgA is to protect mucosal tissue by neutralizing microbes and babies who produce low level of IgA when newborn[41].

Immunoglobulin E is the principal Ig involved in the recognition and immunity against parasites and it is fundamental for the sensitization of mast cells[42].

The most abundant isotope in human is immunoglobulin G (10-20% of plasma protein) and for this reason and its ability to diffuse to extravascular sites, the most

used for anti-cancer treatment. IgG can be subdivided in four subclasses, named in order of decreasing abundance: IgG1, IgG2, IgG3 and IgG4. The IgG1 antibody has many key functions such as recruitment of NK cells, opsonization and activation of the complement system[43]. IgG2 is responsible for the immune recognition and responses against bacterial capsular polysaccharide antigens. A potent inducer of inflammation and activator of the complement system is IgG3, but with a half-life reduced to 7 days (IgG average half-life is 21 days). IgG4 is instead crucial for opsonization and neutralization of pathogens[44].

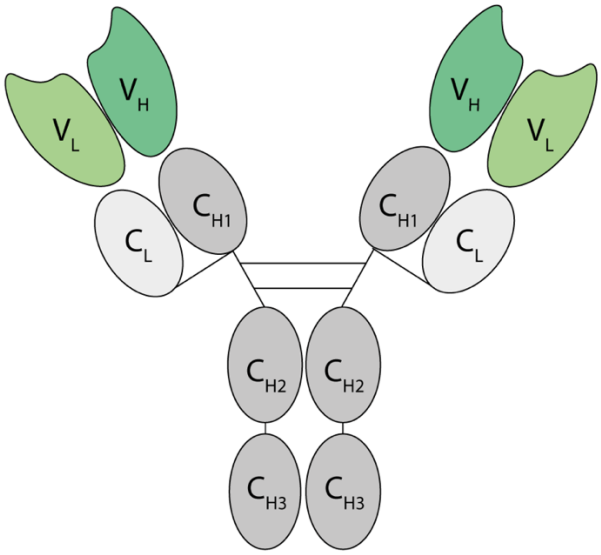

Figure 2.3: Schematic representation of an immunoglobulin composed of two heavy (H) and light (L) chains. Heavy chains contain a variable domain (VH) and three constant domains (CH1, CH2 and CH3), while light chains contain only one constant domain (CL) and a variable one (VL). Disulfide bonds (depicted in black) link heavy chains in the hinge region as well as light chains. Adapted from (44).

Antibodies capitalize from three primary mechanisms to exert their function:
i) Neutralization: antibodies inhibit the infectivity of a virus or the toxicity of a toxin molecule by binding to the pathogen.
ii) Opsonization: antibodies coat the pathogens and foreign particles, making it more easily ingested by phagocytes.
iii) Complement activation: bound antibodies form the binding site for the first protein of the complement complex, which leads to a series of events resulting in the killing of pathogens.

Anti-cancer therapeutic antibodies have been developed to either block growth receptors (signal disruption), specifically sequestering tumor growth factor (signal disruption) or by inducing the complement-dependent cytotoxicity (CDC) and antibody-dependent cell-mediated cytotoxicity (ADCC).

2.3 Recombinant antibodies

2.3.1 Monoclonal antibodies

During a humoral response, our immune system produces a wide variety of antibodies capable of recognizing different portions of a pathogen surface ("epitopes")[45,46]. The polyclonal response starts when different B cell clones are exposed to the pathogen and, upon antigen encounter in secondary lymphoid organs, these lymphocytes proliferate and secrete antibodies. This kind of response plays a fundamental role in immunology since it ensures an efficient recognition of multiples antigens avoiding escaping mechanism from the pathogen. In case of infection with monomeric toxin, for example, it is necessary that toxin's non overlapping epitopes are recognized by different antibodies to assure an efficient removal of the pathogen from the circulation by the phagocytic system[34]. A monoclonal response would be inefficient, and it would lead to an exacerbation of the disease. For certain clinical conditions (e.g., toxin, virus and venoms), serum preparation of polyclonal antibodies (mixture comprising two or more monoclonal antibodies as a single drug) are still currently used. On the other hand, products consisting in mixture of polyclonal antibodies are cumbersome to industrialize due to batch-to-batch variation. For pharmaceutical applications, the use of monoclonal antibody leads to product with defined characteristics and quality standards, and it is less time-consuming.

Several methods have been developed for the generation of monoclonal antibodies. In late 1970s started the "antibody's era" with the pioneer work of Köhler and Milstein who first described the generation of murine monoclonal antibodies[47]. They pioneered a methodology for the preparation of monoclonal antibodies termed "hybridoma technology" that awarded the Nobel Prize in Medicine and Physiology in 1984[47,48]. This procedure is based on the immortalization of B cells producing antibody (splenocytes) by fusion with myeloma cells (P3-X63-Ag8) conferring unlimited proliferation to hybridomas and leading to the isolation of large repertoire

of monoclonal antibodies[47]. The hybridoma technology allowed the production of rodent-derived monoclonal antibodies of a single specificity. Unfortunately, non-human antibodies isolated with hybridoma procedure resulted in immune response in treated patient due to the generation of human anti-mouse antibodies (HAMAs)[49]. HAMAs are responsible for severe allergic reaction in patient with a reduced efficacy of the drug when administered for multiple times. Moreover, a suboptimal recruitment of effector cells was due to a weaker activity towards the murine Fc portion of the antibodies[50,51].

To reduce immunogenicity and increase the effector function activity, "chimeric antibodies" have been developed by Morrison and coworkers in 1984. They consist in an engraftment of the variable regions of murine antibodies (from the S107 myeloma cell lines) into human constant regions (from human IgG1 molecule)[52]. However, even this format, named with suffix -Ximab, suffered from immunogenicity when infused in patient. Nevertheless, the methodology was subsequently used for the generation of various monoclonal antibodies which gained marketing authorization[53]. Rituximab (Rituxan®, Genentech/Roche), antibody targeting CD20, was the first monoclonal antibody that received marketing approval for the treatment of non-Hodgkin's lymphoma in 1997[54].

To overcome the limitation due to the immunogenicity of chimeric antibodies, Sir Gregory Winter and his collaborators improved the technology developing "humanized antibodies" in 1988. They are based on human antibodies in which the CDR regions were replaced with murine CDR regions of selected antibodies[55]. This methodology minimizes the portions of rodent origin within the antibody molecule aiming to a decrease of immunogenicity[55,56]. Humanized antibodies (-Zumab) retained binding affinity for the cognate antigen and display minimal residual risk of immunogenicity (**Figure 2.4**). For this reason, humanized antibodies have gained fast acceptance in the market as effective and safe class of therapeutics like Daclizumab (Zenapax, anti CD25 antibody) and Bevacizumab (Avastin, anti VEGF-A antibody) [5357].

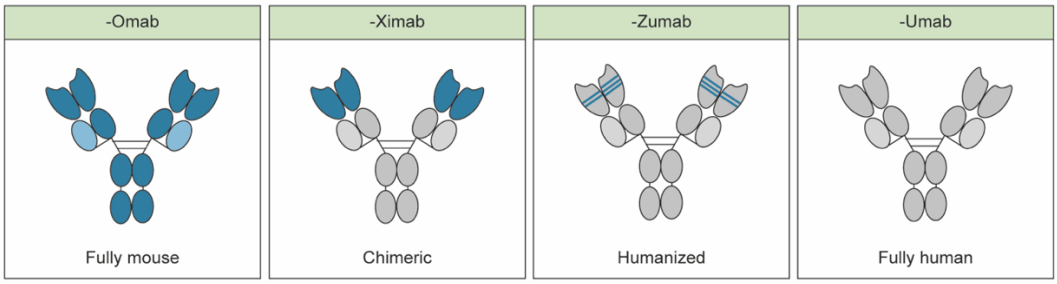

Figure 2.4: Schematic representation of fully mouse, chimeric, humanized and fully human antibodies. Adapted from (34).

2.4 Generation of fully human antibodies

The development of new technologies such as transgenic mice expressing human antibodies or phage display enabled the isolation of fully human antibodies, capable to retain high affinity for the target and effector functions, without any immunogenicity issues.

The first technology involved the use of transgenic mice capable of stimulating a human humoral response. The mice used for this procedure incorporate the entire human immunogloblulin loci[58–60]. Different approaches can be adopted to the generation of transgenic mice: Abgenix (acquired by Amgen in 2005) established, through XenoMouse technology, six different mouse strains making human IgG1, IgG2 and IgG4 antibodies[61]. Fully human antibodies derived by transgenic mice have the advantage to be already affinity matured for the antigen using the evolution-tuned mechanisms of the murine humoral system. However, the need for immunogenic antigens remains a limitation for this methodology. Some proteins of pharmaceutical interested present indeed completely conserved sequence (e.g. Tenascin C, EDA and EDB domains of fibronectin, calmodulin) and would therefore induce a mechanism of tolerance when injected into transgenic rodents.

2.5 Phage display technology

Phage display technology revolutionized the way antibodies are produced. This *in vitro* technology allows the discover of antibodies to almost every type of antigen with a broader range of epitope since it does not require any immune response[62,63]. "For the phage display of peptide and antibodies" George P. Smith and Sir Gregory Winter were awarded with the Chemistry Nobel Prize in 2018.

Phage antibody technology is a simple and powerful methodology that allows the selection of a particular phenotype (i.e. a ligand specific to a desired antigen) from a repertoire of protein displayed on the surface of bacteriophages, capable of yielding specific monoclonal antibody fragments in a limited time of experimental work[64]. This example of *in vitro* selection does not depend on the *in vivo* immune response and can be used to discover binders against a large variety of antigen which may be suppressed by the immune system[57].

Phage display was originally described in 1985 by Smith: he presented the use of non-lytic filamentous bacteriophage, fd, for the display of specific binding peptides on the phage coat[62]. The ability of displaying functional folded protein on phage surface, such as monoclonal antibodies or hormones, has been corroborated respectively by the groups of Winter and Wells[63,65].

Phage display technology mimics what happens in B cells. The technology is indeed based on the fact that a polypeptide can be displayed on the phage surface by inserting the gene coding for the polypeptide into the phage genome, linked to the phage minor coating protein (pIII) gene (**Figure 2.5**)[66]. Thus, the phage particle links genotype to phenotype.

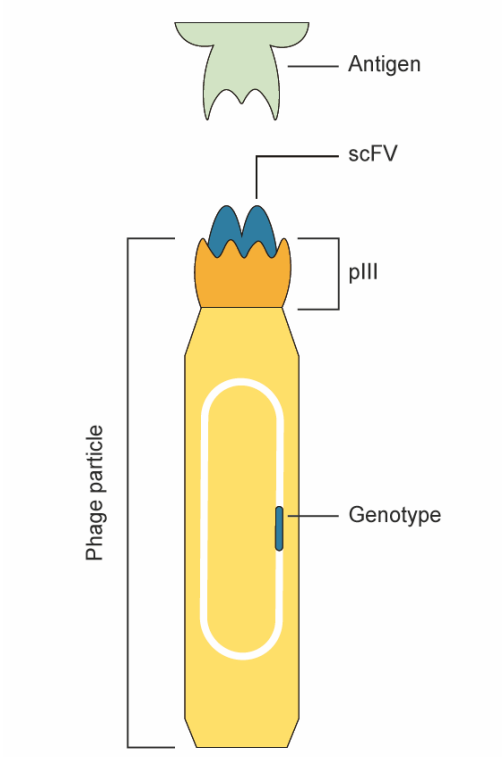

Figure 2.5: Phage displaying a binding protein (in this case a scFv fragment) as fusion protein of a minor coat protein pIII.

Repertoires of phage, so called phage display libraries, could be created displaying on each phage proteins which are slightly different from each other (10^6–10^{11} different ligands in a population of > 10^{12} phage molecules)[67]. The procedure of specific binding selection is termed as panning, since it resembles the procedure used to extract gold nuggets or flakes from a vast excess of silt and it is essential to enrich the desired molecule level. The selection of a binding specificity from a repertoire of binders is composed by different steps: the phage library is biopanned against the target of interest (i.e. tumor antigens) which is immobilized on solid support, magnetic beads or column matrix. Unbound phage is then discarded through washing processes, whereas binder phage is collected and amplified in bacteria. Several rounds of biopanning (usually 2-4 for antibody phage libraries) allow the enrichment of specific molecules with desired activity of monoclonal phage antibodies (**Figure 2.6**)[68]. To determine the binding properties of selected antibodies, different test can be performed such as enzyme-linked immunosorbent assay (ELISA), chromophore-assisted laser inactivation (CALI) or fluorometric microvolume assay technology (FMAT)[69–71]. As a consequence of the multiples round of biopanning and the stringency of the test performed, very rare phenotypes present in large phage libraries can be selected and amplified[72].

The *in vitro* selection of specific antibodies by phage display technology presents many advantages[73,74], which will be described below. The stability of phage particles and their retained ability to remain infective when treated with acids, bases, proteases and denaturants allow a variety of selective elution protocols and the use of this technology not only for selection of binders but also for the selection of catalytically active enzymes, of proteins with altered thermal stability, or aggregation resistant domain antibodies selected on phage by heat denaturation[75–77].

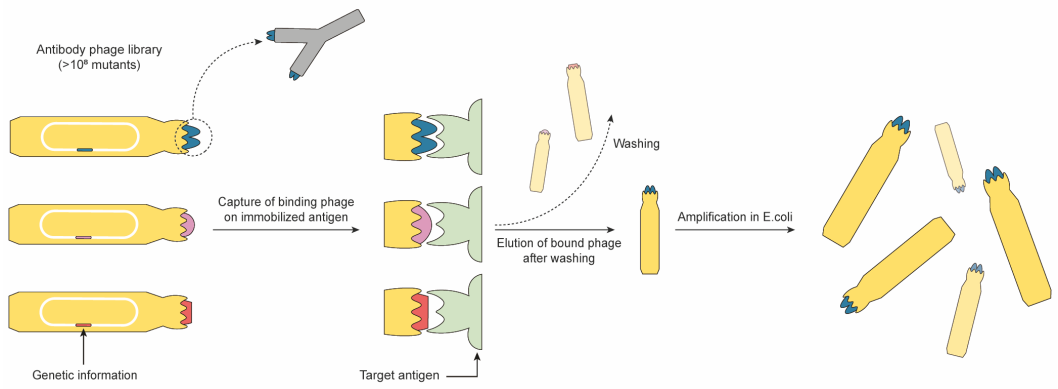

Figure 2.6: Binder's selection from a phage display library. A library of proteins displayed on the phage surface is used as input for the selection. Phage which display a binding protein are captured on immobilized target molecules, and after unbound phage are washed off, bound phage can be eluted. The eluted phage population is then used to infect *E. Coli* cells, propagated in bacterial cultures, and can be used for further rounds of selection.

Filamentous phage are capable of infecting strains of *E. Coli* that harbor the F conjugative episome by attaching to the tip of the F pilus and by translocating the phage genome into the bacterial cytoplasm. The genome is then replicated involving both host-derived and phage proteins and packaged into elongated viral particles of approximately 6 nm diameter and 900 nm length. For this reason, selected phage could be amplified in bacteria enriching the pool of phage with the desired phenotype. Several thousand copies of small major coat protein (pVIII) cover filamentous phages, whereas few copies of the minor coat proteins pIII and pVI and pVII and pIX are displayed at the two-opposite extremity of the phage particle. Peptides and proteins have been displayed on the minor coat protein III which is expressed in 3-5 copies on the phage particle. It is fundamental for the phage particle since it mediates the adsorption of the phage to the bacterial pilus or pVIII[62,78,79].

Phage vectors (with suitable cloning sites for pVIII or pIII fusions and an antibiotic resistance gene) were the first used to display peptides and proteins on the phage particle. In phage vectors in which proteins are fused to the pIII, each pIII minor coat proteins displayed on the phage is fused to heterologous polypeptide. Short peptides of 6-7 aminoacids containing no cysteine are instead better displayed when

fused to the pVIII. Phage vectors were used due to the advantage of keeping all the genetic information for the phage cell life cycle (**Figure 2.7**)[80].

Phagemids are plasmid vectors that carry the gene III with appropriate cloning site and a packaging signal[81]. Helper phage particles must superinfect phagemid containing bacteria to produce functional phage particle. Phagemid vectors encoding the polypeptide-pIII fusion are preferentially packaged into the phage particles, because the typically used helper phage (M13K0715 or VCS-M13) have a slightly defective origin of replication, which also serves as packaging signal. pIII derived from the helper phage or the polypeptide-pIII fusion can be incorporated in the resulting phage particles. Ratios of polypeptide-pIII:pIII range between 1:9 and 1:10000 can be achieved depending on the nature of the polypeptide fused, the growth conditions and the type of phagemid[76,82].

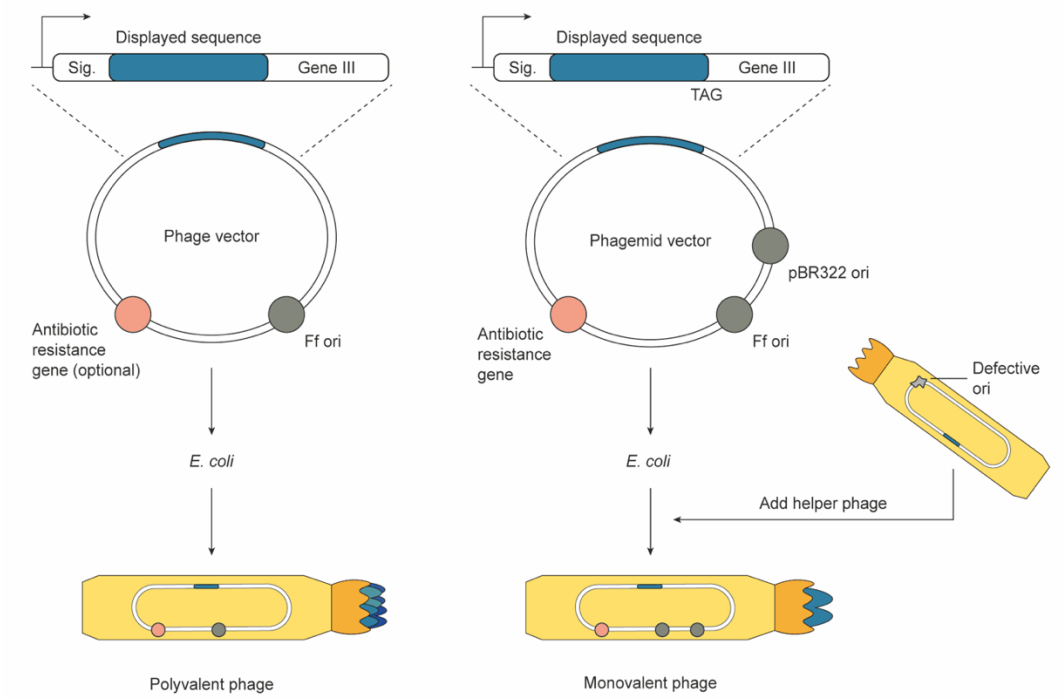

Figure 2.7: General scheme for phage display using phage or phagemid vectors. The difference between phage and phagemid vectors is illustrated for pIII display. Sequences for display are inserted between a secretion signal sequence (Sig.) and gene III. Both phage and phagemid vectors carry an Ff origin of replication to permit production of ssDNA and hence virions. Phagemid vectors also have a plasmid origin (here pBR322) and an antibiotic resistance marker to allow propagation as plasmids in *E. Coli*. Phage vectors are also often modified with antibiotic resistance markers for convenience, as illustrated here. In many phagemid vectors, an amber stop codon (TAG) is interposed between the displayed sequence and gene III to allow soluble protein expression by transferring the vector into a non-supE suppressor strain. Adapted from "Phage display: a practical approach" Edited by ClacksonT. and Lowman HB. Oxford University Press.

2.5.1 Phage display derived antibodies in clinical development

Several monoclonal antibodies discovered by phage display have received approval in the market or are currently in clinical development.

The first human antibody phage display-derived approved by FDA in 2002 is Adalimumab (Humira®). Its target is the tumor necrosis factor (TNF) which is a key mediator of the pro-inflammatory cytokine cascade: it binds to TNF receptor 1 and 2 leading to cell activation, inflammation and fever, acute phase responses and

sepsis. Humira is used for the therapy of moderate to severe chronic rheumatoid arthritis, psoriasis and psoriatic arthritis, pediatrics and adult Crohn's disease and other pathologies driven by important status of inflammation[83,84].

Belimumab (Benlysta®) is a human monoclonal antibody that has been approved by FDA in 2011. The antibody inhibits the B-cell activating factor (BAFF), known as B-lymphocyte stimulator (BLyS). Benlysta® is now primarily used in patients with systemic lupus erythematosus[85].

Another antibody derived by phage display which was approved for the market is Ranibizumab (Lucentis®), created from the same parent mouse antibody as Bevacizumab. The Fab of Ranibizumab is used for the treatment of macular edema following retinal vein occlusion, for the treatment of diabetic macular edema and diabetic retinopathy[86].

The Neri group has spent the last decades working on synthetic human antibody phage display libraries (e.g., ETH-2 Gold, PHILO and PHILODiamond) containing more than 10^{9-11} antibody clones[87–89]. Various products based on antibodies derived by these libraries are currently in clinical phase. Darleukin (L19-IL2) is an immunocytokine specific for EDB domain of fibronectin, now in Phase III for the treatment of melanoma[90]. Dekavil (F8-IL10) is a fusion protein direct to EDA domain of fibronectin in Phase II for the treatment of rheumatoid arthritis[91]. Fibromun (L19-TNF) is a scFv-fusion with TNF in clinical phase III for melanoma and soft tissue sarcoma[92,93].

2.6 Yeast display

Yeast surface display of antibody fragments has become an increasingly popular tool for protein engineering and library screening applications (**Figure 2.8**)[94]. A major strength of this methodology is the possibility to characterize the binding properties of a clone directly by Fluorescent-Activated-Cell-Sorting (FACS) without the need of subcloning, expression and purification of antibodies fragment. The clone of interest can be isolated based on its ability to bind fluorescently labelled antigen. In the yeast display, the heterogeneous immunoglobulin gene pool is cloned into the yeast display plasmid into a vector as an in-frame fusion with Aga2p. In *S. Cerevisiae*, the a-agglutinin receptor, which consists of two proteins Aga1 and Aga2, acts as an adhesion molecule to stabilize cell-cell interactions and facilitate fusion between mating *a* and α haploid yeast cells[95]. GAL1, a galactose

inducing promoter, tightly regulates the expression of both the Aga2 fusion protein from the vector and the Aga1 protein in the host strain. Upon induction with galactose, the Aga1 protein and Aga2-scFv fusion protein associate within the secretory pathway, and the epitope tagged scFv antibody is displayed on the cell surface at 10'000-100'000 copies per cell, minimizing any potential interaction with other molecules of the yeast wall[96]. The use of GALI promoter allows the expansion of a scFv library 10^{10}-fold without any recognizable changes in either the percentage of antibody expression or the frequency of specific clones within the library[96].

Yeast display technology allows the selection of monoclonal antibody fragments *in vitro*, which are expressed with high fidelity and some level of post-translational modifications. Library screening can proceed in a more rapid and reliable way minimizing avidity effects and gaining accurate control over selection parameters during FACS screening. One disadvantage of this technique is the expression of proteins with a differential glycosylation in yeast compared to mammalian cells; from a library perspective instead, the total number of unique antibody clones in yeast libraries is lower than phage libraries due to the lower transformation efficiency of yeast cells.

Yeast display technology has demonstrated its potential to be suitable for the generation of therapeutic antibodies. Sintilimab, a PD-1 blocking antibody, which received marketing authorization in China for the treatment of refractory classical Hodgkin's lymphoma[97,98] was isolated by yeast display.

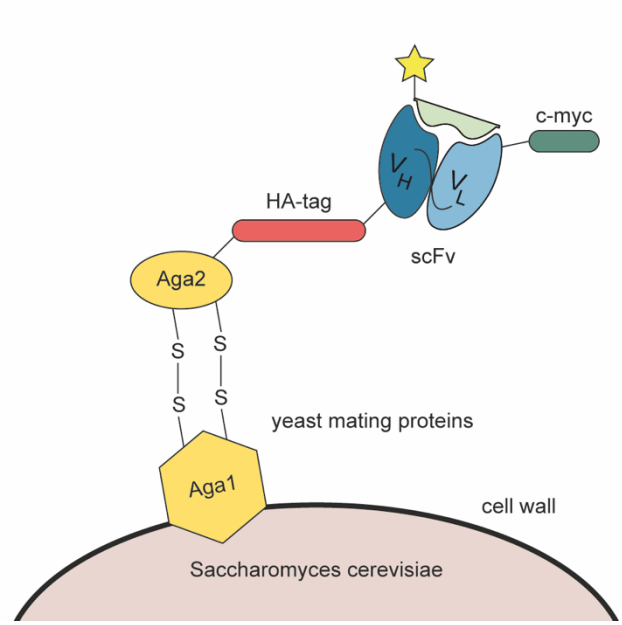

Figure 2.8: The scFv Aga2 fusion protein surface expression system. Aga1 is bound to a cell wall glucan and connected by a disulfide bond to Aga2. The protein to be displayed is cloned in frame with Aga2 protein. The N-terminal hemagglutinin (HA) tag and C-terminal c-myc tag allow the monitoring of fusion protein display by suitable anti-peptide tag antibodies. By addition of labeled antigen, yeast cells displaying antibody fragments that bind to the antigen can be isolated by FACS (e.g. fluorescently labeled antigen) or affinity purification (e.g. biotinylated antigen).

2.7 Mammalian display

Another powerful methodology for the discovery of high affinity ligands is the mammalian cell surface display technology[99]. Libraries of antibody fragments are generated by the genetic fusion of the C-terminus of the heavy chain constant region to a transmembrane domain of a mammalian cells, for example human platelet-derived growth factor (PDGF) receptor[100]. The plasmid encoding for the library is transfected into mammalian cells; selections are subsequently carried as for yeast display using FACS to identify clones with highest affinity for the incubation with fluorophore-labeled antigen[101].

Since most of the therapeutic antibodies are produced in mammalian cells, a great advantage of this technology is the use of cells suitable for both selection and production of the desired clones. However, one of the biggest disadvantages is the construction of large libraries comparable to those in yeast or phage display.

Furthermore, the incorrect antibody assembly can limit the library stability when antibodies libraries are complex[102].

2.7 Ribosome display

Cell-free *in vitro* methods combine two important aspects for identifying and optimizing ligands: they allow the generation of higher library diversity by obviating the need to transform cells and secondly, they make PCR-based mutagenesis strategies convenient including it as an internal step[103,104].

Ribosome display the coupling of genotype with phenotype by fusing the library candidates to its corresponding mRNA (**Figure 2.9**). After the selection, the mRNA is reverse-transcribed to DNA, PCR-amplified and sequenced. Since the mRNA lacks the information of the terminal stop codon at the end of the sequence encoding for the protein of interest, the ribosome is stalled at that position on the mRNA during the translation leading to the formation of mRNA-ribosome-polypeptide complexes. Selections are carried using magnetics beads coupled with the target antigen or antigen-coating on microtiter plates. After the incubation with the antigen and successive washing steps, complexes that are not binding are removed whereas in situ RT-PCR followed b PCR amplification allows to identify the binders sequence[105].

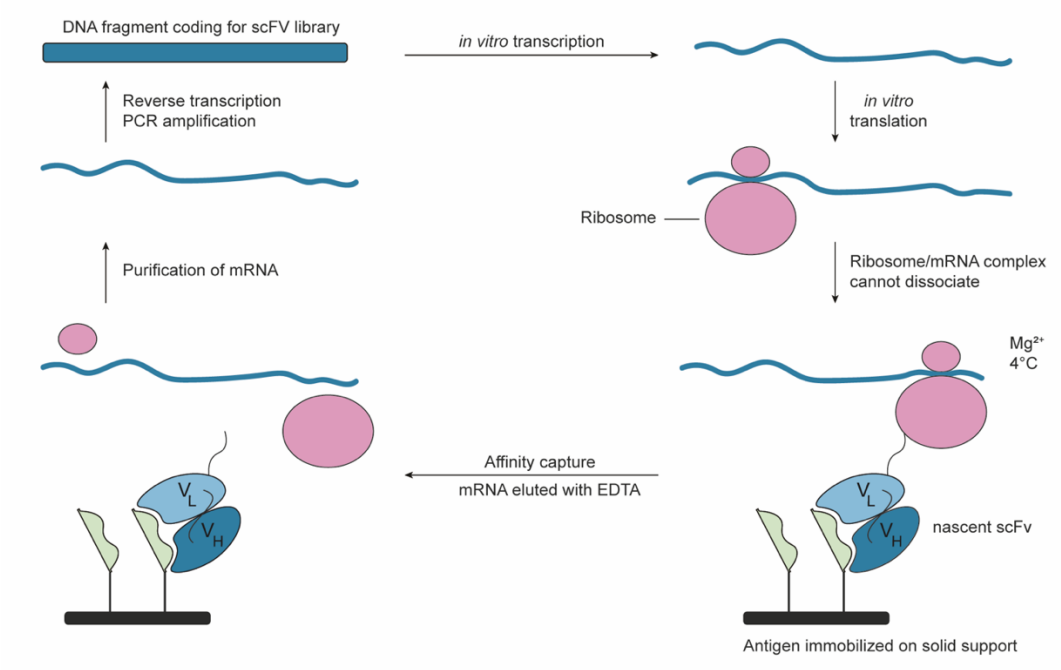

Figure 2.9: Schematic representation of a selection cycle of ribosome display. Linear DNA fragments coding for a protein library (here scFv variants) are transcribed in vitro and purified before subsequent translation in vitro. After having reached the end of the mRNA during translation, the ribosome is unable to dissociate from the mRNA because the stop codon is missing. The resulting ternary complex comprising the ribosome, mRNA and the nascent polypeptide can be stabilized by high concentrations of magnesium ions and low temperature, thereby creating a stable linkage between the mRNA (genotype) and the encoded polypeptide (phenotype). Ribosomes displaying a binding protein can be isolated by affinity selection on immobilised antigen, the selected mRNA molecules can be eluted, and the genetic information is amplified by reverse transcription and PCR, which allows to introduce further variability by error prone PCR.

2.8 Antibody therapeutics

Monoclonal antibodies represent the most important class of pharmaceutical recombinant proteins on the market. As May 2016, over 50 antibodies and their conjugates have been approved by FDA or EMA and only during 2021, 18 investigational antibody therapeutics are in regulatory review in either the US or EU. Most therapeutic antibodies are approved for cancer and autoimmune diseases with a total annual sales revenue exceeding 75 billion US$ in 2013[106].

2.8.1 Intact antibodies

The predominant molecular format used in current antibody therapeutics is the IgG, although the number of products based on non-IgGs formats is increasing[107]. For pharmaceutical application, IgG1 and IgG2 are the favorite choice due to their half-life and the possibility to induce antibody-dependent cellular cytotoxicity (ADCC). IgG_3 does not find any clinical application as these antibodies hold a long hinge region prone to proteolytic cleavage whereas IgG_4 are preferred for the development of blocking antibodies[108]. Intact antibodies for cancer therapy may act through different mechanism of action: Rituximab, for example, is capable to induce ADCC mechanism. Bevacizumab instead blocks the function of the target protein inhibiting cancer cells proliferation and dissemination.

One of the first monoclonal antibodies that gained marketing authorization is the humanized IgG_1 Trastuzumab (commercial name Herceptin®) generated by Paul Carter and Mike Shepard at Genentech. The antibody is capable of binding Her-2 (Receptor tyrosine-protein kinase erbB-2) blocking its activity. Trastuzumab was the first one able to induce complete remissions in patients with solid tumors (e.g. breast cancer) and clinical trial conducted in women with Her-2 positive metastatic breast cancer showed that Herceptin could improve the progression-free survival of the patients by 65%[109]. Trastuzumab is currently used for treating breast and stomach cancer, alone or in combination with chemotherapy. Another intact antibody that received marketing authorization by FDA in 2004 is Cetuximab (Erbitux®), a chimeric epidermal growth factor receptor (EGFR)-specific IgG1 monoclonal antiboby[110]. Erbitux® is used alone or in combination with irinotecan in the treatment of metastatic colorectal cancer and it explicates its activity by preventing binding of activated ligand or the receptor dimerization[111]. Natalizumab (Tysabri®) is the first α4 integrin antagonist IgG_4 monoclonal antibody acting as selective adhesion molecule inhibitor. As intact IgG_4, it demonstrates reduced binding to Fcγ receptors and lack of ability to fix complement *in vitro*. FDA approved Natalizumab for the treatment of multiple sclerosis (2004) and Chron's disease (2008)[112,113].

2.8.2 Armed antibodies

Armed antibodies consist in a subclass of therapeutic antibodies in which a payload (e.g., a potent cytotoxic drug, a radionuclide, a growth factor, a second antibody

moiety or a cytokine) is fused to an antibody capable of selective localization to the tumor site (**Figure 2.10**). The fusion to antibodies in IgG format or fragments has provided a strategy to increase the therapeutic index of cytotoxics (i.e., antibody-drug conjugates), radionuclides (i.e., radioimmuno-conjugates), antibodies of different specificities (i.e., bispecific antibodies), cells (i.e., chimeric antigen receptor-T cells) and cytokines (i.e., immunocytokines)[108,114,115]. The killing mechanism of armed antibodies relies on the property of the bioactive payload rather than on the anti-cancer activity of the antibody that, in this context, is chosen as selective vehicle for the payload. Due to the ability of IgG to bind the salvage neonatal receptor (FcRn) and their large structure which allows longer half-life, IgG was the preferred format by pharmaceutical companies for several years. Interestingly, armed IgGs typically show a much faster clearance compared to naked antibody[116]. For this reason, antibody fragments may be preferred over full IgGs. Antibody fragments lead to a preferential tumor to blood ratio due to their fast clearance and exhibit a more efficient tumor penetration and tumor uptake. The monovalent scFv format could be suitable for pharmacodelivery applications although its small size (27 kDa) and its monomeric structure leads to rapid renal excretion. The diabody format (Db) consists in a non-covalent homodimer (54 kDa) composed of two scFv fragments and it can be generated by using short linkers (usually less than 10 amino acids) to connect VH and VL domains, preventing their intramolecular pairing. This homodimeric format exhibits higher avidity due to the two antigen binding sites with longer tumor penetration if compared with scFv[117]. Armed fragments antibodies may also be generated from the small immunoprotein (SIP) format, a covalent homodimer (74 kDa) in which each monomeric unit contains a scFv linked to the CH4 domain of an IgE. The tumor targeting and clearance properties of this format are an intermediate between the diabody and the IgG format[118].

However, the absolute antibody uptake at the tumor site of armed antibodies can be at best only 0.01-0.1 percent of injected dose per gram (%ID/g) of tissue to the neoplastic mass, even with the best tumor targeting antibodies[119–121].

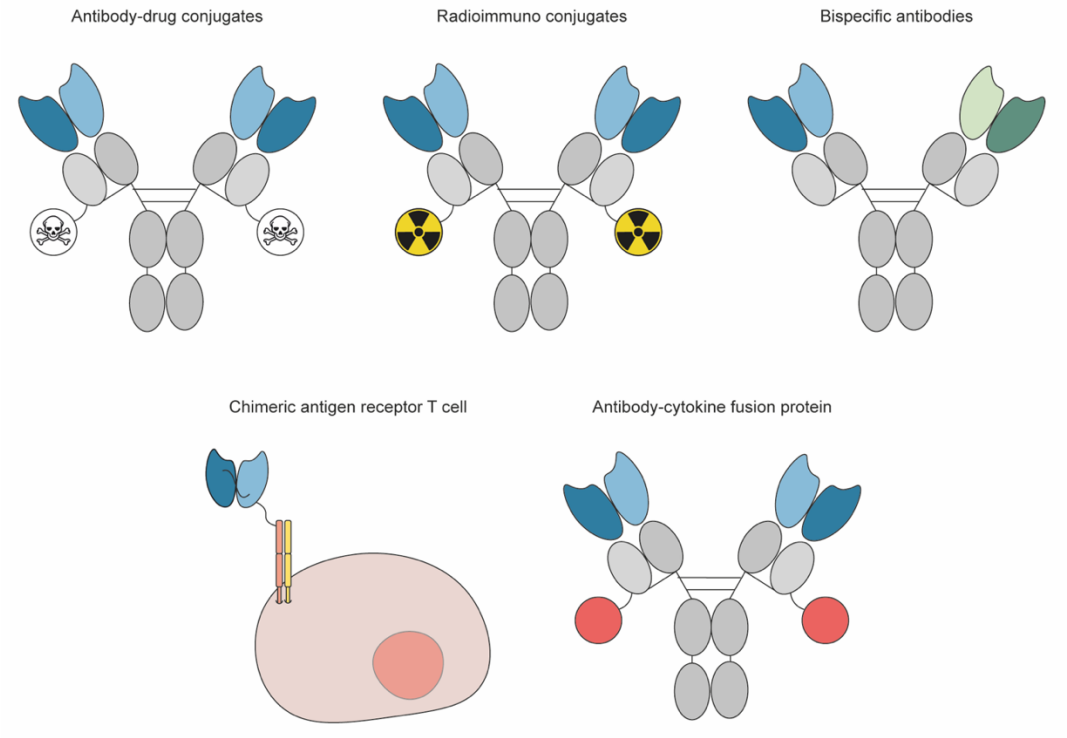

Figure 2.10: Schematic representation of armed antibodies. For simplification, the antibody is depicted in the IgG format (except for the chimeric antigen receptor-T cell that displays the antibody molecule as scFv).

2.8.3 Antibody-drug conjugates (ADCs)

Antibody-drugs conjugates consist of three components: (i) an antibody molecule targeting a suitable antigen, (ii) a cleavable linker stable in the circulation but capable to release the drug at the proper time and (iii) a potent cytotoxic payload[122]. ADCs take advantage of the selective targeting offered by the monoclonal antibody are based on and from the cytotoxic activity of the drug coupled to it. Many pharma companies are currently investing in these molecules due to their ability to increasing the therapeutic window of the chemotherapeutic agent[108]. The number of sites of the appended drug molecules (drug-to-antibody ratio or DAR) must be also efficiently tailored: ADCs with high DAR and hydrophobic linkers typically experience a more rapid clearance from circulation. Cytotoxic agents are related in structure and mode of action to Auristatine and Maytansine derivatives, which are potent microtubulin-targeting or DNA damaging agents[123–125]. So far, eight therapeutic ADCs have been approved for the treatment of various oncological indications.: Adcetris®, Kadcyla®, Besponsa®, Polivy®, Mylorag®, Enhertu®, Padcev®, Trodelvy® and Blenrep®[126–132].

2.8.4 Radioimmuno-conjugates

Radiolabeled antibodies consist of immunoglobulins linked to a suitable radionuclide by using chelating agents (e.g. for radiometal labelling) or by chemical reaction (e.g. radioiodination using oxidizing agents). These therapeutic products are capable of selectively deliver cytotoxic radiations to the neoplastic mass reducing radiotoxicity to normal tissue. Depending on the radionuclide of choice, radioimmuno-conjugates can be used for imaging (when linked to γ (SPECT) or β+ (PET)-emitting radionuclides such as 99mTc and 18F, 11C, 124I) or for therapy applications when combined with β^-emitting radionuclides (e.g., 90Y, 177Lu, 131I). Two anti-CD20 radiolabeled antibodies have gained marketing authorization, Zevalin® and Bexxar®, for the treatment of Non-Hodgkin-Lymphoma[133,134]. However, these products are rarely used in the clinic as they do not show any superiority compared to Rituximab in combination with chemotherapy[135].

2.8.5 Bispecific antibodies

A rapidly expanding group of targeting protein consists of bispecific antibodies, considered a special class of armed antibodies. The first antigen-binding domain serves as pharmacodelivery vehicle, as seen for typical armed antibody, but in this case the payload is represented by a second antibody directed against a leukocyte surface marker or tumor associated antigens[114,135]. Bispecific antibodies usually aim to recruit effector cells, such as T cells or NK cells, to form an artificial "immunological synapse" with the cells at the tumor site. A product which gained marketing authorization in 2012 is Blinatumomab (Blincyto®), a bispecific T cell engager (BiTE) capable of simultaneously binding to the T cell receptor CD3 and to CD19 (an antigen expressed both on B cells and in hematological malignancies of B cell origin). Blincyto is used for the treatment of Acute Lymphoblastic Leukemia: its clinical success is the result of schedule optimization for the administration of the drug enhancing its tolerability profile[136].

The IgG format is the most used. However, the development of a product with two different binding site offers many opportunities for protein engineering which led to the generation of more than 100 bispecific formats[137]. Several strategies, for example, have been developed to overcome the problem of possible mispaired IgG contaminants when producing the IgG format in single host cells[138]. A possible

solution, named "knob-into-holes", relies on point mutations in the constant domain to promote the correct formation of heterodimeric bispecific antibodies[139]. An example of a full-size IgG bispecific approved in the market is Emicizumab (Hemlibra™ , anti-coagulation factor IX fused to anti-coagulation factor X), used as an enzyme-cofactor replacement in a bleeding disorder.

2.8.6 Antibody-cytokine fusion proteins

Antibody-cytokine fusion proteins, termed immunocytokines, represent an emerging class of armed antibody capable of inducing a selective activation of the immune system against the tumor cells are selective for. As previously mentioned, immunocytokine consist of an antibody fused to a cytokine moiety. Cytokines are small proteins (5-20 kDa) able to modulate the activity of the immune system. 60 different cytokines have been discovered so far, and they have been named considering their presumed functions (e.g. pro- or anti-inflammatory, chemotactic, growth factors), cell from which they are secreted, or cell that they influence[34]. Pro-inflammatory cytokines are typically generated by cells of innate immunity after the recognition of pathogens. They are present in the blood at extremely low concentrations (e.g., in the picomolar concentration range) but their production can increase in pathological conditions[140]. The dissociation constant between cytokine and their cognate receptors is extremely low and for this reason, cytokine can mediate their biological effects when present at picomolar concentration. For cancer therapy, pro-inflammatory payloads are the most used, while autoimmune disease or chronic inflammation are treated with immunocytokine based on anti-inflammatory cytokine. Due to their potent activity at picomolar concentrations, researchers have considered the use of recombinant cytokine for malignant diseases. Unfortunately, short circulatory half-life, inability of accumulate at the tumor mass and systemic toxicity when administered have represent major setbacks for the clinical development of these drugs[29,141]. Few recombinant cytokines have gained marketing authorization. An example is Proleukin (IL2) which is currently used for the treatment advanced renal cell carcinoma and metastatic melanoma[25,142]. Beromun, recombinant TNFα is used for soft tissue sarcoma of the limb in combination with melphalan whereas IFNα based products (Intron A and Roferon-A) have been approved for the treatment of hairy cell leukemia, follicular non-Hodgkin lymphoma, melanoma and AIDS-related Kaposi's sarcoma[143,144].

Immunocytokine have been designed with the aim to reduce toxicity in patients compared to untargeted recombinant cytokines to increase the therapeutic activity and selectivity of these molecules avoiding severe side-effects. The antibody-based delivery of IL2 has been explored in different indications such as neuroblastoma (ch14.18-IL2), B cell malignancies (Lym1-IL2), and in a pan-solid tumoral setting when directed to degenerated necrotic areas associated with the malignancy (chTNT3-IL2)[145–147]. Fusion proteins based on IL4, IL12, IL21, GM-CSF and cytokine of TNF superfamily (e.g. CD137L) had also been characterized[148].

The *in vivo* targeting properties of immunocytokine products and their relative biological activity depends on the nature of the payload itself, but also on the antibody format used for development. Roche and Merck-Serono have generated antibody-cytokine fusions using the IgG format. When IgGs are used to generate cytokine fusions (e.g., with IL2 or IL12), their long half-life in the bloodstream may induce cytokine-dependent side effects[149,150]. The Neri's group has instead typically used antibody fragments to facilitate long retention at the tumor mass and faster clearance from blood circulation[32,119]. When immunocytokines are based on homotrimeric cytokines (e.g. TNF, TRAIL and FasL), the monovalent scFv is preferred to other formats since the oligomerization of the antibody could lead also to the product polymerization.

As seen by immunodetection of radiolabeled monoclonal antibody in human patients, the intratumoral concentration of immunocytokines is around 0.01-0.03 % ID/g, meaning that only a small fraction of the fusion proteins accumulates at the tumor site[121]. It is indeed fundamental the choice of appropriate payload which facilitates the egress of the protein at the neoplastic lesion from the circulation, thus enhancing the % ID/g in the tumor while minimizing off-target toxicities.

IL12, IL2 and TNF-based immunocytokines are discussed in detail in the next sections.

2.9 Selected examples of recombinant cytokines for cancer therapy

2.9.1 Interleukin 12

Interleukin 12 (previously termed *natural killer cell stimulating factor*) is the first described member of IL12 family (IL12, IL23, IL27 and IL35); it was discovered in 1989 as a "natural killer – stimulating factor" and as "cytotoxic lymphocyte maturation factor"[151,152]. IL12 is a heterodimeric cytokine comprised of the IL12-p35 (a 35 kDa light chain or IL12α) and of the IL12-p40 (a 40 kDa heavy chain, or IL12β) (**Figure 2.11**) subunits which are covalently linked by a disulfide-bridge giving raise to the active form IL12-p70[153]. P35 has homology with IL6, whereas p40 shows homology to IL6 receptor α chain, providing evidence that IL12 p70 is evolutionary correlated with the IL6 superfamily. IL12 p40 can be secreted outside the cell independently of the association with other subunits but has no or little pro-inflammatory. P35 is instead the responsible domain whole pro-inflammatory activity exerted by IL12 (at least for the mouse homologue) resulting as the rate limiting factor for IL12 function[154].

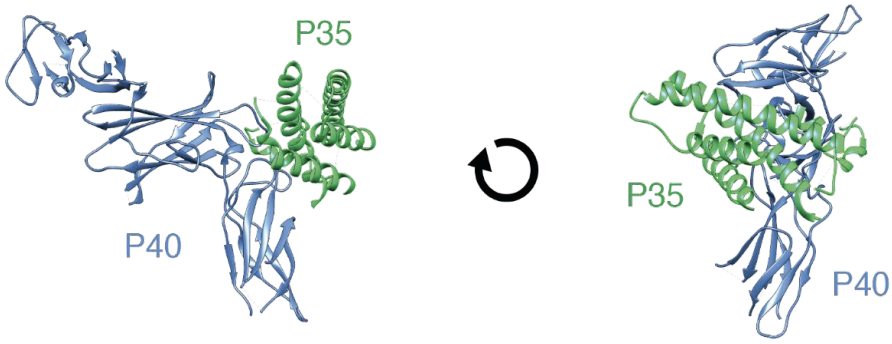

Figure 2.11: Crystal structure of interleukin 12 from different angles. The P40 subunit is depicted in blue, while the P35 is represented in green.

The protein is physiologically and mainly produced by antigen presenting cells (APC) such as dendritic cells (DCs) and macrophages in response to "danger signals" like pathogen associated molecular patterns. The high affinity receptor for IL12 (IL12-Rβ1/IL12-Rβ2) is expressed on activated T cells, DCs and natural killer cells (NKs) and activates various pathway such as TYK2, JAK2 and STAT resulting in a dose dependent induction of IFN-γ[155,156]. IFN-γ is a proinflammatory mediator which favor a Th1 differentiation of CD4+ T cells; IL12 is able to boost the proliferation of CD8+ T cells and NK, to increase the antigen processing and

presentation by APC, enhance IgG production, inhibit Treg activity and alter the expression patterns of endothelial adhesion molecules (e.g. VCAM-1)[157–160]. The mechanism of action of IL12 converge during the immune response creating an interconnection between innate and adaptive immunity (**Figure 2.12**).

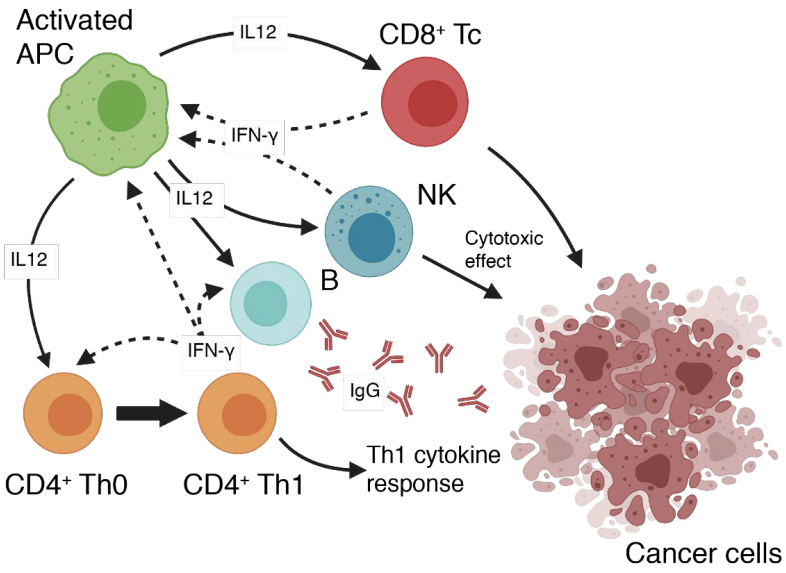

Figure 2.12: Graphical representation of some of the main effects of IL12. Activated antigen-presenting cells (APCs) release IL12, which stimulates CD8+ T cells and natural killer cells (NK), activates the IgG production from B cells and drives the CD4+Th0 towards the Th1 phenotype differentiation. Adapted from (152), created with BioRender.com.

IL12 is a highly appealing therapeutic agent and for this reason, several groups are investigating the preclinical and clinical activity of IL12[161–164]. In the late 90s, recombinant human IL12 was brought to the clinic for the first time showing excessive toxicity and an overall low response rate[165–167]. For this reason, the U.S FDA decided to discontinue the clinical development. In the past years, many clinical trials involving the use IL12 have started: most of them relate with the delivery of the cytokine through gene therapy mechanism.

However, two products based on antibody fused to IL12 (NHS-IL12 and BC1-IL12) are currently in phase I clinical trials to determine tolerability and Maximal Tolerated Dose (MTD) in patients with solid tumors. The activity of the two immunocytokines is associated with increased serum concentration of IFN-γ and

IP10 with a toxicological profile consistent with preclinical studies with decreased white blood cells count and elevated levels of transaminases[168,169].

Our group generated various IL12-based immunocytokines in the last twenty years. IL12 has been fused to L19 and F8 antibody in various format (e.g. scFv, SIP, single and tandem diabody) due the heterodimeric architecture if the cytokine which allows different protein engineering strategies[170–172]. To abrogate systemic toxicity, the p40 and p35 subunits have been devised as two distinctive products reconstituting the full heterodimeric p70 *in vivo*[154].

2.9.2 Interleukin 2 and TNF as possible payloads for antibody fusions

Interleukin 2 is a monomeric 16 kDa cytokine considered as main regulator of immunity. It was discovered by Gallo and co-workers in 1976, and isolated one year later by Gillis

and Smith[173,174]. At resting condition, IL2 is mainly produced by CD4+ helper T cells, while after immune activation T cells, NK cells, dendritic cells and mast cells start to secrete the cytokine. Its activity explicates as inducer of the proliferation of proliferation of cytotoxic T cells, NK cells, B cells and monocytes. It also potentiates the action of regulatory T cells[175,176]. IL2 receptor has three forms generated as different combination of three chains: CD25 (also called IL2-Rα), CD122 (IL2-Rβ) and CD132 (IL2-Rγ).

The IL2-Rα chain bins IL2 with low affinity, whereas the complex of β and γ chains expressed by memory T cells and NK cells is capable of biding IL2 with an intermediate affinity. The three receptors chain complex is instead the one binding IL2 with the highest affinity (Kd ~ 10^{-11} M) and it is expressed by T cells and T regs (**Figure 2.13**).

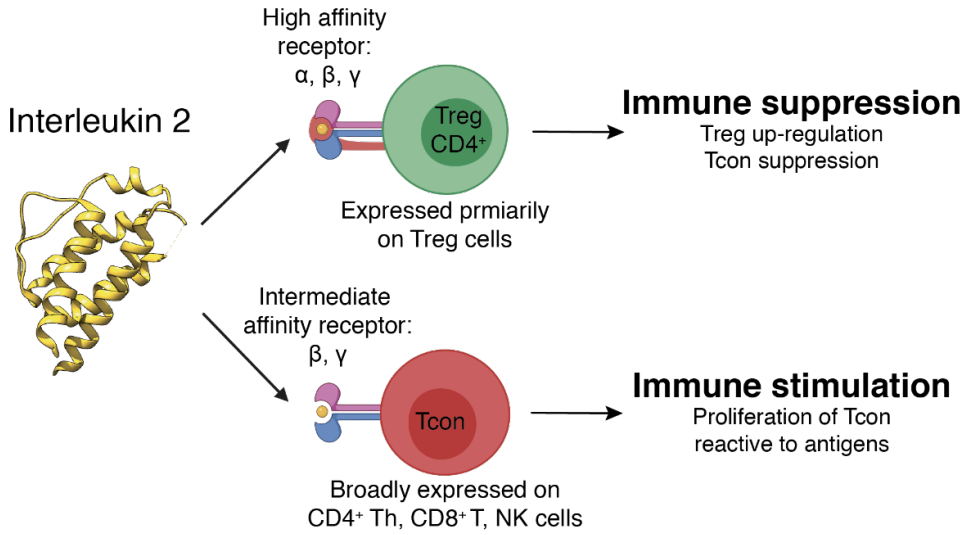

Figure 2.13: Crystal structure of IL2 (yellow) and graphical representation of the dual pharmacology of IL2. IL2 can bind both to high-affinity trimeric receptors on regulatory T cells (represented in green) and to intermediate-affinity dimeric receptors on conventional T cells (Tcon, represented in red). Depending on the immune cells activated, IL2 can cause either a suppressive or a stimulatory immune response. Adapted from (173), created with BioRender.com.

In 1985, Steve Rosenberg showed that the administration of high dose of IL2 in combination with autologous T cells brought to the remission of tumor in patients with advanced melanoma[34]. Recombinant IL2 got the approval from FDA as non-targeted product (aldesleukin, Proleukin®) based on the long remission induced by IL2 in patient with metastatic kidney cancer and melanoma. Even if used as low dose regimen (72'000 IU/kg), the administration of Proleukin induced several toxicities (e.g. vascular leak syndrome, nausea and fever) limiting the applicability of this biopharmaceutical[177–179]. The reason for these toxicities is correlated to the expression by T regs of the high affinity receptor for IL2 composed by the subunits $\beta\gamma\alpha$, thus outcompeting naïve T cells for their natural ligand.

To improve the therapeutic index of recombinant IL2, several strategies have been employed. Nektar therapeutics has, for instance, developed NKTR-214 (bempegaldesleukin), a site-specific PEGylated version of the cytokine that allow to increase the drug's circulatory half-life, while improving its tolerability profile[180,181]. PEG site specific conjugation prevents the interaction with CD25, mainly expressed by T regs.

The targeted delivery of IL2 at the site of disease was another strategy used to improve the therapeutic index of the protein[182]. Our group has generated several IL2-fusion proteins, featuring cancer-specific antibodies targeting splice isoforms of fibronectin (EDB and EDA) and tenascin-C (domain D) (e.g., L19-IL2, F8-IL2 and F16-IL2, respectively)[183–185]. The developed products showed promising activity as single agents in preclinical studies in various solid and hematological tumor models. The anti-tumor activity was then improved when administered in combination with immune checkpoint-inhibitors, cytotoxic agents, external beam radiation, other immunocytokines, or IgG antibody molecules that induce ADCC. L19-IL2 is being studied (i) in combination with Rituxan in patients with relapsed or refractory diffuse large B-cell lymphoma (Phase I, NCT02957019), (ii) in combination with stereotactic body radiation therapy (Phase II, NCT02735850), (iii) and as neoadjuvant in combination with L19-TNF for intralesional application of stage IIIB and C melanoma patients (Phase III, NCT02938299).

Tumor necrosis factor (TNF) is a pro-inflammatory cytokine mainly produced by macrophages, NK cells and T cells (at first as 26 kDa transmembrane protein, later it is released as 17 kDa cytokine) in response to trauma and infections[34,186]. TNF was discovered by the laboratory Lloyd J. Old at the Memorial Sloan Kettering Cancer Center in New York in 1975 during some studies about the potential anti-tumor effect given by the injection of endotoxins in mouse models. The cytokine was secreted into the serum of mice and capable of inducing hemorrhagic necrosis of sarcomas; for this reason, it has been identified as "tumor necrosis factor" because of the observed cancer-damaging activity[187]. TNF is not involved only in the process of tumor cells apoptosis, whereas it drives the production of other pro-inflammatory cytokines (e.g., IL1 and IL6), promoting the activation of the endothelium and blood coagulation. Moreover, the activation of the immune system due to inflammation at the tumor site leads to an immune mediated anticancer effect[188]. Since TNF can activate the vascular endothelium and trigger blood clotting, local infections are prevented by the spread of TNF into the circulation. However, the systemic activity of TNF could lead to disseminated intravascular coagulation and multi-organ failure (septic shock)[34]. Furthermore, many inflammatory disease (e.g. rheumatoid arthritis, Crohn's disease and inflammatory bowel disease) are associated with unbridled synthesis of TNF[189–191].

Despite the undesirable role of TNF in different pathological disorders, various strategies have been exploited for the treatment of cancer patients. The systemic use of recombinant TNF in the clinic is limited by substantial side effects and the recombinant product (Beromun®) obtained marketing authorization only for locoregional treatments (i.e., for isolated limb perfusion) in patients with soft-tissue sarcoma lesions, in combination with melphalan[192–194]. The targeted delivery of TNF thought antibody fusion proteins has been intensively investigated in various cancer mouse models[195]. The anti-cancer activity that was observed relied on the induction of vascular shut-down and activation of adaptive immunity.

Our group has developed an immunocytokine consisting of human TNF fused to the anti-EDB antibody L19; L19-TNF is currently being tested in various clinical trials. The immunocytokines has been administered either in combination with doxorubicin for the treatment of metastatic soft tissue sarcoma (Phase III clinical trial, EudraCT Number 2016-003239-38) or in combination with L19-IL2 for intralesional application of stage IIIB and C melanoma (Phase III, NCT02938299), as well as in combination with dacarbazine in pre-treated soft tissue sarcoma (Phase II starts in 2020), and in monotherapy for the treatment of glioma (Phase I, NCT03779230).

The fusion TNF and IL2 with tumor-targeting monoclonal antibodies has been proposed for oncological applications and extensively studied by our group. Complete and durable tumor remissions have been observed in mouse model when treated with immunocytokines products based on pairs of synergistic payloads (e.g. IL4/IL12, IL2/IL12, IL12/TNF and IL2/TNF)[196–201]. Our group has been studying the synergistic effect of IL2 and TNF both as administered as dual cytokine product (at a preclinical level) or as simultaneous injection of L19-IL2/L19 TNF. Encouraging results in a Phase II study in patients with Stage IIIB/C melanoma have led to the initiation of a Phase III clinical trial in Europe and in the U.S.A., involving the intralesional administration of L19-IL2 plus L19-TNF to patients with fully-resectable Stage IIIB/C melanoma lesions [EudraCT number 2015-002549-72].

2.10 Tumor microenvironment associated antigens for selective drug delivery

Tumor growth is not only determined by malignant cells themselves but also by the tumor stroma. Main actors in cancer progression are angiogenesis (i.e., the

formation of new blood vessels from pre-existing ones) and inflammatory cells that can also contribute to the tumor growth[202,203]. Over the last decades, the importance of tumor microenvironment (TME) for solid tumor development and progression became increasingly recognized. On one hand, tumor stroma holds essential functions fostering tumor growth. On the other hand, that same environment typically produces unique antigens that can be exploited for pharmacodelivery applications[204]. Antigens expressed either on new blood vessels or in the matrix represents attractive targets for selective therapy of cancer. Furthermore, since angiogenesis is a common feature of malignancies, the same agent could in principle be used for a variety of tumors. Other interesting characteristics of TME associated antigens are their abundancy and stable expression in the tumor stroma with less antigen heterogeneity compared to non-TME associated antigens[205].

2.10.1 Oncofetal fibronectin

Tumor-associated extracellular matrix (ECM) components such as fibronectins, collagens, tenascins and proteoglycans are produced by stromal, endothelial and tumor cells[206]. Fibronectins are high-molecular weight glycoproteins which are present in large amounts in the ECM and in the plasma[207]. Monomers are flexible and folded in a series of proteins domains (e.g. type I, type II and type III domains) with functionally distinctive properties[208]. Secreted fibronectins are usually linked in dimers whereas in tissue, fibronectins forms fibronectin matrices build by disulfide-crosslinked fibrils[209]. These matrices are important for cell adhesion and spreading in the ECM. Moreover, they play a fundamental role in cellular morphology, differentiation, and proliferation. In particular, during tissue remodeling events and in malignancies, extra-domain B (EDB), extra-domain A (EDA), and IIICS region is inserted in the protein by a mechanism of alternative splicing[210,211]. EDB and EDA are some of the most extensively studied ECM tumor associated antigens[212,213].

2.10.2 Tenascin C

Tenascin C was the first member of the tenascin family discovered in 1983 as a protein enriched in the stroma of gliomas[214]. Its name reflects two sites where TNC is mainly expressed: tendons and embryos[215]. TNC is indeed expressed during embryogenesis, and it is not detectable in healthy tissue. During pathological

conditions such as infection, inflammation, and tumorigenesis, TNC is rapidly produced by activated fibroblasts, endothelial cells or by cancer cells. Many growth factors, for example TGF-β, and mechanical stress have been shown to induce tenascin C expression in cultured cells or tissues[216].

Tenascins are all built from a common set of structural motifs. From a structural point of view, TNC is a hexameric, multimodular extracellular matrix glycoprotein with several forms that are created through protein modification and alternative splicing[217]. It comprises several fibronectin type 3 (FNIII) like domains; eight FNIII domains are constitutionally present in the protein, whereas nine repeats (FNIII A-D) located between FNIII5-6 are subject to alternative splicing giving rise to small and large isoforms of TNC[218]. *In vitro* assay demonstrates that the alternative splicing of normal cells can be controlled by extracellular pH, whereas malignant cells accumulate large TNC isoforms regardless of the pH of the culture media[219].
Large isoforms of tenascin C are undetectable in most healthy tissues but they have been associated with angiogenesis during tissue remodeling and invasiveness of carcinomas (Jones et al. 2000) as well as with wound healing[220,221]. By contrast, large isoforms of TNC are over-expressed in several tumors including oral squamous cell carcinomas, breast carcinomas, prostatic adenocarcinoma, lung cancers, colorectal cancer, astrocytoma and other brain tumors[222–228].
In the first part of this thesis, we focused on the isolation of a highly specific antibody against the Domain D of Tenascin C. TNC-D is highly conserved between mouse and man, thus representing an ideal target for the development of novel fully human monoclonal antibodies, which can be used for preclinical experiments in mice and for subsequent clinical application[229].

TNC exerts different effects on different cell types during tumor growth. It promotes angiogenesis and inhibits the immune response. By modulating cell adhesion and cell spreading, TNC promotes tumor cell proliferation or their trans-differentiation into cells with endothelial properties[230,231]. Whereas cells on fibronectin are flat and assemble a network of actin stress fibers, cells on tenascin C are rounded and extend actin-rich processes. The activities of focal adhesion kinase (FAK) and RhoA are repressed on a tenascin C substratum[232]. Recent studies

revealed that TNC promotes multiple events during metastasis stimulating angiogenic switch with the formation of poorly functional blood vessel.

Several antibodies have been raised against Tenascin C, in particular against large Tenascin C isoforms[214,233,234]. A murine antibody specific for the alternative spliced A4 domain of TNC, termed BC2, was discovered and used as radiolabeled preparation (^{131}I-BC2 IgG1 or^{111}I -BC2 IgG1) for imaging in patients with glioma and malignant glioblastoma[235,236]. Furthermore, a three-step pre-targeted imaging method consisting of the injection of biotinylated BC2 followed by avidin and (^{99m}Tc)PnAO-biotin was tested to detect cerebral gliomas[237]. During Phase 2 clinical studies, the murine 81C6 antibody (specific to TNC-D) was investigated as ^{131}I radio-conjugate for the treatment of glioma patients[238]. Phase I studies with fully human 81C6 IgG2 have been conducted for the treatment of non-Hodgkin lymphoma[239]. Sigma Tau (Italy) developed murine antibodies specific to the large (named ST2485) and small (named ST2146) isoform of TNC[240]. ST2146 (later called tenatumomab), was investigated in a Phase 1 clinical trial as a delivery agent for radionuclides to neoplastic lesions (NCT02602067).

Our group worked extensively on the generation of high-affinity antibodies against markers for angiogenesis, in particular the EBD and EDA domains of Fibronectin and A1, C and D domains of Tenascin C (**Figure 2.14**).
L19 and F8 antibodies recognize EDB and EDA domains, respectively; both antigens are conserved from mouse to man thus facilitating translational activities from preclinical models to clinical trials. After the validation of these antibodies in several mouse models of cancer, L19 and F8 are currently being studied in late-stage clinical trials as fusion protein with different payloads such as IL2, TNF, IL12 and IL10[30,32,33].
Brack and coworkers described the generation of F16, an antibody specific for the A1 domain of TNC. The antibody showed excellent tumor targeting performances comparable with the one of L19. P12 was instead an antibody generated against the D domain of TNC: it displayed excellent *in vitro* properties, but sub-optimal *in-vivo* targeting performance[229]. For this reason, the isolation of novel antibodies against this target is still needed.

Silacci and Neri's group reported on the generation of G11, an antibody specific for TNC-C, strongly expressed in the majority of lung cancers, with a vascular and stromal pattern of expression[229].

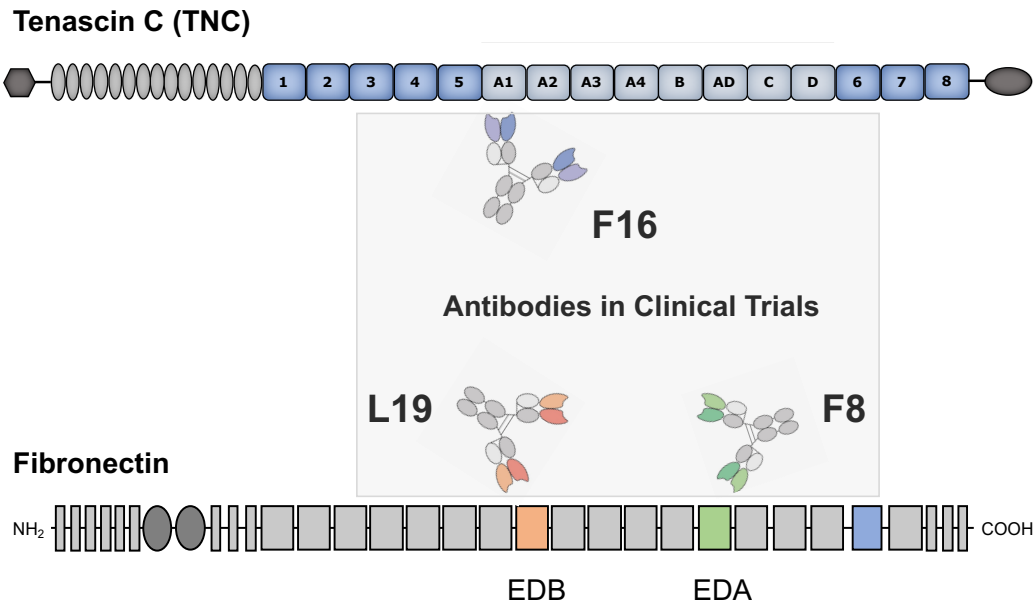

Figure 2.14: Schematic representation of the domain structure of Fibronectin and Tenascin-C. The alternatively spliced extra-domains A and B of Fibronectin are recognized by the antibodies F8 and L19, respectively. The F16 antibody is specific for the A1 domain of Tenascin C.

2.10.3 Fibroblast Activation Protein

Fibroblast Activation Protein (FAP) is a cell-surface serine protease emerges as promising candidate for the specific targeting of cancer associated fibroblasts (CAFs), important tumor stroma's components which promotes tumor growth and progression[241].

FAP was discovered in the mid 1980s by two groups that were investigating surface antigens to define activated fibroblasts and membrane-bound proteases. Both groups identified a 170-kDa gelatinase with dipeptidyl peptidase activity that was later recognized as FAP[242–244]. FAP enzymatically active form consists of a homodimer that cleaves peptide bond between proline and other amino acids modifying various bioactive molecules. The main form of FAP is a type II membrane-bound glycoprotein with a transmembrane region (20 aa), a cytoplasmic region (6 aa) and an extracellular region (734 aa) which contains the catalytic site[245].

FAP is best known for its presence in the tumor microenvironment of over 90% types of malignant tumors. FAP can be expressed by stromal activated fibroblasts of epithelial tumors and bone and soft tissue sarcomas. Furthermore, its expression is also detected in tumor cells (e.g. melanoma, malignant breast, colorectal, skin, prostate and pancreatic cancers, bone and soft sarcomas)[242–244,246,247]. FAP protein levels can be elevated not only in CAFs but also in tumor vasculature as well. The absence of FAP in healthy adult tissue renders this peptidase an attractive target for both imaging and therapeutic applications. The antigen has been described as the "next billion-dollar nuclear theranostics target", as more than 28 different tumor types have successfully been imaged in patients with radiolabeled FAP ligands (e.g., FAPI-04, FAPI-46)[248,249].

The first monoclonal antibody capable of selectively target FAP was F19. The antibody could strongly stain pancreatic, breast, ovarian and colorectal cancers[242,243,250]. For this reason, a radiolabeled preparation of the humanized version of F19, Sibrotuzumab, was used to image metastatic cancer patients of different origins. The slow clearance of the immunoglobulin from the bloodstream impaired the development of the product for imaging activities.

Several others recombinant immunoglobulins targeting FAP have been developed over the last decades. Fisher and coworkers described in 2012 the generation of two novel FAP-specific antibodies, termed ESC11 and ESC14. In preclinical experiments, radiolabeled preparation of the ESC11 antibody (i.e., ESC11-^{177}Lu) showed preferential accumulation in human melanoma xenografts and induced tumor growth retardation[251].

Claus and coworkers described the generation of a bispecific antibody which simultaneously recognizes FAP on tumor cells and 4-1BBL on lymphocytes. The product was able to induce long-term cancer remissions in mouse tumor models and is currently being investigated in a Phase I clinical trial[252]. Klein and coworkers developed a novel fusion protein consisting of an anti-hFAP antibody fused to an Interleukin 2 variant (IL2v)[253]. MP0310 (NCT04049903) and MP0317 are two early-stage clinical products, based on the DARPin® platform, that combine tumor-restricted FAP binding with 4-1BB and CD40 agonistic ligands, respectively[254].

Our group recently developed a small molecule targeting hFAP. OncoFAP binds to human FAP with affinity in the sub-nanomolar concentration range and cross-reacts with the murine isoform of the protein. The small molecule derivatives targeting properties have been evaluated in biodistribution studies in mouse models showing a rapid and homogeneous penetration within the neoplastic tissue[255].

3. Aim of the thesis

The aim of my PhD thesis was the isolation and validation of monoclonal antibodies selective for tumor microenvironment-associated antigens. In the first part of this thesis, the generation of a novel antibody against the spliced domain D of Tenascin C (TNC-D) by phage display technology is described. TNC is a glycoprotein overexpressed in the extracellular matrix of various solid tumors. The second part of this work focuses on the isolation of an antibody selective for Fibroblast Activation Protein (FAP), serine protease *de novo* expressed during carcinogenesis and inflammation in the tumor microenvironment.

Experience with L19 and F8 antibodies has shown that targeting the extracellular matrix is an efficient and promising strategy for cancer therapy. Fully human antibodies selective for well-established antigens such as TNC-D and FAP are interesting candidate for clinical developments. Furthermore, the generation of immunocytokines based on IL12 allowed to understand the therapeutic properties of the two newly discovered antibodies in tumor models in mice.

4. Novel human monoclonal antibodies specific to the alternatively spliced domain D of Tenascin C efficiently target tumors in vivo

This chapter is based on the study published in 2020 on the journal "mAbs". The paper is the result of the work of several scientists. My research contribution was represented by the isolation by phage display, *in vitro* and *in vivo* characterization and cloning of different formats of the monoclonal antibodies described in the article. R. Corbellari and Dr. T. Weiss helped in the execution of the experiments. Dr. A. Villa, Dr. M. Weller, Dr. D. Neri and Dr. R. De Luca supervised the experiments.

Antibodies targeting the spliced domain D of Tenascin have been selected from the synthetic library "ETH2Gold" by phage display technology. After the process of screening of different clones by Size Exclusion Chromatography and Surface Plasmon Resonance Analysis, R6N demonstrated to be the best candidate with a K_D of 24 nM. The antibody was capable of selectively accumulate at the neoplastic lesion when inject in tumor bearing mice. Furthermore, the molecule resulting from the fusion of R6N in tandem diabody format with interleukin-12 was tested in different mouse tumor models. The immunocytokine R6N-IL12 exhibited potent antitumor activity leading to tumor growth inhibition and regression. In the future, the antibody could be used as platform for the generation of immunocytokines specifically targeting various models of Tenascin C-positive cancers.

Lisa Nadal[1,2†], Riccardo Corbellari[1,2†], Alessandra Villa[2], Tobias Weiss[3], Michael Weller[3], Dario Neri[4] and Roberto De Luca[2*]

[1] University of Trento, Italy, CiBIO (Department of Cellular, Computational and Integrative Biology), Via Sommarive 9, 38123 Povo (Trento)
[2] Philochem AG, Libernstrasse 3, 8112 Otelfingen, Switzerland
[3] Department of Neurology and Brain Tumor Center, University Hospital Zurich and University of Zurich, Zurich, Switzerland
[4] Department of Chemistry and Applied Biosciences, Swiss Federal Institute of Technology (ETH Zürich), Zurich, Switzerland

*** Corresponding author**

Roberto De Luca, Philochem AG, Philogen Group, Libernstrasse 3, CH-8112 Otelfingen (Switzerland),

Telephone: +41-43-5448819

e-mail: roberto.deluca@philogen.com

Key words: Monoclonal antibodies, phage display technology, Tenascin C, antibody-cytokine fusions, Interleukin 12**.**

4.1 Abstract

Antibody-based delivery of bioactive molecules represents a promising strategy for the improvement of cancer immunotherapy. Here, we describe the generation and characterization of R6N, a novel fully human antibody specific to the alternatively spliced domain D of Tenascin C, which is highly expressed in the stroma of primary tumors and metastasis. The R6N antibody recognized its cognate tumor-associated antigen with identical specificity in mouse and human specimens. Moreover, the antibody was able to selectively localize to solid tumors *in vivo* as evidenced by immunofluorescence-based biodistribution analysis. Encouraged by these results, we developed a novel fusion protein (termed mIL12-R6N) consisting of the murine interleukin 12 fused to the R6N antibody in homodimeric tandem single-chain variable fragment arrangement. mIL12-R6N exhibited potent antitumor activity in immunodeficient mice bearing SKRC52 renal cell carcinoma, as well as in immunocompetent mice bearing SMA-497 glioma. The experiments presented in this work provide a rationale for possible future applications for the R6N antibody for the treatment of cancer patients.

4.2 Introduction

Over the past two decades, antibody-based therapy has become an established and successful strategy to treat hematological and solid malignancies[256–258]. The targeted delivery of bioactive payloads (e.g., radionuclides, cytotoxic drugs, cytokines, procoagulant factors) to the tumor environment, by means of antibodies specific to tumor-associated antigens, represents an avenue for the development of selective anti-cancer agents[259–262]. In addition to antibodies specific to cell surface antigens (e.g., carcinoembryonic antigen, fibroblast activating protein, carbonic anhydrase IX), markers of tumor angiogenesis expressed in the extra-cellular matrix (ECM) of the tumor microenvironment exemplify attractive molecules for the targeted delivery of therapeutics[220]. ECM components are well accessible to antibodies due to their low shedding profile and their abundancy and stability[229]. Our group has extensively studied ECM-associated antigens, such as the spliced extra domains A (EDA) and B (EDB) of fibronectin[64,263] and Tenascin C (TNC)[218,229].

In this work, we describe the generation and validation of a new antibody specific to the alternatively spliced domain D of Tenascin C (TNC-D). TNC is a highly conserved glycoprotein, which comprises multiple fibronectin type 3 (FNIII) like domains. A total of eight FNIII domains are constitutionally present in the protein, whereas nine repeats (FNIII A-D) located between FNIII5-6 undergo to alternative splicing giving rise to small and large isoforms of TNC[217,264,265]. *In vitro* assay demonstrates that the alternative splicing of normal cells can be controlled by extracellular pH, whereas malignant cells accumulate large TNC isoforms regardless of the pH of the culture media[219]. The large isoform of TNC is physiologically expressed during embryogenesis, but it is not detectable in adult healthy tissues. However, it can be rapidly expressed *de novo* in response to pathological stress condition such as chronic inflammation and cancer[219,266,267]. Domain D of Tenascin C is highly conserved between mouse and man[229], thus representing an ideal target for the development of novel fully human monoclonal antibodies, which can be used for preclinical experiments in mice and for subsequent clinical application.

Several antibodies have been raised against Tenascin C, in particular against large Tenascin C isoforms[214,233,234]. The murine antibody BC2 in IgG1 format (specific to

an epitope of the alternative spliced A4 domain of TNC) was radiolabeled with ^{131}I or^{111}I and used as an imaging agent in patients with glioma and malignant glioblastoma[235,236]. Furthermore, a three-step pre-targeted imaging method consisting of the injection of biotinylated BC2 followed by avidin and (^{99m}Tc)PnAO-biotin was tested to detect cerebral gliomas[237]. The murine 81C6 antibody (specific to TNC-D) was investigated in Phase 2 clinical trials as ^{131}I radio-conjugate for the treatment of glioma patients[238,268]. In order to minimize murine Fc-mediated immunogenicity in patients, the murine variable regions of the 81C6 antibody were grafted in a human IgG2 background[52]. The monoclonal chimeric antibody was studied in Phase 1 clinical trials for the treatment of non-Hodgkin lymphoma[269]. Sigma Tau (Italy) developed murine antibodies specific to the large (named ST2485) and small (named ST2146) isoform of TNC[240,270]. ST2146 (later called tenatumomab), was investigated in a Phase 1 clinical trial as a delivery agent for radionuclides to neoplastic lesions (NCT02602067). An antibody against TNC-D (named P12) had previously been reported by our group. P12 displayed excellent *in vitro* properties, but sub-optimal *in-vivo* targeting performance[229]. For this reason, the isolation of novel antibodies against this target is still needed.

Phage display is one of the most versatile and reliable platforms for discovery and affinity maturation of monoclonal antibodies, peptide and protein therapeutics[271–273]. The large number of clinical grade antibodies generated by phage display technology (e.g., Humira®, Benlysta®, Lucentis®), suggest the value of this *in vitro* methodology[57]. Phage-derived antibodies directed against ECM components are particularly suited for the delivery of bioactive payloads (e.g., drugs, radionuclides, cytokines) to the tumor site, helping spare normal tissues[30,119,140] Among the cytokine payloads, Interleukin 12 (IL12) is one of the most attractive candidates for tumor therapy because of its unique ability to potently activate natural killer (NK) cells, CD4+ T cells and CD8+ T cells[31,150]. We and others have previously described antibody-IL12 fusion proteins[170], and two of these products have moved to clinical trials for the treatment of various types of malignancies (NCT00625768, NCT04303117).

Here we describe the generation by phage display technology of R6N, an antibody selective for the TNC-D. The antibody was capable of recognizing the antigen both

in human and mouse specimens and showed encouraging targeting properties in mouse model of cancer. To investigate the therapeutic potential of R6N for the active delivery of payloads to the tumor site, we fused it to IL12. The resulting novel fusion protein, termed mIL12-R6N, consisted of a murine IL12 sequentially fused to the N-terminus of R6N in homodimeric tandem single-chain variable fragment (scFv) arrangement[274]. Preclinical studies were performed with the murine analogue of IL12 since the human protein is not able to recognize the cognate receptor in mice[275]. mIL12-R6N was able to induce cancer regression in SKRC52 and SMA-497 orthotopic syngeneic tumor-bearing mice, without showing signs of toxicity. The fully human product (IL12-R6N) may find clinical applications for cancer immunotherapy.

4.3 Materials and Methods

Cell lines

The human renal cell carcinoma SKRC52 was kindly provided by Professor E. Oosterwijk (Radbound University Nijmegen Medical Center, Nijmegen, the Netherlands). CHO cells, U87 cells, A431 cells, A375 cells, Colon 26 cells and C51 cells, were obtained from the ATCC. Cell lines were received between 2018 and 2020, expanded, and stored as cryopreserved aliquots in liquid nitrogen. SMA-497 and SMA-540 cells were obtained from Dr. D. Bigner (Duke University Medical Center, Durham, North Carolina, USA) and cultured as previously described[276].
Cells were grown according to the supplier's protocol and kept in culture for no longer than 14 passages. Authentication of the cell lines also including checks of post-freeze viability, growth properties, and morphology test for mycoplasma contamination, isoenzyme assay, and sterility test were performed by the cell bank before shipment.

Cloning, expression and biotinylation of BSP-hTNC-D

The gene encoding for TNC-D was amplified and cloned into the bacterial expression vector pQE-12 with the BirA target sequence "BirA Substrate Peptide" (BSP), LHHILDAQKMVWNHR, to specifically biotinylate the antigen. Primers were designed to fuse the BSP tag sequence to the N-terminus of human TNC-D. PCR fragments were assembled and cloned into the expression vector by EcoRI and HindIII restriction site as described previously[277]. The BSP-hTNC-D protein was expressed in *E. coli* TG-1 as described before[278,279]. The protein biotinylation was carried with BirA enzyme, an *E. coli* enzyme able to achieve precise biotin modification. The biotinylation was carried in BirA buffer (10 mM Tris pH 7.5, 200 mM NaCl, 5 mM $MgCl_2$) following the protocol described by Fairhead et al[278].

In vitro protein characterization

The fusion proteins described here were produced through transient gene expression (TGE) in CHO-S cells[280] and purified from the cell culture medium by protein A Sepharose (Sino Biological) affinity chromatography, dialyzed against phosphate-buffered saline (PBS) and stored in PBS at -80°C. SDS-PAGE was performed with 10% gels under reducing and non-reducing condition. Purified

proteins were analyzed by size-exclusion chromatography using a Superdex 75 increase or 200 increase 10/300 GL column on an ÄKTA FPLC (GE Healthcare, Amersham Biosciences). Affinity measurements were performed by SPR using BIAcoreX100 instrument (BIAcore AB, Uppsala, Sweden) on human TNC-D coated CM5 chip and on mouse TNC domains BCD coated CM5 chip. Differential scanning fluorimetry was performed on an Applied Biosystem StepOnePlus RT-PCR instrument for R6N diabody and R6N IgG1. Protein Thermal Shift Dye Kit (Thermo Fisher) was used for thermal stability measurements, where the temperature range spanned from 25 to 95°C with a scan rate of 1°C/min. For electrospray ionization-mass spectrometry (ESI-MS) analysis samples were diluted to 0.1 mg/mL and LC-MS was performed on a Waters Xevo G2XS Qtof instrument (ESI-ToFMS) coupled to a Waters Acquity UPLC H-Class System using a 2.1 Å~ 50 mm Acquity BEH300 C4 1.7 µm column (Waters).

Selections of antibodies from the ETH-2 Gold library by phage display

Human monoclonal antibody L7D specific to human TNC-D was isolated by two rounds of biopanning from ETH-2 Gold library[87] following the protocol described by Viti et al[67]. Briefly, 120 pM of biotinylated BSP-hTNC-D were incubated with 60 μL of streptavidin-coated magnetic beads (Invitrogen, M-280); coated dynabeads were subsequently incubated with preblocked 10^{12} transforming units of phage antibodies. Beads were washed with 0.1% Tween 20 in PBS and with PBS (100 mmol/L NaCl, 50 mmol/L phosphate, pH 7.4). Bound phage was eluted with triethylamine (Sigma) and amplified in *E. coli* TG-1 using VCS-M13 Interference-Resistant Helper Phage (Agilent, Santa Clara, CA). Phage particles were precipitated from culture supernatant using a solution of 20% polyethylene glycol /2.5 M NaCl. Two rounds of panning were performed against the target antigen. Induced supernatants of individual clones were screened by ELISA on human TNC-D and on mouse TNC domains BCD as described by Viti et al[67].

Affinity maturation of scFv L7D

The scFv(L7D) affinity maturation library was constructed in a phagemid vector by introducing sequence variability in the CDR1 loops of both heavy and light chain using degenerated primers as described by Brack et al[229]. A point mutation N-Q was introduced at position 88 of the light chain to remove a potential glycosylation

site[281]. The ligation was electroporated into *E. coli* TG-1 cells; phage was rescued by superinfection with helper phage VCS-M13. The library had a theoretical variability of 6.4×10^7; the obtained library had a size of 1.4×10^6. The library was subjected to two rounds of panning following the same protocol used for the parental antibody selection. R6N, together with L7D, were subcloned into the mammalian expression vector pcDNA 3.1 (+) by NheI/HindIII restriction site, produced and characterized as described.

Cloning, expression and purification of R6N in IgG1 and IgG2a format and of P12 in IgG1 format

R6N IgG1, IgG2a and P12 IgG1 cloning started from the cloning of the light chain of the immunoglobulin into suitable vector by HpaI/SpeI restriction sites. Cloning procedures continued with R6N/P12 IgG1/IgG2a heavy chain cloning using HindIII and XhoI as restriction sites. The same cloning strategy was used to design KSF IgG1. R6N IgG1, IgG2a and P12 IgG1 format were expressed using TGE in CHO-S cells, purified and characterized *in vitro* as described.

Cloning, expression and purification of R6N in diabody format

R6N was reformatted in diabody format into the mammalian expression vector pcDNA 3.1 (+) using NheI and NotI restriction enzymes. The same cloning strategy was used to design KSF diabody (specific for an irrelevant antigen, here used as negative control). R6N in diabody format was expressed using TGE in CHO-S cells, purified and characterized as described.

Cloning, expression and purification of mIL12-R6N and IL12-R6N

The fusion protein mIL12-R6N contains the R6N antibody in homodimeric tandem scFv arrangement fused to murine IL12 at N-terminus. The gene encoding for R6N in diabody format and the gene encoding for the murine IL12 or human IL12 were PCR amplified, PCR assembled and cloned into pcDNA 3.1 (+) by NheI/HindIII restriction site. mIL12-R6N and IL12-R6N were expressed using TGE in CHO-S cells, purified and characterized *in vitro* as described. The biological activity of mIL12-R6N was evaluated by an IFN-γ release assay as described by Puca et al[282].

Immunofluorescence studies

Antigen expression was confirmed on ice-cold acetone–fixed 10-μm cryostat sections of A431, U87, SKRC52, A375, Colon 26, C51, SMA-540, SMA-497, of frozen tumor and normal tissue specimens in microarray (Amsbio, T2635700) and of patient-derived glioblastoma stained with R6N IgG1-FITC (protein was FITC labelled according to manufacturer protocol; Sigma) (final concentration 10 μg/mL) and detected with rabbit anti-FITC (Bio-Rad, 4510-7804) and anti-rabbit AlexaFluor488 (Invitrogen; A11008). For vascular staining, rat anti-CD31 (BD Biosciences, 550274) and anti-rat AlexaFluor594 (Invitrogen; A21209) antibodies were used. Cell nuclei were stained with DAPI (Invitrogen; D1306). For the immunofluorescence-based biodistribution analysis, mice were injected with 200 μg/mouse of R6N IgG1 or KSF IgG1 and of R6N Diabody or KSF Diabody when tumor size reached 100-250 mm^3 and sacrificed 24 hours after injection. Tumors were excised and embedded in cryo-embedding medium (Thermo Fisher) and cryostat sections (10 μm) were stained and detected with Protein A-Alexa 488 conjugate (Thermo Fisher, P11047). Slides were mounted with fluorescent mounting medium (Dako) and analyzed with Axioskop2 mot plus microscope (Zeiss). Quantification of the fluorescent signal, using Image J software, is depicted in **Supplementary Figure S4.12**.

Animal Study design

The immunofluorescence-based biodistribution analysis were performed with 6 BALB/c nude mice bearing A431 epidermoid carcinoma or A375 malignant melanoma. One control group (mice injected with KSF IgG or Diabody) was used for the experiment. The quantitative biodistribution analyses were performed with groups of 4-5 BALB/c nude mice bearing U87 glioblastoma or A431 epidermoid carcinoma, respectively, and one control group (mice injected with KSF diabody) was used for each experiment. The therapy with mIL12-R6N was performed with 10 BALB/c nude mice bearing SKRC52 renal cell carcinoma; one control group with mice injected with saline was used during the experiment. The therapy with R6N IgG2a and diabody was performed with 15 BALB/c nude mice bearing A375 malignant melanoma. The therapy with mIL12-R6N and mIL12-KSF was performed with 15 VM/Dk mice bearing SMA-497 glioma. Mice were randomized

into groups according to their tumor volume; tumor volume measurements were taken by the same experimenter to minimize any subjective bias.

Experimental animals

A total of 51 female BALB/c nude mice, aged 8 weeks with an average weight of 20 g were used in this work. Mice were purchased from Janvier (Route du Genest, 53940 Le Genest-Saint-Isle, France) and raised in a pathogen-free environment with a relative humidity of 40-60%, at a temperature between 18 and 26°C and with daily cycles of 12 hours light/darkness according to guidelines (GV-SOLAS; FELASA). The animals were kept in a specific pathogen free (OHB) animal facility in cages of maximum 5 mice, left for one-week acclimatization upon arrival, and subsequently handled under sterile BL2 workbenches. Specialized personnel were responsible for their feeding; food and water were provided *ad libitum*. Mice were monitored daily (in the morning) in weight, tumor load, appearance (coat, posture, eyes and mouth moisture) and behavior (movements, attentiveness and social behavior). Euthanasia criteria adopted were body weight loss > 15% and/or ulceration of the subcutaneous tumor and/or tumor diameter > 1500 mm and/or mice pain and discomfort. Mice were euthanized in CO_2 chambers.
VM/Dk mice were bred in pathogen-free facilities at the University of Zurich. Female and male mice of 6 to 12 weeks of age were used in all experiments.

Ethical statement

Mouse experiments were performed under a project license (license number 04/2018) granted by the Veterinäramt des Kantons Zürich, Switzerland, in compliance with the Swiss Animal Protection Act (TSchG) and the Swiss Animal Protection Ordinance (TSchV).

Tumor models and biodistribution studies

The *in vivo* targeting performance of the R6N antibody was evaluated by quantitative biodistribution analysis, as previously described[263]. 10 μg of ^{125}I radio-iodinated R6N diabody protein was injected into the lateral tail vein of U87 and A431 tumor-bearing BALB/c nude mice. Mice were sacrificed 24 hours after injection, organs were excised, weighed, and the radioactivity of organs and tumors was measured using a Cobra gamma counter and expressed as percentage of

injected dose per gram of tissue (%ID/g ± SEM; n = 4 mice/group). An immunoreactivity test on TNC-D coated CNBr sepharose resin (GE Healthcare) was conducted as quality control analysis of the radiolabeling process of the antibody. Pooled fractions of radiolabeled antibody were loaded on a resin previously coated with TNC-D (according to manufacturer protocol) and the flow through was collected. Afterwards, TNC-D resin was washed with 1 column volume of PBS and fractions were collected. Finally, radiolabeled antibody was eluted with 1 M triethylamine pH 11.0 and fractions were collected. The radioactivity of the single fractions and of the resin was measured and normalized to the initial radioactivity input.

Tumor model and therapy studies

1×10^7 SKRC52 and 5×10^6 cells A375 tumor cells were implanted subcutaneously in the flank of BALB/c nude mice with 0.5 ml 29G insulin syringes (MicroFine™ +, BD medical). Mice were monitored daily; tumor volume was measured with a caliper and volume was calculated using the formula: tumor size = (Length[mm]*Width^2[mm])/2. When tumors reached a suitable volume (approx. 100 mm^3), mice were injected three times into the lateral tail vein with the pharmacological agents. mIL12-R6N was dissolved in PBS (pH: 6.9) and administered at a dose of 24 μg/mouse every 48 hours. A saline group was included as control. R6N Diabody and IgG2a were dissolved in PBS (pH:7.4) and administered at a dose of 100 μg/mouse every 72 hours for three times. Intracranial tumor cells SMA-497 implantation has been performed as previously described[283]. SMA-497 tumor-bearing mice were treated intravenously at days 5 and 10 after tumor implantation with 100 μl PBS, 100 μl containing 8 μg mIL12-KSF or 100 μl containing 8 μg mIL12-R6N μg. Survival data are presented as Kaplan-Meier plots.

Statistical Analysis

Data were analyzed using Prism 7.0 (GraphPad Software, Inc.). Differences in tumor volume between therapeutic groups (until day 27, when n = 5) were evaluated with the two-way ANOVA followed by Bonferroni as post-test. $P < 0.05$ was considered statistically significant ($^*P < 0.05$, $^{**}P < 0.01$, $^{***}P < 0.001$, $^{****}P < 0.0001$). Kaplan Meier survival analysis was performed to assess survival

differences among the treatment groups and p values were calculated with Gehan-Breslow-Wilcoxon test. Significance was tested at *$p < 0.05$ and **$p < 0.01$.

4.4 Results

Isolation and characterization of antibodies specific to the spliced domain D of TNC

Monoclonal antibodies were isolated from the synthetic human scFv ETH-2 Gold library[87] by phage display technology. The BirA Substrate Peptide (BSP) was fused to human TNC-D (**Fig. 4.1**) at the N-terminus of the protein, in order to coat magnetic beads used for the selection (**Supplementary Fig. S4.1**). The addition of BSP sequence to the antigen allowed a site-specific biotinylation of the antigen[278]. After two rounds of panning, the clone L7D (**Supplementary Fig. S4.2**) was chosen based on the enzyme-linked immunosorbent assay (ELISA) signal and used for further studies (**Supplementary Fig. S4.3**). L7D in scFv format was expressed in Chinese hamster ovary (CHO) cells and characterized by analytical methods, showing homogeneity in size exclusion chromatography and sodium dodecyl sulfate-polyacrylamide gel electrophoresis (SDS-PAGE) (**Fig. 4.1 B and C**). Monomeric fractions from gel-filtration experiments were used for affinity measurements. Surface plasmon resonance (SPR) analysis on TNC-D coated chip showed a biphasic dissociation profile, with a first fast dissociation phase followed by a slow dissociation phase. The calculated KD value was 41 nM. (**Fig. 4.1 D**). To confirm the cross-reactivity of L7D for the mouse antigen, BIAcore analyses were performed on a mouse TNC domains BCD-coated chip (**Fig. 4.1 E**). A microscopic immunofluorescence analysis on U87 glioblastoma section confirmed that the L7D antibody could recognize its cognate antigen in tissues (**Fig. 4.1 F**).

In vitro CDR1 affinity maturation of L7D scFv

The binding properties of the L7D antibody were further improved using a previously described *in vitro* affinity maturation methodology[68]. Sequence variability in the complementarity-determining region 1 (CDR1) loops of the antibody heavy and light chains was introduced. Since residue 88 of the light chain encoded for a potential glycosylation site, the amino acid was mutated into glutamine during the cloning of the library[281]. The best clone isolated from affinity maturation library selections was R6N (**Fig. 4.1 and Supplementary Fig. S4.4**). BIAcore analysis on TNC-D coated chip showed an improvement in binding properties with an affinity in the two-digit nanomolar range, with a KD value of 24

nM. The cross-reactivity for the mouse antigen was further confirmed by SPR (KD value of 3 nM) (**Fig. 4.1 L**).

Antigen specificity was evaluated for L7D and R6N scFvs by ELISA. Both antibodies bound to their antigen in a specific manner (TNC-D and TNC domains CD6) and were cross-reactive for the mouse TNC-BCD. As expected, L7D and R6N did not bind to closely related proteins, including the alternatively-spliced extra-domains A (EDA) and B (EDB) of fibronectin, as well as domain A1 of TNC and recombinant human tumor necrosis factor (**Supplementary Fig. S4.5**). Furthermore, the antibody specificity for the Domain D of Tenascin C was confirmed by immunofluorescence analysis using R6N IgG2a (**Supplementary Fig. S4.6**) co-stained with P12 IgG1 (**Supplementary Fig. S4.7**) on SKRC52 tissue slides. Both antibodies showed a comparable pattern of staining, thus verifying antigen specificity. (**Supplementary Fig. S4.8**)

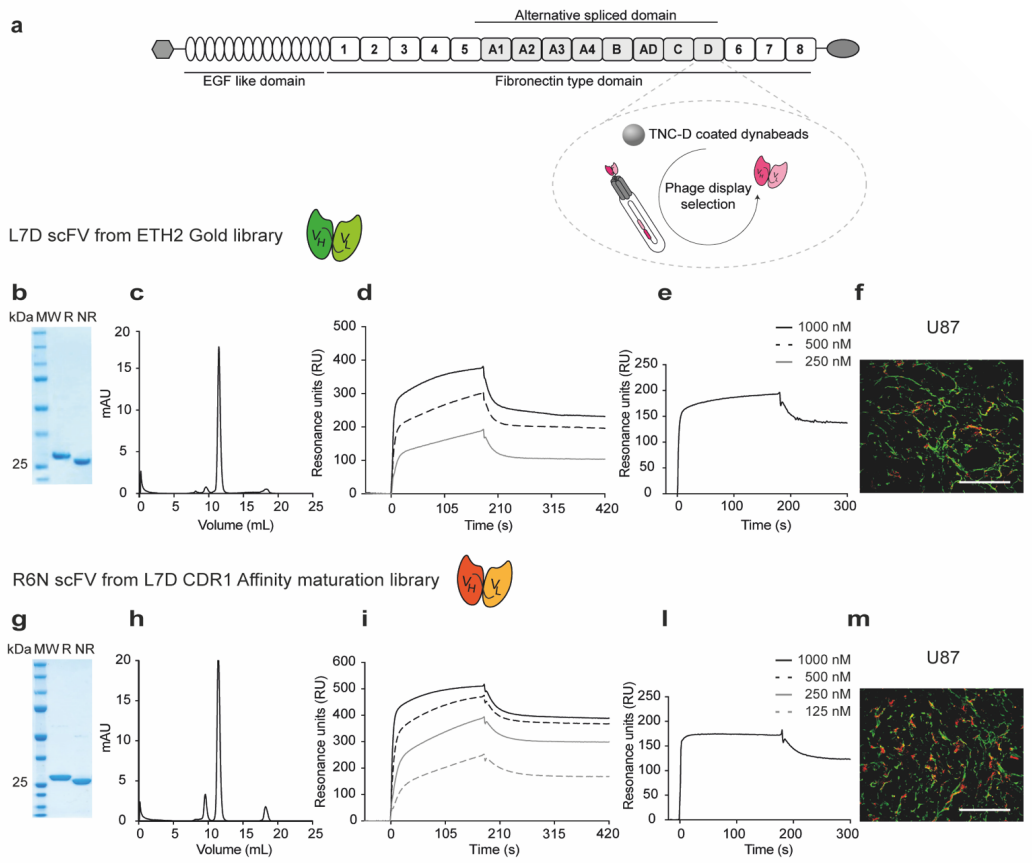

Figure 4.1: Characterization of antibodies against the human spliced isoform D of Tenascin C (hTNC-D). (a) Structural model of one subunit of Tenascin C. Structural domains: hexagon, Tenascin assembly domain; ellipses, epidermal growth factor (EGF) like repeats; white squares, constant fibronectin type 3 homology repeats; gray squares, alternatively spliced fibronectin type 3 homology repeats; circle, fibrinogen globe. Schematic representation of phage display. Characterization of L7D and R6N scFv selected from ETH-2 library; (b, g) SDS-PAGE, 10% gel in reducing (R) and non-reducing (NR) condition of purified scFvs; (c, h) Size exclusion chromatogram, the major peak eluting at about 11.5 mL corresponds to the molecular weight of monomeric fraction of scFvs; (d, i) BIAcore sensograms of monomeric scFvs on hTNC-D coated CM5 chip; (e, l) BIAcore sensograms of scFvs on mouse TNC-BCD domains coated CM5 chip; (f, m) Microscopic fluorescence analysis of TNC-D on U87 tumor section detected with scFvs (green, AlexaFluor 488) and anti-CD31 (red, AlexaFluor 594). Cell nuclei were counterstained with DAPI (blue). Representative pictures of the samples were taken 20x magnification, scale bars = 100 µM.

Immunofluorescence analysis on xenografts, mouse tissue sections and tissue microarray

R6N in IgG1 (**Supplementary Fig. S4.9**) format was studied by immunofluorescence staining on tissue sections. The protein was labelled with fluorescein isothiocyanate (FITC-labelled) and used to stain xenografts tumor models (SKRC52, U87, A431 and A375) and mouse tumor sections (Colon 26, C51, SMA-540 and SMA-497) (**Fig. 4.2**). R6N exhibited an intense staining in all sections, confirming the capability of the antibody to recognize both human and mouse antigen *in vitro*. Moreover, R6N-IgG1-FITC exhibited intense staining in most human solid tumors (particularly ovarian, breast and uterine tumors), but not in healthy adult organs (**Fig. 4.3**). Immunofluorescence analysis on brain sections from a glioma patient revealed that expression of TNC-D and EDB (detected with the L19 antibody) was comparable (**Fig. 4.4**).

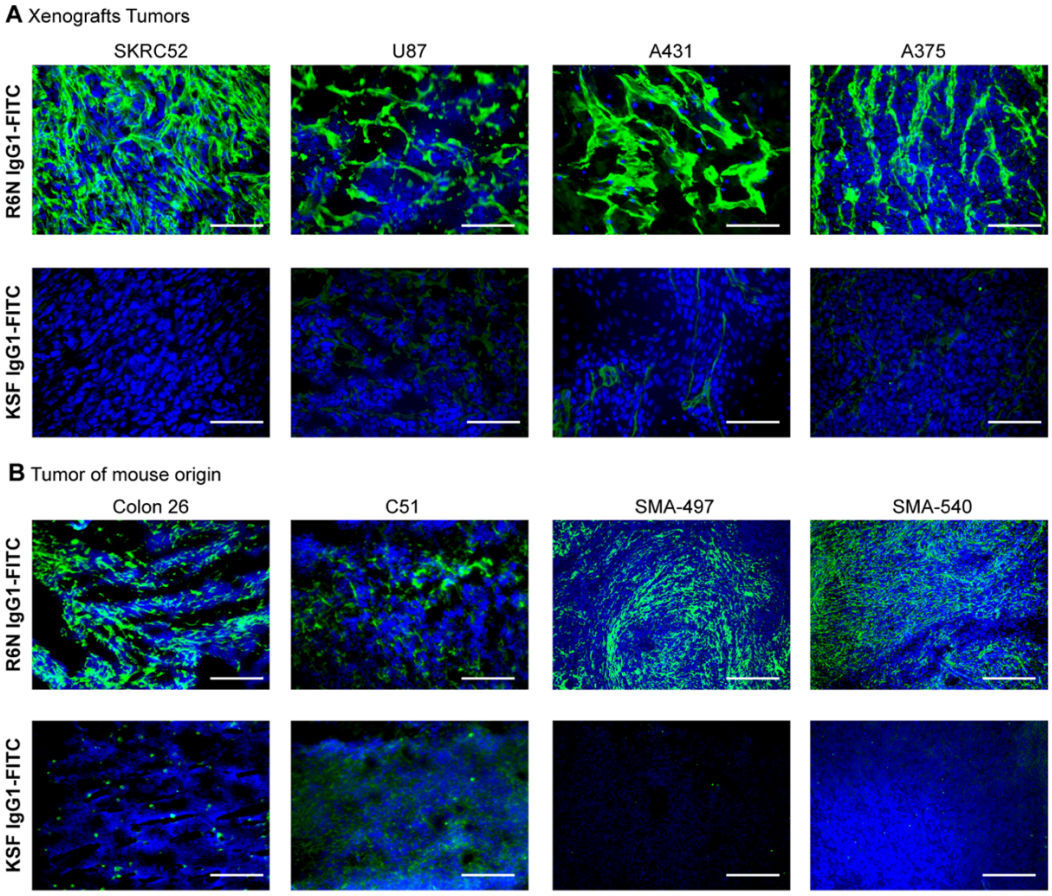

Figure 4.2: Microscopic fluorescence analysis of TNC-D expression on xenografts and tumors of mouse origin section with R6N IgG1-FITC. (a) Microscopic fluorescence analysis of human TNC-D expression on xenograft tumor: SKRC52, U87, A431 and A375 detected with R6N-IgG1-FITC and KSF IgG1-FITC (negative control); (b) Microscopic fluorescence analysis of mouse TNC-D expression on tumors of mouse origin: Colon 26, C51, SMA-497 and SMA540 detected with R6N IgG1-FITC and KSF IgG1-FITC (negative control). Cryosections were stained with anti-FITC (green, AlexaFluor 488); cell nuclei were stained with DAPI (blue). Representative pictures of the samples were taken at 10x magnification, scale bars = 100 μM.

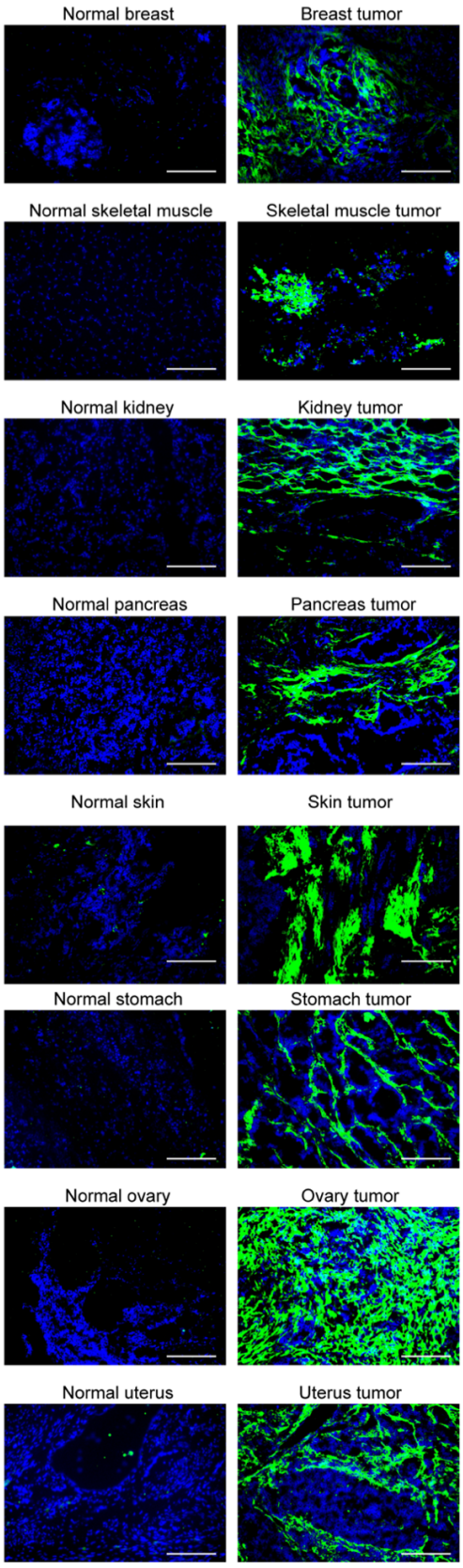

Figure 4.3: Microscopic fluorescence analysis of TNC-D expression of frozen tumor and normal tissues. A tissue microarray containing normal tissue specimens (left) and their tumoral counterpart (right) was stained with R6N IgG1-FITC (green, AlexaFluor 488); cell nuclei were stained with DAPI (blue). Representative pictures of the samples were taken at 10x magnification, scale bars = 100 μM.

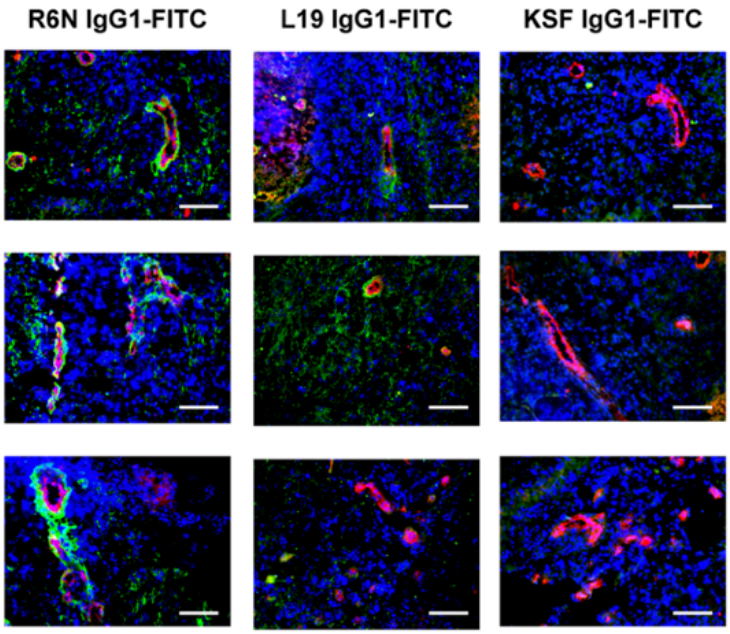

Figure 4.4. **Microscopic fluorescence analysis of TNC-D expression on glioblastoma tissue section from a patient with R6N IgG1 and L19 IgG1**

Microscopic fluorescence analysis of human TNC-D expression on glioblastoma tissue section from a patient detected with R6N IgG1-FITC, L19 IgG1-FITC and KSF IgG1-FITC (used as negative control). Cryosections were stained with anti-FITC (green, AlexaFluor 488); anti CD31 (red, AlexaFluor 594) and cell nuclei were stained with DAPI (blue). Representative pictures of the samples were taken at 10x magnification, scale bars = 100 µM.

Immunofluorescence-based biodistribution analysis

The *in vivo* tumor-targeting performance of R6N was evaluated through immunofluorescence-based biodistribution in A375 (**Fig. 4.5A**) or A431 (**Fig. 4.5B**) tumor-bearing mice. Tumor cell lines were inoculated in immunodeficient mice and when the tumor reached a size of 100-250 mm^3, R6N in IgG1 (in A375 tumor-bearing mice) or diabody (in A431 tumor-bearing mice) (**Fig. 4.6**) format were injected intravenously (KSF in IgG1 or diabody formats were used as negative control). After 24 hours mice were sacrificed, organs and tumor were examined by immunofluorescence procedure. R6N in both IgG1 and diabody format localized to tumors, while no detectable antibody was found in the other organs. No preferential accumulation of the KSF antibody was observed in the neoplastic mass, confirming the requirement of TNC-D binding for an active targeting process. Signal quantification validated the expression of TNC-D only in the tumor mass and not in healthy organs (**Fig. S4.6A**). Quantitative biodistribution analysis in immunodeficient mice bearing subcutaneously grafted U87 glioblastoma (Supplementary **Fig. 4.11A**) or A431 epidermoid carcinoma (**Supplementary Fig. 4.11B**) confirmed the capability of R6N diabody to localize to solid tumors with a good tumor:blood ratio (11.07 in U87 tumor-bearing mice and 7.15 in A431 tumor-bearing mice).

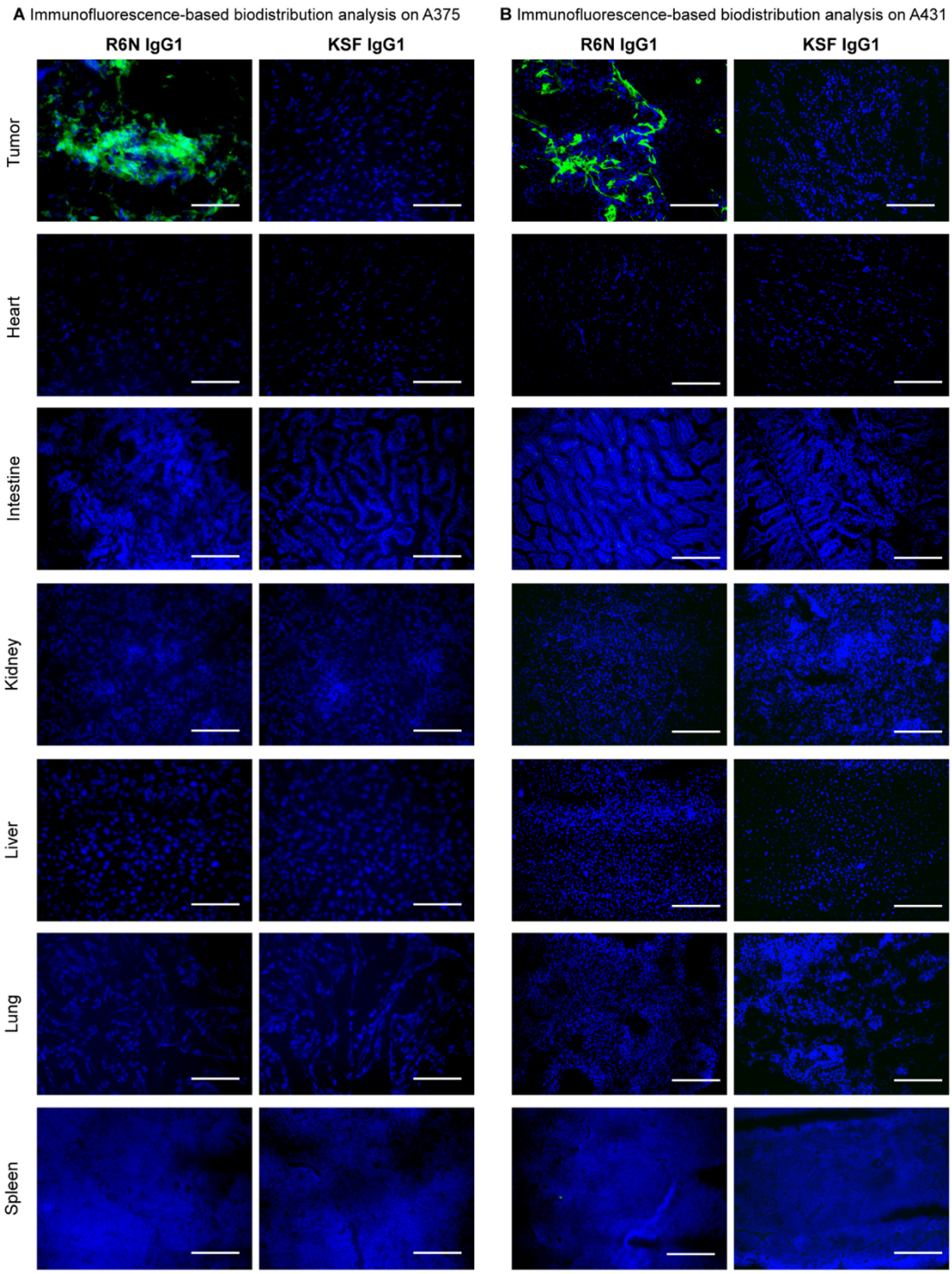

Figure 4.5: Immunofluorescence-based biodistribution analysis with R6N IgG1. Microscopic fluorescence analysis of tumor-targeting performance on A375 (a) and A431 (b) tumor and organs from BALB/c nude tumor-bearing mice. Two hundred micrograms of R6N IgG1 or KSF IgG1 (negative control) was injected intravenously into the lateral tail vein and mice were sacrificed 24 hours after injection, tumor and organs were excised and embedded in cryoembedding medium; cryostat sections were stained with Protein A (green, AlexaFluor 488) and DAPI (blue). Representative pictures of the samples were taken at 20x magnification, scale bars = 100 µM.

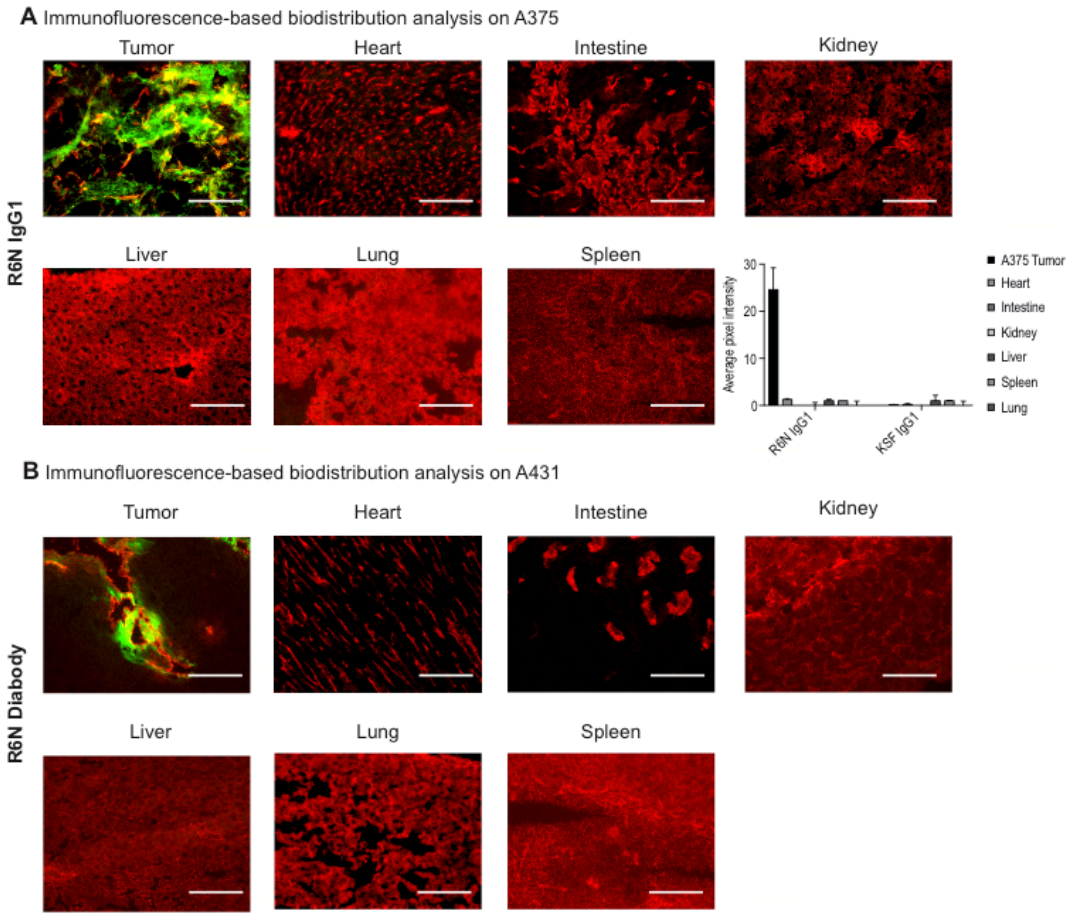

Figure 4.6. Immunofluorescence-based biodistribution analysis with R6N IgG1 and diabody

Microscopic fluorescence analysis of tumor targeting performance on A375 (**A**) and A431 (**B**) tumor and organs from BALB/c nude tumor bearing mice. 200 µg of R6N IgG1 or diabody were injected intravenously into the lateral tail vein and mice were sacrificed 24 hours after injection, tumor and organs were excised and embedded in cryoembedding medium; cryostat sections were stained with Protein A (green, AlexaFluor 488) and anti-CD31 (red, Alexa 594). Representative pictures of the samples were taken at 20x magnification, scale bars = 100 µM. Average pixel intensity was calculated using Image J software for A375 tumor and organs.

Generation of mIL12-R6N and tumor therapies

We first evaluated the potential antitumor activity of R6N in IgG2a and diabody formats in A375 tumor-bearing mice. Both formats without the cytokine were not able to induce any tumor growth retardation (**Supplementary Fig. S4.6 and S4.10**). **Figure 4.7** depicts the amino acid sequence and a schematic representation of mIL12-R6N in the format previously described[170]. The product was well-behaved in biochemical assays and mIL12 retained its biological activity as evidenced by an interferon (IFN)-γ release experiment (**Fig. 4.7 C**). *In vivo* therapy studies with mIL12-R6N revealed strong anti-cancer activity in immunodeficient mice, bearing SKRC52 renal cell carcinoma (**Fig. 4.7F**) and in immunocompetent mice bearing SMA-497 glioma model (**Fig. 4.7G**). Both in xenograft and orthotopic syngeneic cancer models, a sustained tumor growth retardation was observed, with a significant difference compared to the untargeted antibody mIL12-KSF (**Fig. 4.7C**). No significant change in body weight was detected during the therapy in SKRC52, indicating good tolerability of the fusion protein at the dose used (**Supplementary Fig. S4.12**).

Figure 5

a

mIL12 p40 – Linker – mIL12 p35 – Linker – R6N VH – Linker – R6N VL – Linker – R6N VH – Linker – R6N VL

MWELEKDVYVVEVDWTPDAPGETVNLTCDTPEEDDITWTSDQRHGVIGSGKTLTITVKE
FLDAGQYTCHKGGETLSHSHLLLHKKENGIWSTEILKNFKNKTFLKCEAPNYSGRFTCS
WLVQRNMDLKFNIKSSSSSPDSRAVTCGMASLSAEKVTLDQRDYEKYSVSCQEDVTCPT
AEETLPIELALEARQQNKYENYSTSFFIRDIIKPDPPKNLQMRPLKNSQVEVSWEYPDS
WSTPHSYFSLKFFVRIQRKKEKMKETEEGCNQKGAFLVERTSTEVQCKGGNVCVQAQDR
YYNSSCSKWACVPCRVRSGGGGSGGGGSGGGGSRVIPVSGPARCLSQSRNLLKTTDDMV
KTAREKLKHYSCTAEDIDHEDITRDQTSTLKTCLPLELHKNESCLATRETSSTTRGSCL
PPQKTSLMMTLCLGSIYEDLKMYQTEFQAINAALQNHNHQQIILDKGMLVAIDELMQSL
NHNGETLRQKPPVGEADPYRVKMKLCILLHAFSTRVVTINRVMGYLSSAGGGGSGGGGS
GGGGSEVQLLESGGGLVQPGGSLRLSCAASGFTFSQYSMSWVRQAPGKGLEWVSAISGS
GGSTYYADSVKGRFTISRDNSKNTLYLQMNSLRAEDTAVYYCAKGRRIFDYWGQGTLVT
VSSGGSGGSSELTQDPAVSVALGQTVRITCQGDSLRPTMASWYQQKPGQAPVLVIYGKN
NRPSGIPDRFSGSSSGNTASLTITGAQAEDEADYYCQSSRMDVPTVVFGGGTKLTVLGD
IGGGSGGGGSGGGGEVQLLESGGGLVQPGGSLRLSCAASGFTFSQYSMSWVRQAPGKGL
EWVSAISGSGGSTYYADSVKGRFTISRDNSKNTLYLQMNSLRAEDTAVYYCAKGRRIFD
YWGQGTLVTVSSGGSGGSSELTQDPAVSVALGQTVRITCQGDSLRPTMASWYQQKPGQA
PVLVIYGKNNRPSGIPDRFSGSSSGNTASLTITGAQAEDEADYYCQSSRMDVPTVVFGG
GTKLTVLG*

b

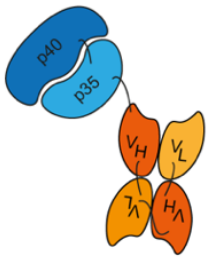

c

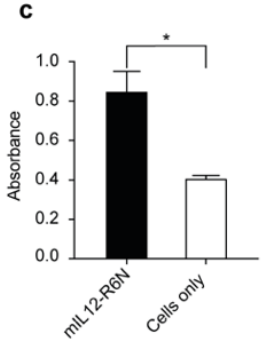

d

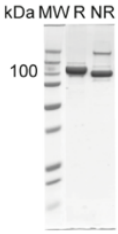

e

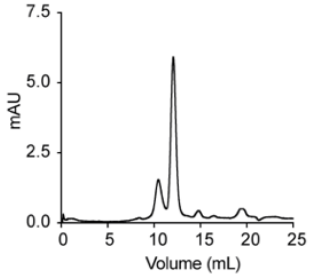

f

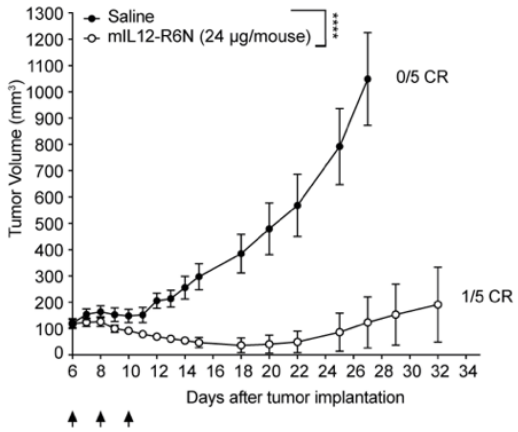

g

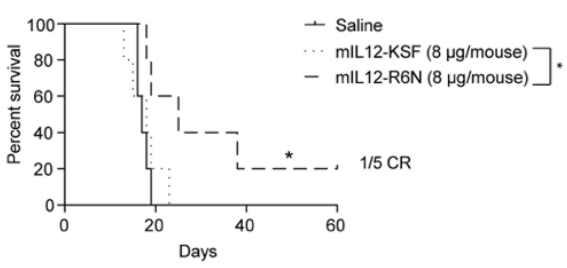

Figure 4.7: Therapy in BALB/c nude mice bearing SKRC52 human renal cell carcinoma and in VM/Dk mice bearing SMA-497 glioma. (a) Amino acid sequence of mIL12-R6N in tandem diabody format. Starting from the N-terminus: mIL12 and R6N in tandem diabody format; (b) Scheme of the heterodimeric murine IL12 fused to the R6N antibody in tandem diabody format; (c) IFN-γ induction assay by mIL12-R6N in BALB/c lymph nodes confirmed the activity of mIL12 at a concentration of 0.1 ng/mL. The experiment was done in triplicates; (d) SDS-PAGE, 10% gel in reducing (R) and non-reducing (NR) condition of purified mIL12-R6N; (e) Size-exclusion chromatogram, the major peak eluting at 12.16 mL corresponds to the molecular weight of monomeric fraction of mIL12-R6N. (f) Therapeutic performance of mIL12-R6N in BALB/c nude mice bearing SKRC52 human renal cell carcinoma. Data represent mean tumor volume Å} SEM, n = 5 mice per group; CR, complete response. Treatment started when tumors reached a volume of 100 mm3, mice were injected three times intravenously every 48 hours with 24 μg of either mIL12-R6N or PBS. (g) Therapeutic performance of mIL12-R6N and mIL12-KSF in VM/Dk mice bearing SMA-497 glioma. Mice were injected treated intravenously at days 5 and 10 after tumor implantation with 8 μg mIL12-R6N or 8 μg mIL12-KSF or PBS. Survival rate is presented as Kaplan–Meier plots, n = 5 mice per group.

4.5 Discussion

In this work we describe the generation, *in vitro* characterization, and *in vivo* targeting properties of a novel antibody specific to domain D of Tenascin C. L7D scFv was isolated by phage display technology from ETH-2 Gold library[284] and affinity matured *in vitro* by randomization of CDR1 loops of antibody heavy and light chains. The resulting antibody, R6N, featured an increased affinity for the target antigen (with a K_D value in the two digits nanomolar range). Unlike the F16 antibody, specific to the domain A1 of Tenascin C discovered by Brack and colleagues[229], R6N had the advantage of being cross-reactive due to the high sequence homology between the mouse and human antigen, as confirmed by SPR analysis (**Fig. 4.1 D-E**) and immunofluorescence studies (**Fig. 4.2**). Cross-reactivity for the mouse antigen facilitates the preclinical evaluation of the antibody's performance.

R6N was sub-cloned in three different formats, diabody, IgG1 and IgG2a, resulting in bivalent antibodies with improved molecular stability and increased avidity for the cognate antigen. R6N could be expressed in mammalian cells and purified to homogeneity with excellent yield regardless of the format chosen (i.e., scFv, diabody, IgG1 and IgG2a) (**Supplementary Fig. S4.6, S4.9 and S4.10**). Recombinant proteins manufacturing is a critical area in today's pharmaceutical industry[285]: efficient protein expression is essential for the scaling up process, which is required for industrial development.

The *in vivo* targeting performance of R6N was evaluated by immunofluorescence-based biodistribution analysis (**Fig. 4.5 and Fig. 4.6**), which showed a positive pattern of staining in the neoplastic region but not in healthy organs, reinforcing the fact that TNC is an attractive target for cancer immunotherapy.

A novel IL12-based immunocytokine was generated and its therapeutic efficacy was evaluated in immunodeficient SKRC52 tumor-bearing mice and in immunocompetent SMA-497 orthotopic syngeneic tumor-bearing mice (**Fig. 4.7**). A strong anti-cancer activity was observed in both tumor models, with an improvement of survival in mice treated with R6N antibody.

In a SMA-497 glioma model, the antibody-mediated delivery of mIL12 to the tumor mass clearly enhanced the therapeutic performance of this cytokine, compared to the irrelevant antibody mIL12-KSF (**Fig. 4.7G**). Glioblastoma remains one of the most challenging cancer, with still poor prognosis[286]. It is thus conceivable, that using a targeted approach with a fully human IL12-based product (**Supplementary Fig. S4.14**) may provide a benefit to certain groups of patients with malignant gliomas and glioblastomas.

The ability of mIL12-R6N to induce a tumor growth retardation was confirmed also in xenograft model SKRC52 in nude mice (**Fig. 4.7 F**). In an immunodeficient mice setting, NK cells stimulated by IL12 may play an important role in the tumor rejection process[150,282].

In conclusion, we developed an antibody selective for TNC-D with excellent targeting properties confirmed by immunofluorescence-based biodistribution staining. The novel mIL12-R6N fusion protein exhibited potent single agent activity, leading to tumor growth inhibition in treated mice. The data presented here provide a rationale for the clinical development of this human IL12-R6N fusion protein.

4.6 Supplementary information

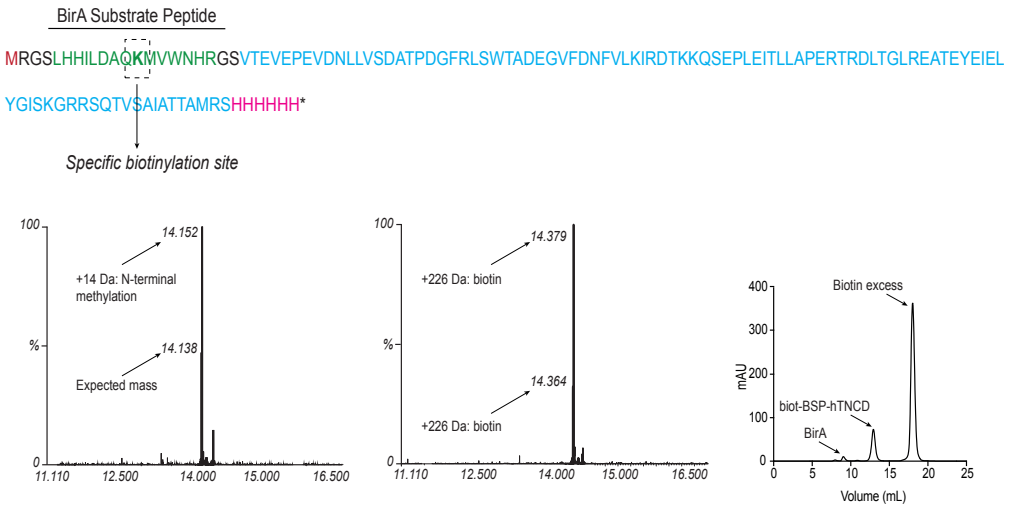

Figure S4.1. **BSP-hTNC-D sequence and biotinylation**

BSP-hTNC-D sequence: in green BSP tag sequence, in bold the lysine where the specific biotinylation was carried; in magenta HIS-tag sequence. Column 1. ESI-MS profile of BSP-hTNC-D non-biotinylated; Column 2. ESI-MS profile of specifically biotinylated BSP-hTNC-D; Column 3. Size exclusion chromatogram of BSP-hTNC-D after biotinylation.

EVQLLESGGGLVQPGGSLRLSCAASGFTFSGYAMSWVRQAPGKGLEWVS
AISGSGGSTYYADSVKGRFTISRDNSKNTLYLQMNSLRAEDTAVYYCAK
GRRIFDYWGQGTLVTVSSGGGGSGGGGSGGGGSSELTQDPAVSVALGQT
VRITCQGDSLRSYYASWYQQKPGQAPVLVIYGKNNRPSGIPDRFSGSSSG
NTASLTITGAQAEDEADYYCNSSRMDVPTVVFGGGTKLTVLG

Figure S4.2. **L7D scFv aminoacidic sequence**

Aminoacidic sequence of L7D scFv. In green, variable heavy chain sequence, in grey linker sequence, in orange variable light chain sequence. CDRs are underlined.

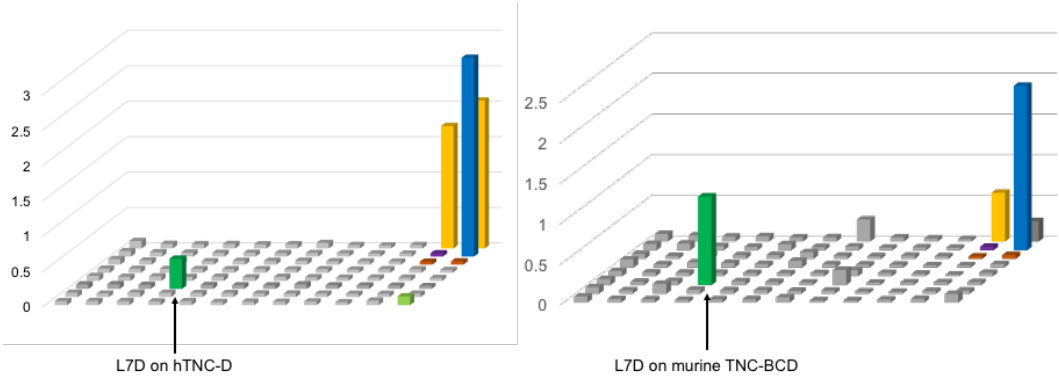

Figure S4.3. ELISA with induced supernatants of individual clones on human TNC-D and on murine TNC domains BCD

At the end of the first selections against TNC-D, ELISA with induced supernatants of individual clones was performed. In green, L7D scFv positive both on the human (left) and murine (right) TNC-D. In yellow, a positive control, in blue anti-HIS tag positive control, in purple PBS and in red 2xYT medium used as negative control.

EVQLLESGGGLVQPGGSLRLSCAASGFTFSQYSMSWVRQAPGKGLEWVS
AISGSGGSTYYADSVKGRFTISRDNSKNTLYLQMNSLRAEDTAVYYCAK
GRRIFDYWGQGTLVTVSSGGGGSGGGGSGGGGSSELTQDPAVSVALGQT
VRITCQGDSLRPTMASWYQQKPGQAPVLVIYGKNNRPSGIPDRFSGSSSG
NTASLTITGAQAEDEADYYCQSSRMDVPTVVFGGGTKLTVLG

Figure S4.4. **R6N scFv aminoacidic sequence**

Aminoacidic sequence of R6N scFv. In green, variable heavy chain sequence, in grey linker sequence, in orange variable light chain sequence. CDRs are underlined.

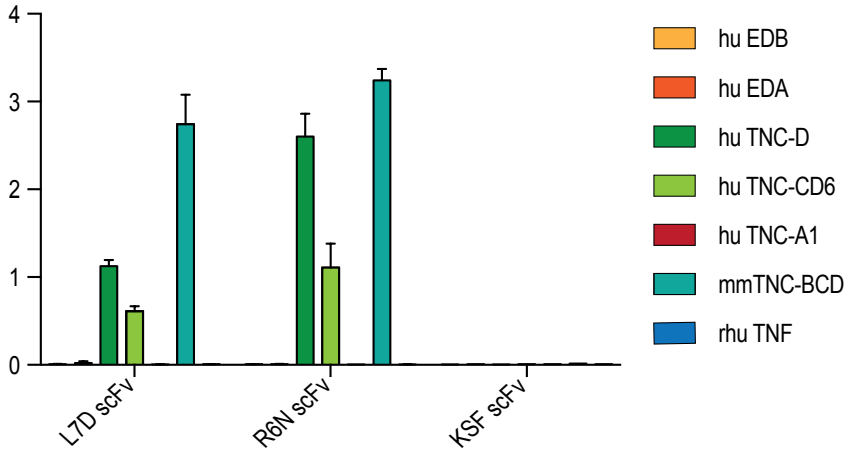

Figure S4.5. **Specificity ELISA of anti-hTNC-D antibodies L7D scFv and R6N scFv**

ELISA signals on different TNC fibronectin type 3 homology repeats showing that both antibodies recognize specifically the cognate antigen (hTNC-D, h-TNC-CD6 and mm-TNC-BCD). L7D and R6N did not bind to h-TNC-A1, fibronectin domains EDA and EDB and recombinant human TNF. KSF scFv, an antibody with irrelevant specificity, was used as negative control.

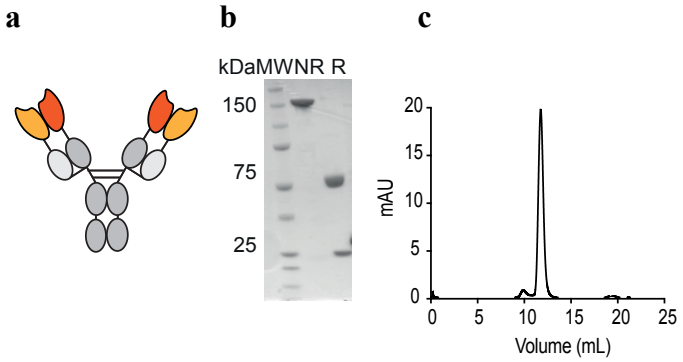

Figure S4.6. **Characterization of R6N in IgG2a format**

A. Scheme of R6N antibody in IgG2a format; **B**. SDS-page, 10% gel in reducing and non-reducing condition of purified R6N IgG2a; **C**. Size exclusion chromatogram, the major peak eluting at 11.83 mL corresponds to the molecular weight of IgG.

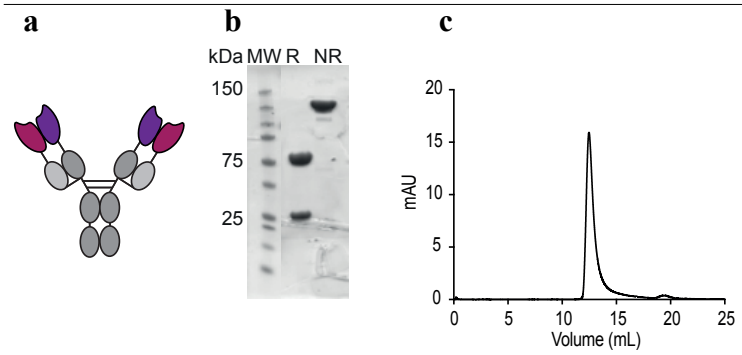

Figure S4.7. **Characterization of P12 in IgG1 format**

A. Scheme of P12 antibody in Ig1 format; **B**. SDS-page, 10% gel in reducing and non-reducing condition of purified R6N IgG1; **C**. Size exclusion chromatogram, the major peak eluting at 12.45 mL corresponds to the molecular weight of IgG.

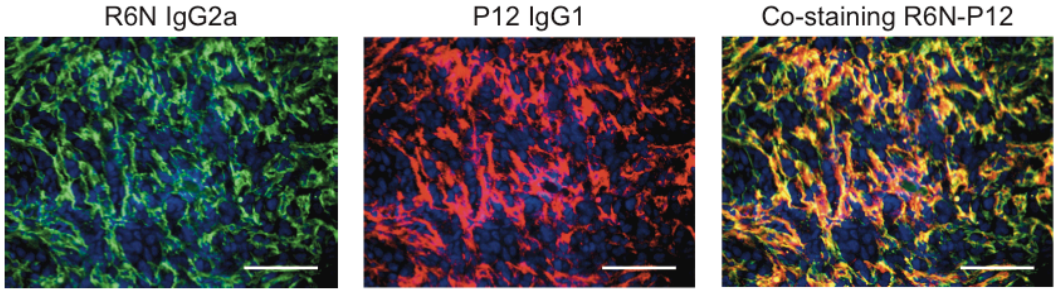

Figure S4.8. **R6N IgG2a and P12 IgG1 double fluorescence on SKRC52**

Microscopic fluorescence analysis of TNC-D on SKRC52 tumor section detected with R6N IgG2a (green, Alexa 488), P12 IgG1 (red, AlexaFluor 594), cell nuclei were counterstained with DAPI (blue). Representative pictures of the samples were taken at 20x magnification, scale bars = 100 µM.

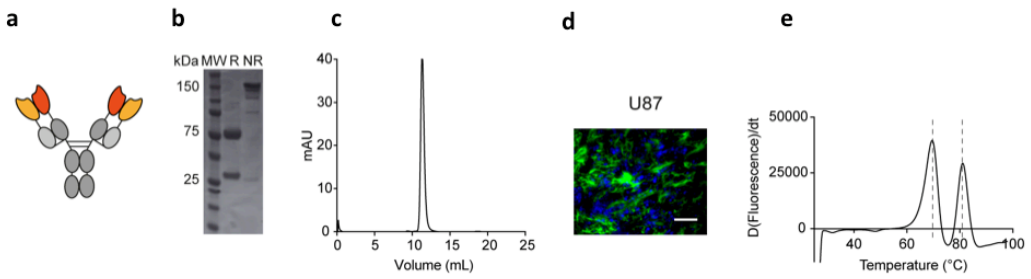

Figure S4.9. **Characterization of R6N in IgG1 format**

A. Scheme of R6N antibody in Ig1 format. **B**. SDS-page, 10% gel in reducing and non-reducing condition of purified R6N IgG1; **C**. Size exclusion chromatogram, the major peak eluting at 11.37 mL corresponds to the molecular weight of IgG1; **D**. Microscopic fluorescence analysis of TNC-D on U87 tumor section detected with R6N IgG1 (green, AlexaFluor 488), cell nuclei were counterstained with DAPI (blue), scale bars = 100 µM. **E**. Differential Scanning Fluorimetry on R6N IgG1: a double denaturation profile can be observed with a transition at 70.14°C and 81.69 °C.

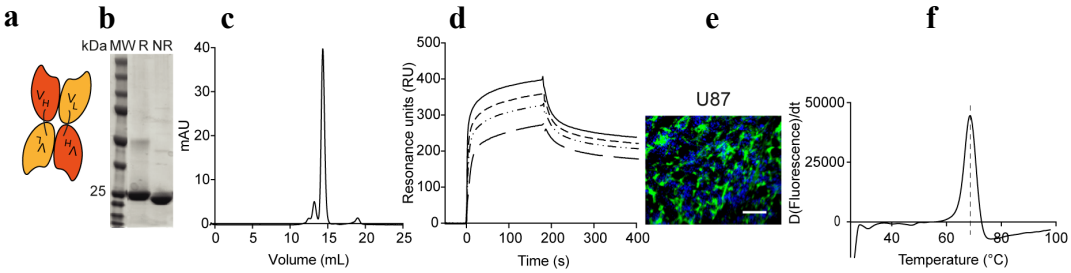

Figure S4.10. **Characterization of R6N in diabody format**

A. Scheme of R6N antibody in diabody format; **B**. SDS-page, 10% gel in reducing and non-reducing condition of purified R6N diabody; **C**. Size exclusion chromatogram, the major peak eluting at 14.67 mL corresponds to the molecular weight of monomeric fraction of R6N diabody; **D**. BIAcore sensograms of R6N diabody on hTNC-D coated CM5 chip: R6N diabody was tested at 4 different concentrations (1000, 500, 250, 125 nM); **E**. Microscopic fluorescence analysis of TNC-D on U87 tumor section detected with R6N diabody (green, AlexaFluor 488), cell nuclei were counterstained with DAPI (blue), scale bars = 100 µM. **F**. Differential Scanning Fluorimetry on R6N diabody: a single peak denaturation profile can be observed with a transition at 69.27°C.

A Quantitative biodistribution in U87

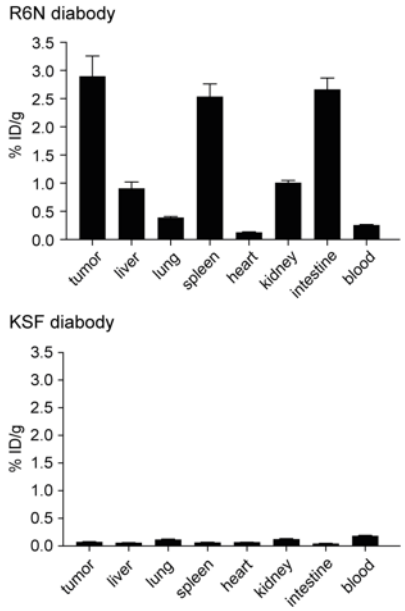

	R6N Db	KSF Db
Tumor:blood	11.075	0.391
Tumor:liver	3.193	1.268
Tumor:lung	7.446	0.624
Tumor:spleen	1.142	1.207
Tumor:heart	22.600	1.154
Tumor:kidney	2.873	0.592
Tumor:intestine	1.089	1.765

B Quantitative biodistribution in A431

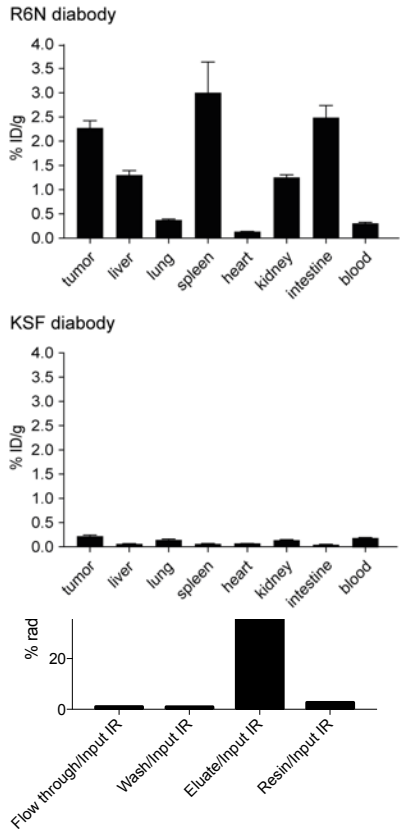

	R6N Db	KSF Db
Tumor:blood	7.154	1.116385
Tumor:liver	1.745	3.494864
Tumor:lung	6.086	1.530668
Tumor:spleen	0.758	3.510922
Tumor:heart	16.877	3.14508
Tumor:kidney	1.811	8.076394
Tumor:intestine	0.914	5.143005

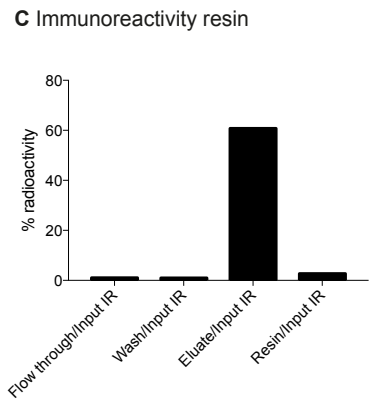

Figure S4.11. Tumor targeting properties of R6N diabody

Quantitative biodistribution analysis of radioiodinated R6N diabody and KSF diabody (negative control) in BALB/c nude mice bearing U87 glioblastoma tumor (**A**) or A431 epidermoid carcinoma (**B**). 8 to 14 µg of radioiodinated diabody were injected intravenously into the lateral tail vein and mice were sacrificed 24 hours after injection, organs were excised, weighed and the radioactivity of organs and tumors was measured. Results are expressed as percentage of injected dose per gram of tissue (%ID/g ± SEM; n = 4-5). Tables shows tumor:organs ratio of R6N and KSF. **C**. Immunoreactivity test performed on TNC-D CNBr-sepharose resin as quality control for the radiolabeling process of R6N antibody for biodistribution quantitative analysis.

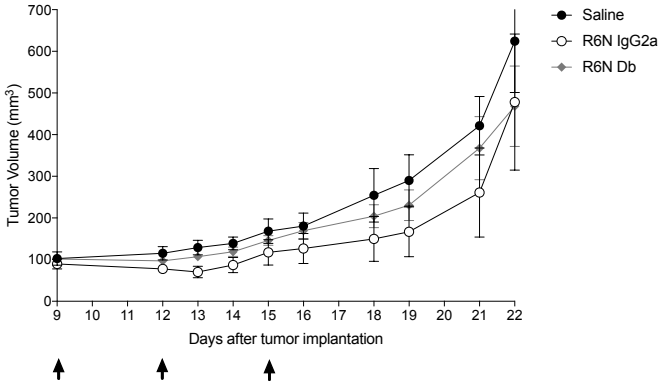

Figure S4.12. **Therapy in BALB/c nude mice bearing A375 human renal cell carcinoma**

Therapeutic performance of R6N in IgG2a and Diabody format in BALB/c nude mice bearing A375 malignant melanoma. Data represent mean tumor volume ± SEM, n=5 mice per group. Treatment started when tumors reached a volume of 100 mm^3, mice were injected three times intravenously every 72 hours with 100 µg of either R6N IgG2a, Diabody or PBS.

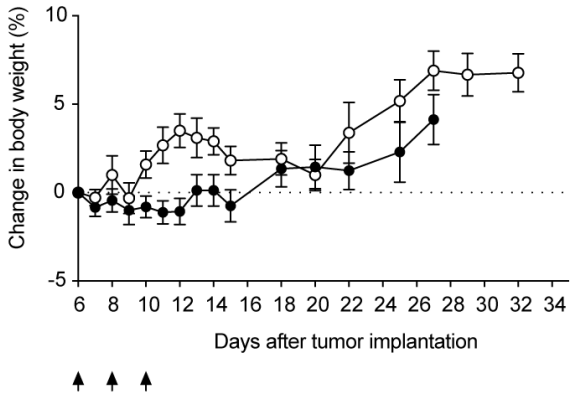

Figure S4.13. Body weight changes of mice treated with IL12-R6N in SKRC52 tumor bearing mice

Body weight changes of mice treated with mIL12-R6N and saline respectively. (Statistic at day 27: $^{****}P < 0.0001$).

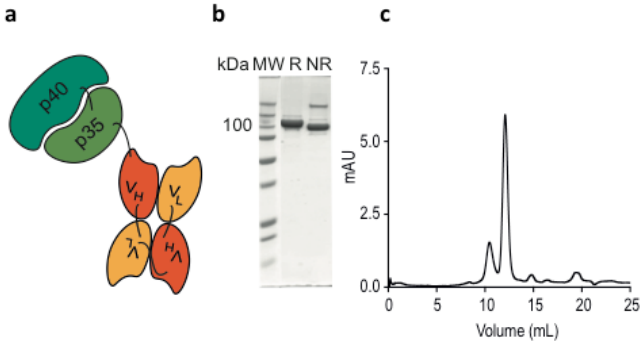

Figure S4.14. Characterization of fusion protein IL12-R6N

A. Scheme of the heterodimeric human IL12 fused to the R6N antibody in tandem diabody format; **B**. SDS-page, 10% gel in reducing and non-reducing condition of purified IL12-R6N; **C**. Size exclusion chromatogram, the major peak eluting at 12.16 mL corresponds to the molecular weight of monomeric fraction of IL12-R6N.

5. Generation and in vivo characterization of immunocytokines based on a novel anti-human FAP monoclonal antibody

This chapter is based on the manuscript in preparation "Generation and in vivo characterization of immunocytokines based on a novel anti-human FAP monoclonal antibody". The paper is the result of the work of several scientists. My research contribution was represented by the isolation by phage display, *in vitro* and *in vivo* characterization and cloning of different formats of the monoclonal antibodies described in the article and on the generation of the stable cell line expressing human FAP (CT26-hFAP). F. Peissert, A. Elsayed, C. Rondinini, R. Corbellari, and J. Millul helped in the execution of the experiments. Dr. D. Neri and Dr. R. De Luca supervised the experiments.

Phage display technology allows the generation of antibodies specific for targets of interest. 7NP2 is a novel monoclonal antibody that has been selected by phage display against the Fibroblast Activation Protein, tumor stroma-associated antigen. The antibody targeting properties were evaluated by *ex-vivo* immunofluorescence based biodistribution analysis: the molecule showed selective accumulation at the tumor site sparing healthy organs. Two immunocytokines have been generated using 7NP2 as building block, IL2-7NP2-TNF^{mut} and IL12-7NP2. Both fusion proteins induced tumor growth retardation and remission when tested in therapy experiments in tumor bearing mice. Favorable pharmacokinetics studies in monkeys revealed a slow clearance of 7NP2 in IgG1 format. Preclinical results provide a rational for future clinical development of 7NP2 antibody.

Lisa Nadal[1,2], Frederik Peissert[2,3], Abdullah Elsayed[1,4], Chiara Rondinini[5], Riccardo Corbellari[1,3], Jacopo Millul[3], Cornelia Halin[4], Dario Neri[5] and Roberto De Luca[3*]

[1] University of Trento, Italy, CiBIO (Department of Cellular, Computational and Integrative Biology), Povo (Trento), Italy
[2] University School for Advanced Studies IUSS Pavia, Pavia, Italy
[3] Philochem AG, Libernstrasse 3, 8112 Otelfingen, Switzerland
[4] Department of Chemistry and Applied Biosciences, Swiss Federal Institute of Technology (ETH Zürich), Zurich, Switzerland
[5] Philogen Spa, Piazza La Lizza 7, 53100 Siena, Italy

*** Corresponding author**

Roberto De Luca

Philochem AG, Philogen Group, Libernstrasse 3, CH-8112 Otelfingen (Switzerland)

Telephone: +41-43-5448819

Fax: +41-43-5448809

e-mail: roberto.deluca@philogen.com

5.1 Abstract

In this study, we describe the generation of a novel fully human monoclonal antibody (named "7NP2") targeting human Fibroblast Activation Protein (FAP), an antigen expressed in the microenvironment of different types of solid neoplasms. 7NP2 was isolated from a synthetic antibody phage display library and was improved by one round of mutagenesis-based affinity maturation. The tumor recognition properties of the antibody were validated by immunofluorescence procedures performed on a commercial tissue microarray as well as on freshly frozen colon cancer biopsies from human patients. An *ex vivo* biodistribution analysis in mice confirmed the ability of the 7NP2 antibody in IgG1 format to selectively localize to solid tumors while sparing healthy organs. Encouraged by these results, two antibody cytokine fusions (IL2-7NP2-TNF^{mut} and mIL12-7NP2) based on the 7NP2 were generated and characterized *in vitro* and *in vivo*, showing a potent anti-tumor activity in immunocompetent and immunodeficient mouse models of cancer. Favorable pharmacokinetic results obtained with IgG1(7NP2) in *Cynomolgus Monkey* provided a rationale for future clinical translation activities using 7NP2 based products.

5.2 Introduction

Over the last decades, the relevance of the tumor microenvironment (TME) in cancer progression has been extensively studies[287]. Cancers are complex diseases, in which malignant cells interact with structures of various nature with the ultimate goal of generating an environment that facilitate their proliferation[288]. On one hand, tumor stroma holds essential functions fostering tumor growth. On the other hand, that same environment typically produces unique antigens that can be exploited for pharmacodelivery applications[204].

One of the major components of the TME (which represents approximately 20–40% of the total tumor mass) are "activated" fibroblasts or cancer associated fibroblasts (CAFs). The latter usually develop a modified phenotype that resembles the fibroblasts involved in wound healing during carcinogenesis[289,290]. CAFs play a key role in cancer progression such as stimulating cancer cells proliferation, angiogenesis, and promoting the production of immunosuppressive cytokines[291,292]. A promising candidate to target CAFs is Fibroblast Activation Protein (FAP), discovered in 1986 using a murine monoclonal antibody called F19[243]. Subsequent studies revealed that FAP can be produced not only by CAFs, but also by other cellular components of the tumor stroma (e.g., endothelial cells) and by cancer cells (e.g., melanoma, malignant breast, colorectal, skin, prostate and pancreatic cancers, bone and soft sarcomas)[242,243,251,293–296]. FAP expression is also correlated with other pathological conditions that are associated with an activated stroma, including rheumatoid arthritis, pulmonary fibrosis and cirrhosis[295].

From a structural point of view, FAP is a 170 kDa homodimeric type II transmembrane glycoprotein, belonging to the family of post-proline dipeptidyl aminopeptidase. FAP can be found in the majority of malignant solid tumors, while being absent in most healthy tissues, rendering it an attractive target for both imaging and therapeutic applications. Secreted FAP can be found in blood circulation as result of cell-surface FAP shedding at invadopodia[250,297]. The exact mechanisms leading this process are still unknown, but it might be useful to understand why circulating FAP levels were inversely proportional to levels of tumor-associated FAP in some solid tumors[248,298].

The antigen has been described as the "next billion-dollar nuclear theranostics target", as more than 28 different tumor types have successfully been imaged in patients with radiolabeled FAP ligands (e.g., FAPI-04, FAPI-46)[248,249].

Several recombinant immunoglobulins targeting FAP have been developed over the last decades. F19 was the first antibody able to target human FAP (hFAP). Immunohistochemistry studies revealed that the F19 antibody could strongly stain pancreatic, breast, ovarian and colorectal cancers[243,250,293]. A radiolabeled preparation of the humanized version of F19, Sibrotuzumab, was used to image metastatic cancer patients of different origins. However, the slow clearance of the intact immunoglobulin from the bloodstream impaired the development of the product as imaging agent. In a phase II clinical trial, focused on the treatment of metastatic colorectal cancer patients, the antibody was found to be well tolerated but showed no therapeutic activity[299]. Fisher and coworkers described in 2012 the generation of two novel FAP-specific antibodies, termed ESC11 and ESC14. In preclinical experiments, radiolabeled preparation of the ESC11 antibody (i.e., ESC11-^{177}Lu) showed preferential accumulation in human melanoma xenografts and induced tumor growth retardation[251].

A number of therapeutic proteins directed against FAP, with promising preclinical results, have recently been generated and moved to clinical trials. A bispecific antibody which simultaneously recognizes FAP on tumor cells and 4-1BBL on lymphocytes was described by Claus and coworkers and induced long-term cancer remissions in mouse tumor models. The product is currently being investigated in a Phase I clinical trial[252]. Klein and coworkers developed a novel fusion protein consisting of an anti-hFAP antibody fused to an interleukin-2 variant (IL2v)[253]. MP0310 (NCT04049903) and MP0317 are two early-stage clinical products, based on the DARPin® platform, that combine tumor-restricted FAP binding with 4-1BB and CD40 agonistic ligands, respectively[254].

Monoclonal antibodies targeting TME antigens have been considered for the delivery of bioactive payloads, such as proinflammatory cytokines[31,140]. Antibody-cytokine fusions (also called immunocytokines) may exploit the tumor-homing properties of the antibody moiety, in order to concentrate the cytokine payload at

the site of disease and enhance the therapeutic index[119,140]. Proinflammatory cytokines, such as interleukin-2 (IL2), tumor necrosis factor (TNF) and interleukin-12 (IL12), have been extensively studied in oncology[25,300,301]. IL2 is a key modulator of Natural Killer (NK) cells and T lymphocytes activity[176]. TNF helps fight cancer by inducing a selective hemorrhagic necrosis in neoplastic mass and by boosting inflammation[302]. IL12 strongly promotes NK cells, CD4+ and CD8+ T cells to produce interferon-gamma (IFN-γ), one of the most relevant mediators of anti-cancer immunity[153,156].

In this work, we describe the generation of a novel anti-FAP immunoglobulin, called 7NP2. The antibody successfully targeted FAP-positive tumors in vivo and served as building block for the development of two immunocytokines products (IL2-7NP2-TNF^{mut} and mIL12-7NP2). IL2-7NP2-TNF^{mut} was generated by combining the IL2 and TNF moieties into a single polypeptide as previously described[195,303]. The second product, mIL12-7NP2, was produced by fusing murine IL12 to the N-terminus of 7NP2 in tandem diabody format, as this strategy had recently shown to be effective for the selective delivery of IL12 to the tumor environment[282].

5.3 Materials and Methods

Cell lines

The human renal cell carcinoma SKRC52 cell line was kindly provided by Professor E. Oosterwijk (Radbound University Nijmegen Medical Center, Nijmegen, the Netherlands). SKRC52-hFAP cells were prepared as previously reported[255]. CHO cells and murine colon carcinoma CT26, CTLL2, L-M fibroblasts were obtained from the ATCC. Cell lines were received between 2018 and 2020, expanded, and stored as cryopreserved aliquots in liquid nitrogen. Cells were grown according to the supplier's protocol and kept in culture for no longer than 14 passages. Authentication of the cell lines also including checks of post-freeze viability, growth properties, and morphology test for mycoplasma contamination, isoenzyme assay, and sterility test were performed by the cell bank before shipment.

Cloning, expression, biotinylation and biochemical characterization of human FAP

Extracellular domain of human FAP (ECD hFAP) was cloned into the mammalian cell expression vector pcDNA3.1(+) (Invitrogen) using NheI/NotI restriction sites. The protein was expressed by transient gene expression in CHO-S cells and purified to homogeneity via Ni-NTA agarose resin (Roche) chromatography. Purified human FAP was dialyzed into HEPES buffer (100 mM NaCl, 50 mM HEPES, pH 7.4). The quality of the proteins was assessed by SDS-PAGE and by Size-exclusion chromatography on a Superdex 200 Increase 10/300 GL column on an ÄKTA FPLC (GE Healthcare). Purified human ECD hFAP recombinant fragment was randomly biotinylated with *N*-Hydroxysuccinimide (NHS) ester-activated biotins (Sigma). The biotin-labelling reaction was carried with an 80X molar excess of NHS-biotin on Hula Shaker for 1h at room temperature. The reaction was then quenched with Tris-HCl (pH:7.4), the biotin-labelled protein loaded on pre-equilibrated PD10 column (GE Healthcare) and dialyzed into HEPES buffer (100 mM NaCl, 50 mM HEPES, pH 7.4) overnight at 4°C.

In vitro protein characterization

The fusion proteins described in this work were produced through transient gene expression (TGE) in CHO-S cells and purified from the cell culture medium by

protein A Sepharose (Sino Biological) affinity chromatography, dialyzed against phosphate-buffered saline (PBS) and stored in PBS at -80°C[280]. Purified proteins were analyzed by size-exclusion chromatography using a Superdex 75 increase or 200 increase 10/300 GL column on an ÄKTA FPLC (GE Healthcare, Amersham Biosciences). SDS-PAGE was performed with 10% gels under reducing and non-reducing condition. Affinity measurements were performed by SPR using BIAcoreX100 instrument (BIAcore AB, Uppsala, Sweden) on ECD hFAP coated SA chip.

Selections of antibodies from a phage display library

Human monoclonal antibody C5 specific to hFAP was isolated by two rounds of biopanning from a phage library following the protocol described by Viti et al.[67,89]. Briefly, biotinylated ECD-hFAP (final concentration 120 pM) was incubated with 60 μL of streptavidin-coated magnetic beads (Invitrogen, M-280); coated dynabeads were subsequently incubated with preblocked 10^{12} transforming units of phage antibodies. Beads were washed with 0.1% Tween 20 in HEPES buffer (100 mM NaCl, 50 mM HEPES, pH 7.4) and subsequently with HEPES buffer. Bound phage was eluted with triethylamine (Sigma). Isolated phage was then amplified in *E. coli* TG-1 using VCS-M13 Interference-Resistant Helper Phage (Agilent, Santa Clara, CA) and precipitated from culture supernatant using a solution of 20% polyethylene glycol /2.5 M NaCl. Two rounds of panning were performed against the target antigen. The supernatants of induced monoclonal selected clones TG-1 cultures expressing scFv antibody fragment were screened by ELISA on hFAP and bound antibodies were detected by 9E10 IgG followed by anti-mouse IgG – HRP conjugate as described by Viti et al.[67].

Affinity maturation of scFv C5

The scFv(C5) affinity maturation library was constructed in a phagemid vector by introducing sequence variability in the CDR2 loops of both heavy and light chain using degenerated primers as described by Brack et al.[229]. The ligation product was electroporated into *E. coli* TG-1 cells; phage was rescued by superinfection with helper phage VCS-M13. The obtained library had a size of 1×10^{8} (theoretical variability of 6.4×10^{7}). The library was subjected to one round of panning following the same protocol used for the parental antibody selection. The resulting best clone

7NP2 and the parental C5 were subcloned into the mammalian expression vector pcDNA 3.1 (+) by NheI/HindIII restriction sites, produced and characterized as described.

Cloning, expression and purification of 7NP2 in IgG1, C5 in IgG1 and IgG2a format

C5 IgG1, IgG2a and 7NP2 IgG1 cloning started from the cloning of the light chain of the immunoglobulin into suitable vector by SpeI/BsiWI restriction sites. Cloning procedures continued with C5/7NP2 IgG1/IgG2a heavy chain cloning using HindIII and XhoI as restriction sites. The same cloning strategy was used to design KSF IgG1 and IgG2a. C5 IgG1, IgG2a and 7NP2 IgG1 format were expressed using TGE in CHO-S cells, purified and characterized *in vitro* as described.

Epitope ELISA

The FAP binding epitope of C5 and 7NP2 antibody was evaluated by ELISA. Biotinylated hFAP was coated on Streptawells (Roche) at a concentration of 100 nM. C5 in IgG2a format and 7NP2 in IgG1 format were co-incubated for 1 h and detected with either anti-human HRP or anti-mouse HRP conjugates. C5 in IgG2a format was also co-incubated with F5 IgG1 (WO2016116399), ESC11 IgG1 [12] and KSF IgG1 (specific to hen egg lysozyme, used as negative control) respectively.

Flow Cytometry analysis

SKRC52-hFAP cells were detached from culture plates using Accutase (Millipore), counted and suspended to a final concentration of 1×10^6 cells/mL in FACS buffer (0.5% BSA, 2mM EDTA in PBS) [37]. Cells were stained with C5, 7NP2 and KSF in IgG1 format and Protein A AlexaFluor488 (Thermo Fisher, P11047). Cells were analyzed on a CytoFLEX cytometer (Beckman Coulter). The raw data were processed with the FlowJo 10.4 software. Similar experiment has been conducted with CT26-hFAP and CT26 WT cell lines to evaluate hFAP expression during the generation of the stable cell line.

Cloning, expression and purification of IL2-7NP2-TNF^{mut}

The fusion protein IL2-7NP2-TNF^{mut} contains the antibody 7NP2 fused to a mutated version of human TNF (arginine to alanine mutation in the amino acid position 108 of the human TNF gene, corresponding to the position 32 in the soluble form) at the C-terminus by a 15-amino acid linker and to human IL2 at the N-terminus by a 12-amino acid linker.

The gene encoding for the 7NP2 antibody and the gene encoding human TNF and human IL2 were PCR amplified, assembled and cloned into the mammalian expression vector pcDNA3.1(+) (Invitrogen) by a NheI/NotI restriction sites as described previously[304].

Cloning, expression and purification of mIL12-7NP2 and IL12-7NP2

The fusion protein mIL12-7NP2 contains the 7NP2 antibody in homodimeric tandem scFv arrangement fused to murine IL12 at N-terminus. The gene encoding for 7NP2 in diabody format and the gene encoding for the murine IL12 or human IL12 were PCR amplified, PCR assembled and cloned into pcDNA 3.1 (+) by NheI/HindIII restriction sites. The two fusion proteins were expressed using TGE in CHO-S cells, purified and characterized *in vitro* as described.

In vitro biological activities

The biological activity of TNF was determined by incubation with mouse L-M fibroblasts, in the presence of 2 μg/mL actinomycin D (Sigma-Aldrich). In 96-well plates, cells (20,000 per well) were incubated in medium supplemented with actinomycin D and varying concentrations of recombinant human TNF or IL2-7NP2-TNF^{mut}. After 24 h at 37°C, cell viability was determined with Cell Titer Aqueous One Solution (Promega). Results were expressed as the percentage of cell viability compared to cells treated with actinomycin D only. The biological activity of IL2 was determined by its ability to stimulate the proliferation of CTLL2 cells. Cells (25,000 per well) were seeded in 96-well plates in the culture medium supplemented with varying concentrations of the fusion proteins. After incubation at 37°C for 72 h, cell proliferation was determined with Cell Titer Aqueous One Solution (Promega). Results were expressed as the percentage of cell viability compared to untreated cells. The biological activity of mIL12-7NP2 was evaluated by an IFN-γ release assay on splenocytes as described by Puca et al.[282].

Immunofluorescence studies

Antigen expression was confirmed on ice-cold acetone–fixed 10-μm cryostat sections of SKRC5-hFAP, slides from a human tissue microarray (AmbsBio, B712100) and patient-derived colon samples CC3, 4 6, 7, 8, 11, 13 and 16 stained with C5, 7NP2 and KSF IgG1-FITC (protein was FITC labelled according to manufacturer protocol; Sigma) (final concentration 10 μg/mL) and detected with rabbit anti-FITC (Bio-Rad, 4510-7804) and anti-rabbit AlexaFluor488 (Invitrogen; A11008). Cell nuclei were stained with DAPI (Invitrogen; D1306). For the immunofluorescence-based biodistribution analysis, mice were injected with 100 μg/mouse of C5 IgG1-FITC, KSF IgG1-FITC and 7NP2 IgG1-FITC when tumor size reached 100-250 mm^3 and sacrificed 24 hours after injection. Tumors were excised and embedded in cryo-embedding medium (Thermo Fisher) and cryostat sections (10 μm) were stained and detected with rabbit anti-FITC and anti-rabbit AlexaFluor488. Slides were mounted with fluorescent mounting medium (Dako) and analyzed with Leika DMI6000B (Leica Microsystems).

Confocal microscopy analysis

SKRC52-hFAP were seeded into 4-well cover slip chamber plates (Sarstedt) at a density of 10^4 cells per well in RPMI medium (1 mL, Invitrogen) supplemented with 10% FCS, AA and HEPES (10 mM) and allowed to grow for 24 hours under standard culture conditions. Hoechst 33342 nuclear dye (Invitrogen) was used to stain nuclear structures. The culture medium was replaced with fresh medium containing 7NP2 IgG1-FITC and KSF IgG1-FITC at a concentration of 10 μg/mL. Randomly selected colonies imaged 1 hour after incubation on a SP8 confocal microscope equipped with an AOBS device (Leica Microsystems).

Transduction of transmembrane human FAP in CT26 cells

Development of stable cell lines expressing FAP was performed as previously described[305,306]. Briefly, CT26 cells were seeded at a density of 1 million cells in a 24 well-plate using RPMI-1640. Next day, 10 μL of the virus aliquot and polybrene (Santa Cruz Biotechnology) to the final concentration of 8 μg/mL were added to the cells. The plate was then centrifuged at 1,000 x g for 90 minutes at 32 °C to enhance the cellular uptake of the virus. In the following day, the media was changed, and cells were kept growing and expanding for three weeks according to

the general cell culture procedures. Finally, positive cells were sorted at the flow cytometry facility (BD FACS Aria III) using 7NP2 IgG1-FITC.

Animal Study design

The immunofluorescence-based biodistribution analysis were performed with 4 BALB/c nude mice bearing SKRC52 renal cell carcinoma transduced with hFAP. One control group (mice injected with KSF IgG1) was used for the experiment. The therapy with IL2-7NP2-TNF^{mut} was performed with 15 BALB/c nude mice bearing SKRC52-hFAP renal cell carcinoma; one control group with mice injected with saline was used during the experiment. The therapy with mIL12-7NP2 was performed with 15 BALB/c nude mice bearing SKRC52-hFAP renal cell carcinoma. Mice were randomized into groups according to their tumor volume; tumor volume measurements were taken by the same experimenter to minimize any subjective bias. The second therapy performed with mIL12-7NP2 was conducted with 10 BALB/c mice bearing CT26-hFAP colon carcinoma.

Experimental animals

A total of 35 female BALB/c nude mice and 10 BALB/c mice, aged 8 weeks with an average weight of 20 g, were used in this work. Mice were purchased from Janvier (Route du Genest, 53940 Le Genest-Saint-Isle, France) and raised in a pathogen-free environment with a relative humidity of 40-60%, at a temperature between 18 and 26°C and with daily cycles of 12 hours light/darkness according to guidelines (GV-SOLAS; FELASA). The animals were kept in a specific pathogen free (OHB) animal facility in cages of maximum 5 mice, left for one-week acclimatization upon arrival, and subsequently handled under sterile BL2 workbenches. Specialized personnel were responsible for their feeding; food and water were provided *ad libitum*. Mice were monitored daily (in the morning) in weight, tumor load, appearance (coat, posture, eyes and mouth moisture) and behavior (movements, attentiveness and social behavior). Euthanasia criteria adopted were body weight loss > 15% and/or ulceration of the subcutaneous tumor and/or tumor diameter > 1500 mm and/or mice pain and discomfort. Mice were euthanized in CO_2 chambers.

Ethical statement

Mouse experiments were performed under a project license (license number 04/2018) granted by the Veterinäramt des Kantons Zürich, Switzerland, in compliance with the Swiss Animal Protection Act (TSchG) and the Swiss Animal Protection Ordinance (TSchV).

Tumor model and therapy studies

6×10^6 SKRC52-hFAP cells were implanted subcutaneously in the flank of BALB/c nude mice with 0.5 ml 29G insulin syringes (MicroFine™+, BD medical). Mice were monitored daily; tumor volume was measured with a caliper and volume was calculated using the formula: tumor size = (Length[mm]*Width^2[mm])/2. When tumors reached a suitable volume (approx. 100 mm^3), mice were injected three times into the lateral tail vein with the pharmacological agents. IL2-7NP2-TNF^{mut} and IL2-KSF-TNF^{mut} were dissolved in PBS (pH: 7.4) and administered at a dose of 30 μg/mouse every 48 hours for four times. A saline group was included as control. mIL12-7NP2 and mIL12-KSF were dissolved in PBS (pH:7.4) and administered at a dose of 8 μg/mouse every 48 hours for three times.

5×10^6 CT26-hFAP cells were implanted subcutaneously in the flank of BALB/c mice. When tumors reached a suitable volume (approx. 100 mm^3), mice were injected into the lateral tail vein with the pharmacological agents. mIL12-7NP2 was dissolved in PBS (pH:7.4) and administered at a dose of 10 μg/mouse every 48 hours for three times.

Non-human Primate Study

The non-human primate study was performed in accordance with the Directive 2010/63/UE of the European parliament and of the council of 22 September 2010 for the protection of animals used for scientific purposes. 1 female *Cynomolgus Monkey*, ~2 years old at the time of allocation and estimated to weigh between 2.59 and 2.66 kg was used in this study. 7NP2 IgG1 was administered slow bolus in peripheral veins (radial vein), using disposable needles and graduated plastic syringes, at a dose volume of 1 mL/kg body weight (which corresponds to 0.1 mg/kg of protein). The dose was administered to the animal on the basis of the body weight measured on the day of administration. Blood samples of ~0.6 mL each were collected from the saphenous or cephalic vein (alternatively from other blood

vessels) of all animals at approximately the following 7 time points: before dosing and at 2, 10, 20 and 30min and 1, 2, and 4 h after treatment. Blood samples were allowed to clot in tubes for maximum 60 minutes at room temperature then spun down by centrifugation (10 minutes 2300 g, +4°C). For each serum sample, 2 aliquots of 100 µL were collected in labeled secondary tubes and stored in a freezer at -80°C.

Pharmacokinetics Analysis

Fusion protein concentrations in serum were assessed by ELISA. Briefly, 100 nM of hFAP were coated on 96 well plates overnight at 4°C. After a blocking step, serum samples were incubated for 1 h and detected with anti-human IgG (Fc specific) – Peroxidase antibody (Sigma A0170).

5.4 Results

Isolation and characterization of antibodies specific to human FAP

Monoclonal antibodies specific to the extracellular domain of human FAP (hFAP) were isolated from the synthetic human scFv library by phage display technology[64]. A recombinant preparation hFAP was biotinylated and used as antigen for antibody phage display selections, using previously described procedures[229] (**Supplementary Fig. S5.1**). After two rounds of panning, the clone C5 (**Fig. 5.1A)** was chosen for future development, based on its strong enzyme-linked immunosorbent assay (ELISA) signal. C5 in scFv format was expressed in Chinese hamster ovary (CHO) cells and purified to homogeneity (**Supplementary Fig. S5.2**). The binding characteristics of scFv(C5) were studied by surface plasmon resonance (SPR) using a monomeric antibody fraction recovered from gel-filtration. SPR analysis on hFAP coated chip revealed a K_D value of 130 nM. (**Fig. 1A**). The C5 antibody was also shown by FACS and immunofluorescence to bind to SKRC52 renal cell carcinoma transduced with hFAP (SKRC52-hFAP) (**Fig. 5.1A**). The C5 antibody bound only to hFAP and not to other irrelevant antigens. (**Supplementary Fig. S5.3A**).

Affinity maturation of the C5 antibody

The binding affinity of the C5 antibody was further improved using a previously described methodology (**Fig. 5.1B**)[64]. Residues 52, 53, 54 and 57 of the complementarity-determining region 2 (CDR2) loop of the variable domain of the antibody heavy chain and residues 51, 54 and 56 of the CDR2 of the light chain were combinatorially mutated and the resulting library was submitted to hFAP selection. The best clone isolated from this affinity maturation strategy was 7NP2 (**Fig. 5.1C, Supplementary Fig. S5.4**). SPR analysis on hFAP coated chip showed an improvement in binding properties, with a K_D value of 10.4 nM, as measured with a monomeric scFv preparation (**Fig. 5.1C**). Both C5 and 7NP2 antibodies gave strong ELISA signals (**Supplementary Fig. S5.3B**). The cross-reactivity for the mouse, canine, ovine, porcine and cyno antigens was evaluated by ELISA for both C5 and 7NP2 in IgG1 format (**Supplementary Fig. S5.3C-D, S5.5, S5.6**). A set of ELISA experiments was also performed with pairs of anti-FAP antibodies (WO2016116399, [251]), in order to better characterize the epitope recognized by

7NP2. The antibody bound to a different epitope, compared to the previously described F5 and ESC11 antibodies (**Fig. 5.2**).

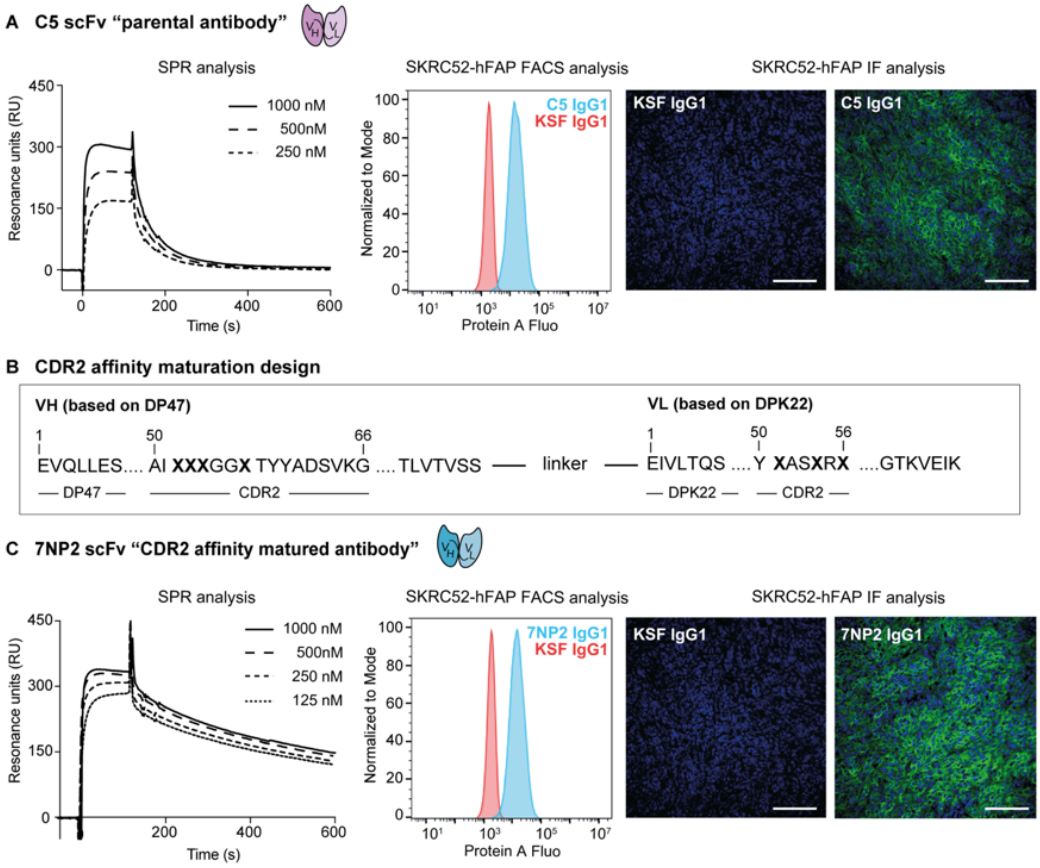

Figure 5.1. Characterization of antibodies against human FAP.

A. Characterization of scFv(C5) selected from synthetic phage display library: BIAcore sensograms of monomeric scFvs on hFAP coated SA chip; FACS analysis on SKRC52-hFAP cells with C5 in IgG1 format (Protein A Fluorescence); Microscopic fluorescence analysis on SKRC52-hFAP section detected with IgG1(C5)-FITC (green, AlexaFluor 488), cell nuclei were counterstained with DAPI (blue). Representative pictures of the samples were taken 20x magnification, scale bars = 100 μm.

B. Schematic representation of scFv(C5) CDR2 affinity maturation design of the phage library.

C. Characterization of scFv(7NP2) from CDR2 affinity matured library of C5: BIAcore sensograms of monomeric scFvs on hFAP coated SA chip; FACS analysis on SKRC52-hFAP cells with 7NP2 in IgG1 format (Protein A Fluorescence); Microscopic fluorescence analysis on SKRC52-hFAP section detected with IgG1(7NP2)-FITC (green, AlexaFluor 488), cell nuclei were counterstained with DAPI (blue). Representative pictures of the samples were taken 20x magnification, scale bars = 100 μm.

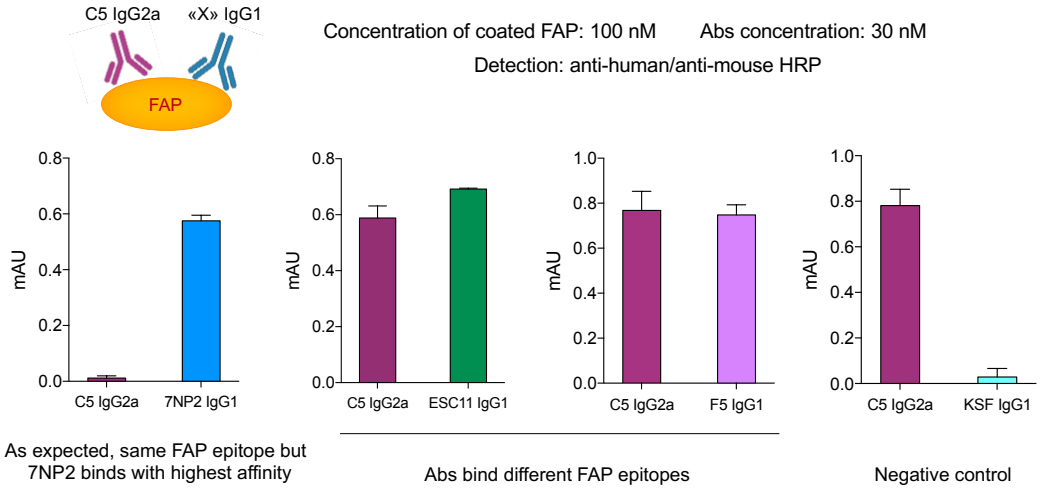

Figure 5.2. FAP binding epitope ELISA

ELISA signals of different antibodies on hFAP. The C5 antibody in IgG2a format was incubated together with the 7NP2 antibody in IgG1 format, the F5 antibody in IgG1 format (WO2016/116399), the ESC11 antibody in IgG1 format (Fisher *et al*., (2012) Clin Cancer Res; 18(22)), or the (negative control) antibody KSF in IgG1 format for 1.5 h at room temperature at a concentration of 30 nM in the antigen-coated wells. After 3 washes with PBS, binding of the antibodies to human FAP was detected using anti-human or anti-murine HRP conjugates.

Immunofluorescence analysis on human colon tissue sections

7NP2 in IgG1 (**Supplementary Fig. S5.6**) format was studied by immunofluorescence analysis on tissue sections. The protein was labelled with fluorescein isothiocyanate (FITC) and used to stain healthy and malignant tissue from a commercial tissue microarray and from patients (**Fig. 5.3**). 7NP2 exhibited an intense staining in colon carcinoma, liver hepatocellular carcinoma, ovary carcinoma and uterus adenocarcinoma but not in healthy tissue, confirming the capability of the antibody to recognize hFAP *in vitro* (**Fig. 5.3A**). After these initial positive results, additional colon tumor specimens were stained, confirming the ability of 7NP2 to recognize colon carcinomas (**Fig. 5.3B**). Confocal analysis on SKRC52-hFAP cells showed no internalization of 7NP2 in IgG1, as for the negative control KSF IgG1 (**Supplementary Fig. S5.6**).

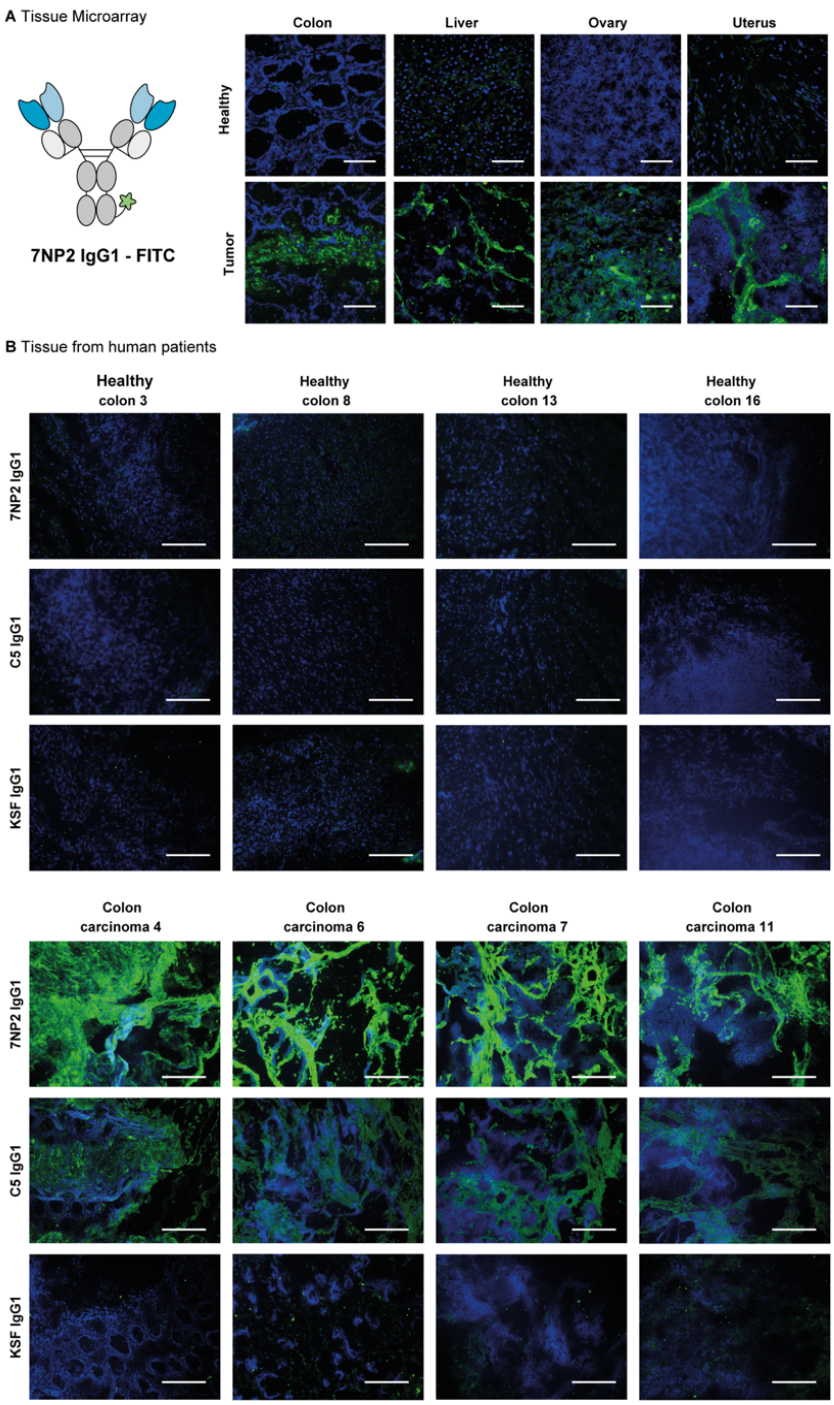

Figure 5.3. Microscopic fluorescence analysis of hFAP expression on tissue human micro array and colon healthy and malignant samples from donors with IgG1(7NP2)-FITC and IgG1(C5)-FITC.

A. Microscopic fluorescence analysis of human FAP expression on tissue microarray detected with IgG1(7NP2)-FITC.

B. Microscopic fluorescence analysis of human FAP expression on healthy and malignant colon samples from donors detected with IgG1(7NP2)-FITC, IgG1(C5)-FITC and IgG1(KSF)-FITC (negative control). Cryosections were stained with anti-FITC (green, AlexaFluor 488); cell nuclei were stained with DAPI (blue). 20x magnification, scale bars = 100 μm.

Immunofluorescence analysis of the tumor homing properties of 7NP2

The *in vivo* tumor-targeting performance of the C5 and 7NP2 antibodies in IgG format was studied by injecting FITC-labelled preparations of these immunoglobulins and of the anti-lysozyme KSF antibody used as negative control, followed by an ex vivo immunofluorescence detection procedure. Tissue sections of SKRC52-hFAP tumors and normal organs, obtained 24h after intravenous administration, revealed a selective accumulation of both C5 and 7NP2 into the tumor mass (**Fig. 5.4 and Supplementary Fig. S5.8**). Targeting selectivity was also confirmed in mice bearing two tumors, one expressing hFAP (SKRC52-hFAP) and the other one devoid of the target antigen (wild-type SKRC52) (**Supplementary Fig. S5.8**).

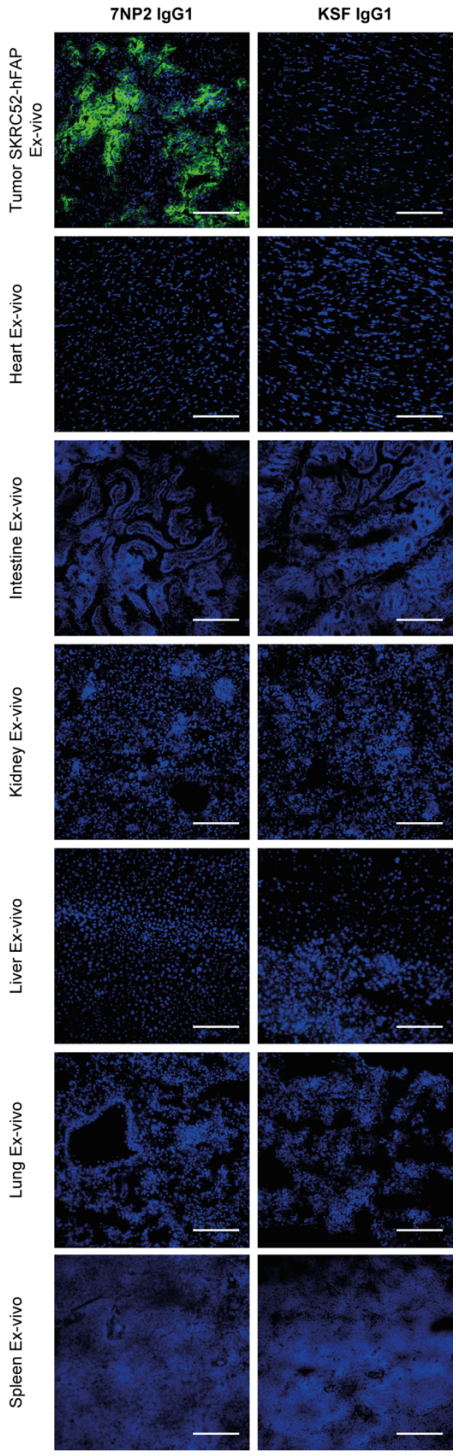

Figure 5.4. *Ex-vivo* immunofluorescence-based biodistribution analysis with IgG1(7NP2)-FITC.

Microscopic fluorescence analysis of tumor-targeting performance on SKRC52-hFAP tumor and organs from BALB/c nude tumor bearing mice. One hundred micrograms of IgG1(7NP2)-FITC or IgG1(KSF)-FITC (negative control) were injected intravenously into the lateral tail vein. The mice were sacrificed 24 hours after the injection, and the tumor and healthy organs harvested for Immunofluorescence analysis. The cryostat sections were stained with anti-FITC (green, AlexaFluor 488) and DAPI (blue). Representative pictures of the samples were taken at 20x magnification, scale bars = 100 μm.

Therapy experiments

The 7NP2 antibody was used as building block for the preparation of antibody cytokine fusion proteins, according to formats which had previously shown anti-cancer activity for other tumor antigens[282,303]. Specifically, the IL2-7NP2-TNF^{mut} and the mIL12-7NP2 fusion proteins were generated. **Figure 5.5A** shows a schematic representation of the IL2-7NP2-TNF^{mut} domain structure[303]. The fusion protein presents a single amino acid substitution in the TNF moiety to de-potentiate the molecule and achieve similar cytokine activity for IL2 and TNF moieties. The product could be purified to homogeneity (**Supplementary Fig. S5.9**). An *in vivo* therapy study, performed by administering 30 μg of protein, revealed a strong anti-cancer activity against SKRC52-hFAP renal cell carcinoma in immunodeficient mice, which was substantially better than the one of a fusion protein with identical format (IL2-KSF-TNF^{mut}), directed against hen-egg lysozyme (**Fig. 5.5B-D**). No notable change in body weight was detected during the therapy experiment, indicating that the fusion protein was well tolerated at the dose used (**Supplementary Fig. S5.10).**

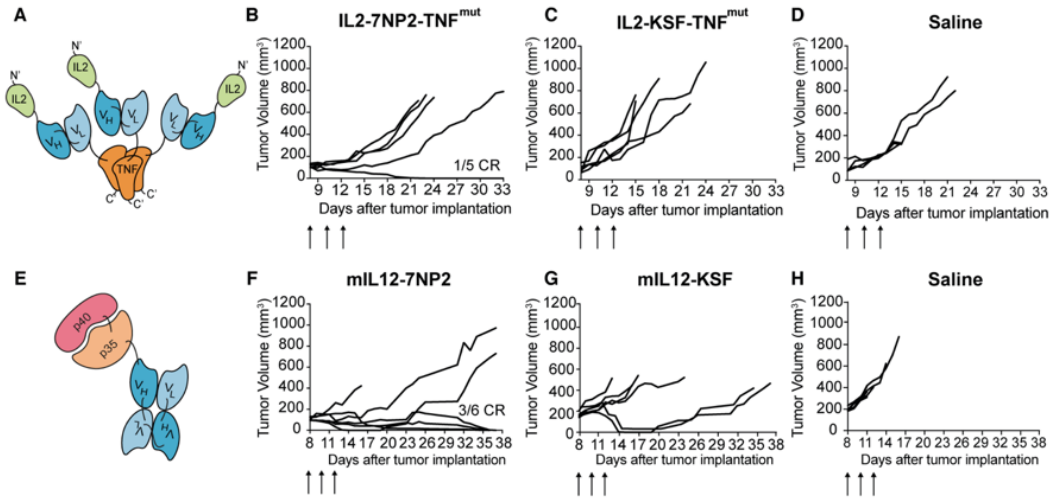

Figure 5.5. Animal experiments in SKRC52-hFAP tumor bearing mice

A. Schematic representation of IL2-7NP2-TNF^{mut}. B, C, D. Therapeutic performance of IL2-7NP2-TNF^{mut} (B) in BALB/c nude mice bearing SKRC52-hFAP human renal cell carcinoma. Data represent tumor volume, n = 5 mice per group; CR, complete response. Treatment started when tumors reached a volume of 100 mm^3, mice were injected three times intravenously every 48 hours with 30 μg of either IL2-7NP2-TNF^{mut} (B), IL2-KSF-TNF^{mut} (C) or saline (D). E. Schematic representation of mIL12-7NP2. F, G, H. Therapeutic performance of mIL12-7NP2 (F) in BALB/c nude mice bearing SKRC52-hFAP human renal cell carcinoma. Data represent mean tumor volume ± SEM, n = 6 mice per group CR, complete response. Once the tumors reached a volume of 100 mm^{3,} the mice were injected three times intravenously every 48 hours with 8 μg of either mIL12-7NP2 (F), mIL12-KSF (G) or saline (H).

The second immunocytokine product (mIL12-7NP2) was produced and purified to homogeneity (**Fig. 5.5E, Supplementary Fig. S5.11**). The motivation for generating the novel fusion protein came from the encouraging results of mIL12-L19, which had previously been reported and which had triggered clinical trials with hIL12-L19 (Eudract number 2019-000613-36/ NCT04471987) (**Supplementary Fig. S5.11**, **Fig. 5.5E-H**). mIL12-7NP2 induced tumor remission in three out of six nude mice, bearing SKRC52-hFAP tumors, without apparent evidence of toxicity (**Fig. 5.5E, Supplementary Fig. S5.12**). In order to test the activity of mIL12-7NP2 in an immunocompetent mouse model, additional therapy studies were performed in BALB/c mice bearing CT26 tumors, stably transfected with hFAP (**Fig. 5.6A-B**). Also in this setting, mIL12-7NP2 showed a strong anti-tumor activity and was able to induce two complete responses in a proportion of treated mice (**Fig. 5.6C-D, Supplementary Fig. S5.13**).

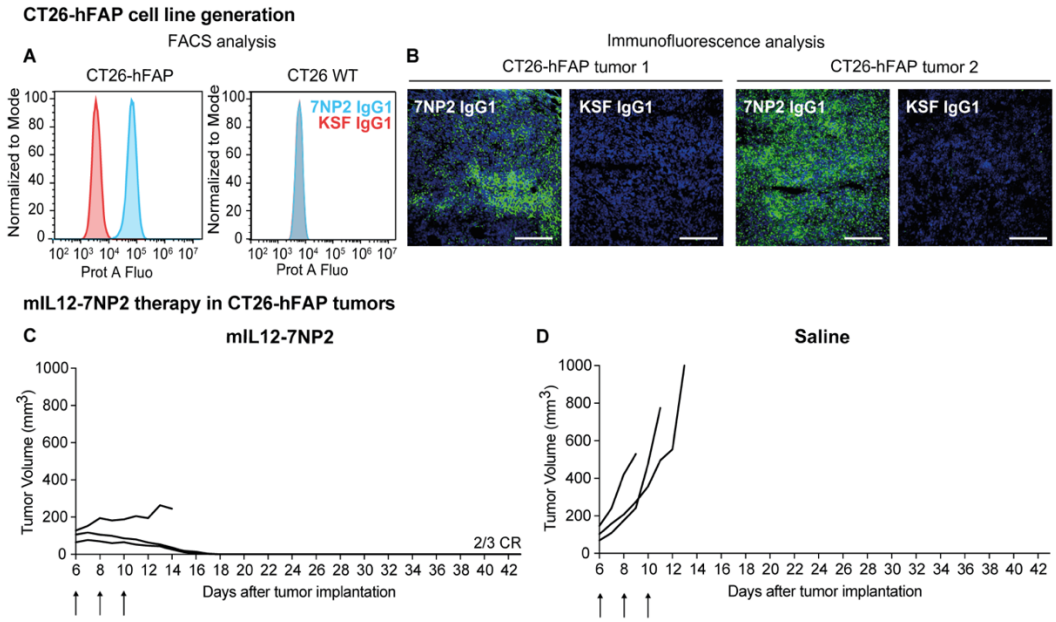

Figure 5.6. CT26-hFAP stable cell line generation and therapeutic performance of mIL12-7NP2.

CT26-hFAP stable cell line generation. A. FACS analysis on CT26-hFAP and CT26 WT with 7NP2 IgG1-FITC and KSF IgG1-FITC. B. Immunofluorescence analysis on CT26-hFAP tissue slides from different tumors grown in BALB/c mice. C, D. Therapeutic performance of mIL12-7NP2 in BALB/c mice bearing CT26-hFAP colon carcinoma. Data represent tumor volume, n = 3 mice per group; CR, complete response. Treatment started when tumors reached a volume of 100 mm^3, mice were injected three times intravenously every 48 hours with 10 μg of either mIL12-7NP2 (C) or saline (D).

Pharmacokinetics studies in Cynomolgus Monkey

Pharmacokinetics (PK) studies in *Cynomolgus Monkey* were conducted with 7NP2 in IgG1 format, in order to check whether the product had the expected circulatory half-life (**Fig 5.7**). Figure **5.7** depicts the concentration of the recombinant immunoglobulin in logarithmic scale as a function of the time, up to 240 minutes. IgG1(7NP2) showed no sink effects at early time points and a slow clearance from bloodstream as expected for IgG1 antibodies.

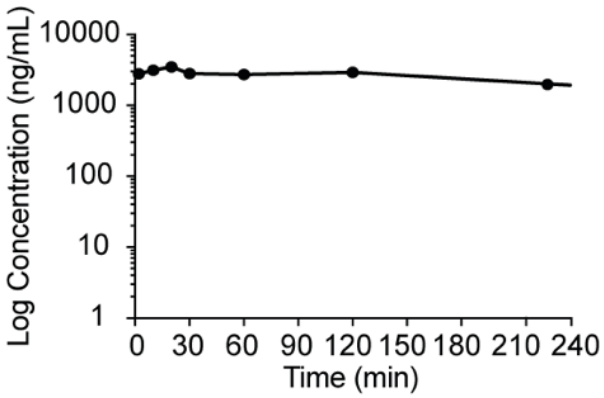

Figure 5.7. Pharmacokinetics in *Cynomolgus* monkeys.

Pharmacokinetics were evaluated in one cynomolgus monkey injected once at the dose of 0.1 mg/kg of IgG1(7NP2). Blood samples were collected before dosing and at 2, 10, 20 and 30 min and 1, 2, and 4 h after treatment.

5.5 Discussion

In this work, we described the *in vitro* and *in vivo* properties of a novel FAP-specific antibody called 7NP2. The recombinant immunoglobulin was isolated by phage display technology from an affinity matured library generated by combinatorial mutagenesis of the parental antibody's scFv(C5) CDR2 loops[64].

The affinity of the 7NP2 antibody (K_D = 10 nM) was improved by more than ten-fold compared to the parental antibody C5 (K_D = 130 nM) (**Fig. 5.1**). The specificity of C5 for hFAP was assessed by ELISA on different antigens (domains A1 and D of Tenascin C, domains EDA and EDB of Fibronectin, Prostate Specific Membrane Antigen, Carbonic Anhydrase II, Prolactin Receptor I and PD-1). In subsequent *in vitro* investigations 7NP2 and C5 were found to be cross-reactive with the murine, canine, ovine, porcine and cyno isoforms of FAP, facilitating translational activities and paving the way to veterinarian applications (**Supplementary Fig. S5.3**).
The binding properties of the 7NP2 antibody were extensively studied *in vitro* on human solid tumors. The protein efficiently bound to the membrane-bound form of hFAP, both in FACS and in immunofluorescence analyses on SKRC52-hFAP tumors (**Fig 5.1**). 7NP2 showed a diffuse stromal staining when tested on commercial tissue microarray of various solid malignancies, as well as on human colon cancer biopsies (**Fig. 5.2A and B**).

The *in vivo* targeting performance of the parental IgG1(C5) antibody was evaluated in mice bearing simultaneously SKRC52-wild type (hFAP-negative; implanted in the right flank) and SKRC52-hFAP (left flank). The antibody could be detected in the hFAP-expressing tumor, while neither FAP-negative lesion nor healthy tissues were found to be C5-postive. The IgG1(KSF) immunoglobulin was used as negative control of the experiment (**Fig. Supplementary Fig. S5.8**). Similar results have been obtained with the affinity matured IgG1(7NP2) antibody injected in SKRC52-hFAP tumor bearing mice, confirming the ability of the immunoglobulin to concentrate into antigen-positive lesions (**Fig. 5.4**).
The 7NP2 antibody could be expressed and purified to homogeneity with excellent yield as naked immunoglobulin (in the scFv and the IgG1 formats) and antibody-cytokine fusion (i.e., IL2-7NP2-TNF^{mut}, mIL12-7NP2 and hIL12-7NP2).

We have here described the production of two novel immunocytokines based on the 7NP2 antibody. IL2-7NP2-TNF^{mut} showed significantly stronger anti-tumor activity in tumor xenografts expressing hFAP (SKRC52-hFAP), compared to the non-targeted product based on the KSF antibody (**Fig. 5.5**). Our group has extensively showed that tumor targeted TNF- and IL2-based products act synergistically in fighting cancer[303]. TNF kills tumor cells though a variety of mechanisms that include the induction of a rapid tumor necrosis, direct killing of tumor cell expressing the TNF Receptor 1 (TNFR1) and by stimulating anti-cancer immunity[307]. Huyghe et al. showed that the anti-cancer properties of TNF are strongly dependent on the expression of TNFR1 on endothelial cells. Transgenic mice expressing TNFR1 on cancer cells, but not on endothelial cells, did not benefit from TNF-based therapeutics. Conversely, animals with TNFR1-expressing blood vessels and tumor-negative TNFR1 responded as well as wild type rodents[308]. This observation entails that the tumor necrosis is mainly mediated by an indirect insult on cancer-associated endothelial cells rather than by the direct interaction of the TNF payload with its cognate receptor on the surface of neoplastic cells. On the other hand, when delivered at the site of disease, IL2 boosts cancer-specific T and NK cells which selectively kill residual living malignant cells[176]. In this study, we showed that NK cells may be sufficient in eradicating cancer, as demonstrated by *in vivo* tumor therapy experiments performed in immunodeficient mice (i.e., which lack of B and T cells). The cytokine activity of a second fusion protein generated (mIL12-7NP2), based on murine IL12, was evaluated in a therapy experiment in mice bearing renal cell carcinomas expressing hFAP. mIL12-7NP2 induced a strong anti-cancer activity, leading to long term cancer eradications in a substantial number of the treated mice (**Fig. 5.5**).

In order to evaluate the activity of cytokine-based therapeutics in an immunocompetent setting, we genetically engineered CT26 colon carcinomas to stably express with hFAP. (**Fig. 5.6**). mIL12-7NP2 was well tolerated at a dose of 10 μg and led to a strong tumor growth retardation (**Fig. 5.6, Supplementary Fig. S5.13**). As previously reported by our group, the targeted delivery of mIL12 to the tumor microenvironment increases the infiltrate of tumor-specific lymphocytes as compared to the control group[282,309].

Pharmacokinetics studies in *Cynomolgus Monkey* were conducted in order to evaluate the circulatory half-life of the IgG1(7NP2) showing slow clearance from bloodstream as expected for IgG1 antibodies (**Fig. 5.7**).

In conclusion, the 7NP2 antibody represents a promising building block for generating immunocytokines with potent anti-tumor properties. The favorable pharmacokinetic profile of the naked immunoglobulin provides a rational for future translation activities of these products.

5.6 Supplementary information

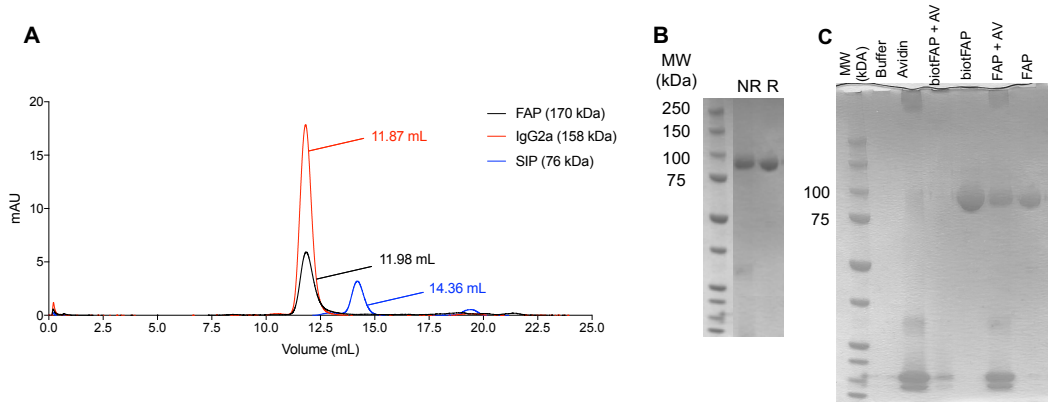

Figure S5.1. hFAP antigen characterization and biotinylation.

A. Size exclusion chromatogram of hFAP; B. SDS-page, 10% gel in non-reducing (NR) and reducing (R) condition of purified hFAP; C. Bandshift assay SDS-page, 10% gel in non-reducing condition.

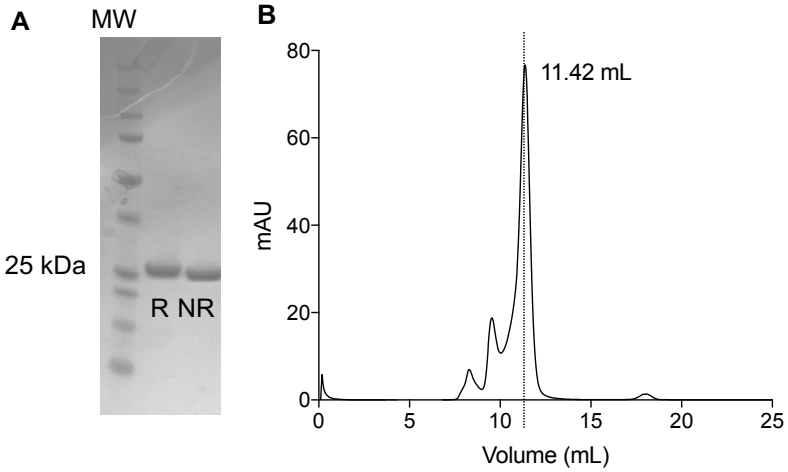

C

EVQLLESGGGLVQPGGSLRLSCAASGFTFSSYAMSWVRQAPGKGLEWVSAIDGSGGSTYYAD
SVKGRFTISRDNSKNTLYLQMNSLRAEDTAVYYCAKRLAWFDYWGQGTLVTVSSGGGGSGG
GGSGGGGGEIVLTQSPGTLSLSPGERATLSCRASQSVSSSYLAWYQQKPGQAPRLLIYGASSRAT
GIPDRFSGSGSGTDFTLTISRLEPEDFAVYYCQQSGKGPLTFGQGTKVEIK

Figure S5.2. scFv(C5) aminoacidic sequence and characterization.

A. SDS-page, 10% gel in reducing (R) and non-reducing (NR) condition of purified scFv(C5); B. Size exclusion chromatogram of scFv(C5). C. Aminoacidic sequence of scFv(C5).

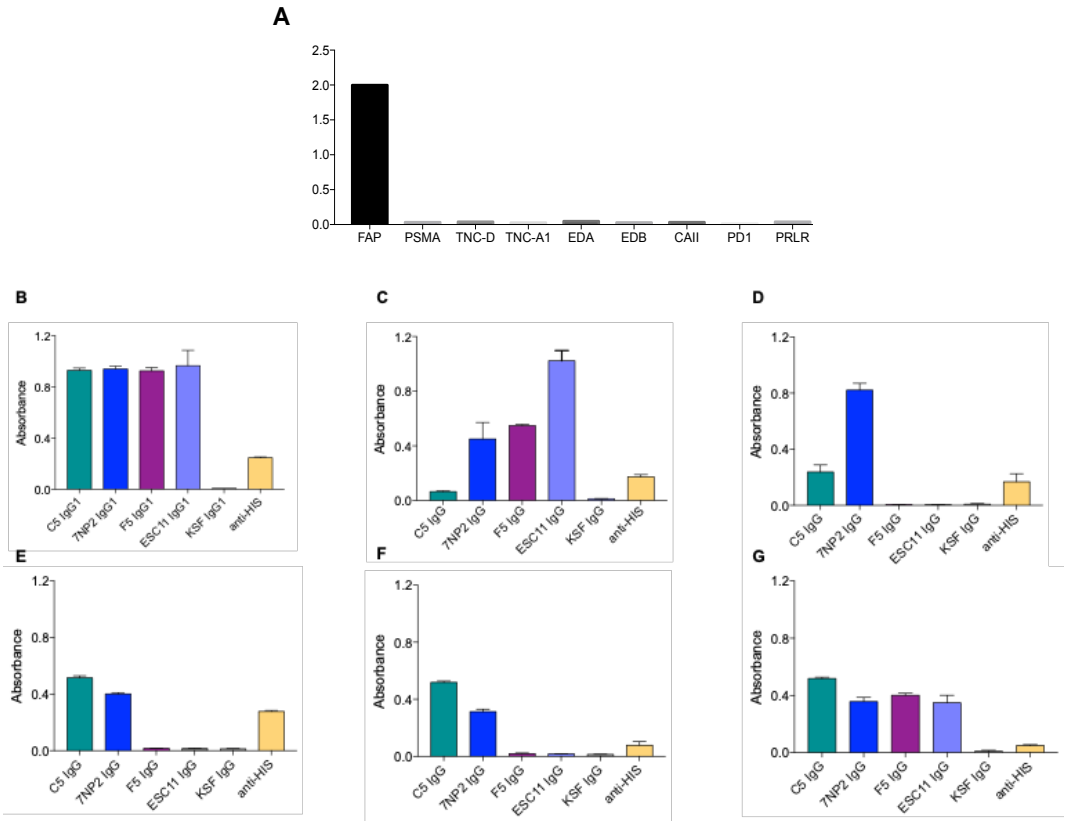

Figure S5.3. C5 antibody specificity ELISA; huFAP, muFAP, caFAP, ovFAP, porFAP and cynoFAP cross-reactivity ELISA.

A. ELISA signals on different antigens (hFAP, PSMA, TNC-D, TNC-A1, Fibronectin domain A and B (EDA and EDB), Carbonic Anhydrase II (CAII), PD1 and Prolactin Receptor (PRLR). scFv(C5) binds only to hFAP.

B. ELISA signals of different anti-FAP antibodies on coated hFAP. 7NP2 retains the ability to bind hFAP in ELISA as the parental C5 scFv. C, D, E, F, G. ELISA signals of different anti-FAP antibodies on murine FAP (C), canine FAP (D), ovine FAP (E), porcine FAP (F) and cynoFAP (G): 7NP2 reveals to be cross-reactive with murine, canine, ovine, porcine and cyno FAP.

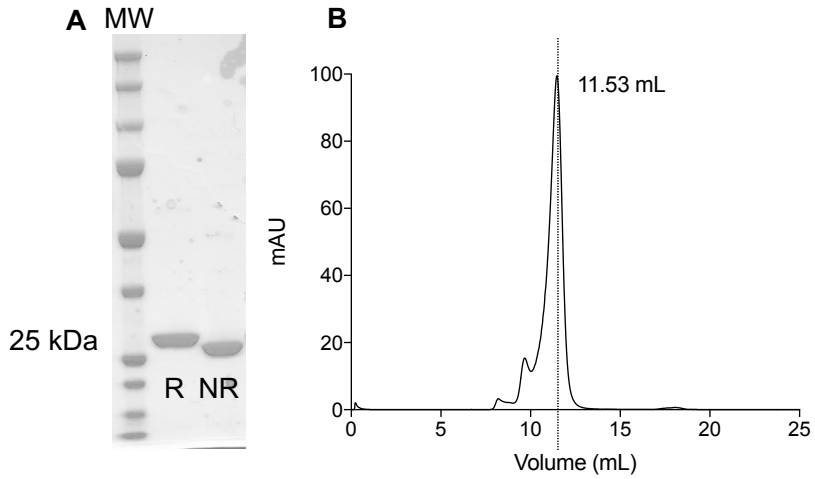

C

EVQLLESGGGLVQPGGSLRLSCAASGFTFSSYAMSWVRQAPGKGLEWVSAIGSVGGPTYYAD
SVKGRFTISRDNSKNTLYLQMNSLRAEDTAVYYCAKRLAWFDYWGQGTLVTVSSGGGGSGG
GGSGGGGEIVLTQSPGTLSLSPGERATLSCRASQSVSSSYLAWYQQKPGQAPRLLIYGASSRAT
GIPDRFSGSGSGTDFTLTISRLEPEDFAVYYCQQSGKGPLTFGQGTKVEIK

Figure S5.4. scFv(7NP2) aminoacidic sequence and characterization.

A**.** SDS-page, 10% gel in reducing (R) and non-reducing (NR) condition of purified scFv(7NP2); B. Size exclusion chromatogram of scFv(7NP2). C. Aminoacidic sequence of scFv(7NP2).

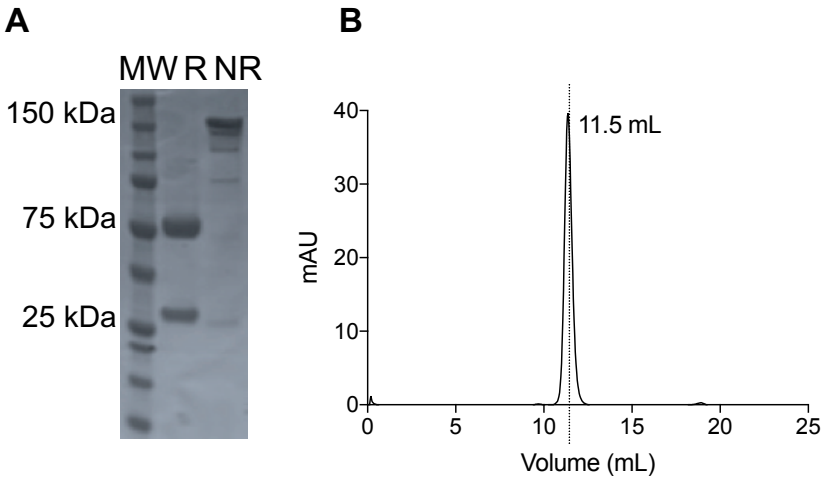

Figure S5.5. IgG1(C5) characterization.

A. SDS-page, 10% gel in reducing (R) and non-reducing (NR) condition of purified IgG1(C5); B. Size exclusion chromatogram of IgG1(C5).

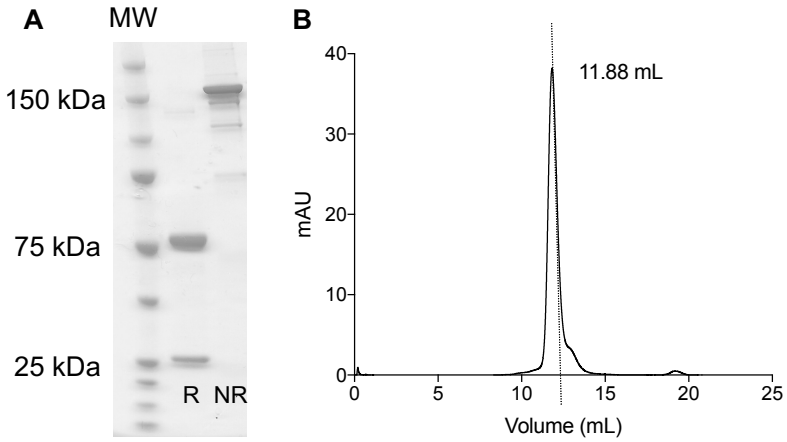

Figure S5.6. IgG1(7NP2) characterization.

A. SDS-page, 10% gel in reducing (R) and non-reducing (NR) condition of purified IgG1(7NP2); B. Size exclusion chromatogram of IgG1(7NP2).

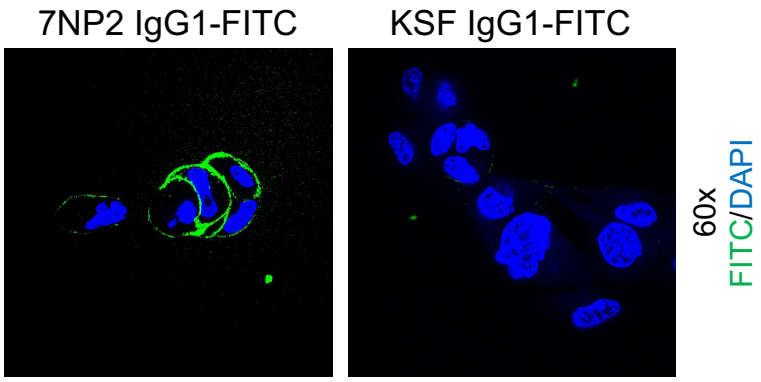

Figure S5.7. Confocal microscopy images after exposure to IgG1(7NP2)-FITC on SKRC52-hFAP cells.

7NP2 was mainly bound to the SKRC52-hFAP cell surface showing lack of internalization (left panel). IgG1(KSF)-FITC (right panel) has been used as negative control for the experiment and it did not show any binding to the cell membrane.

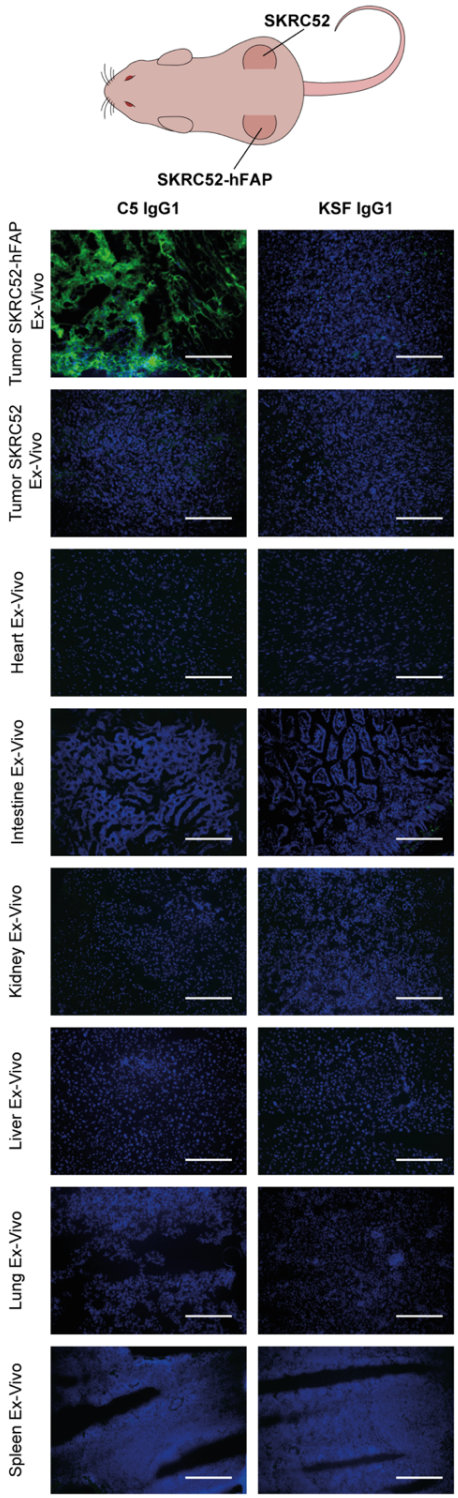

Figure S8. Immunofluorescence-based biodistribution analysis with IgG1 (C5).

Microscopic fluorescence analysis of tumor-targeting performance of IgG1(C5) on SKRC52-hFAP tumor and organs from BALB/c nude tumor-bearing mice. One hundred micrograms of IgG1(C5)-FITCor IgG1(KSF)-FITC (negative control) was injected intravenously into the lateral tail vein and mice were sacrificed 24 hours after injection, tumor and organs were excised and embedded in cryoembedding medium; cryostat sections were stained with ant-FITC (green, AlexaFluor 488) and DAPI (blue). Representative pictures of the samples were taken at 20x magnification, scale bars = 100 µM.

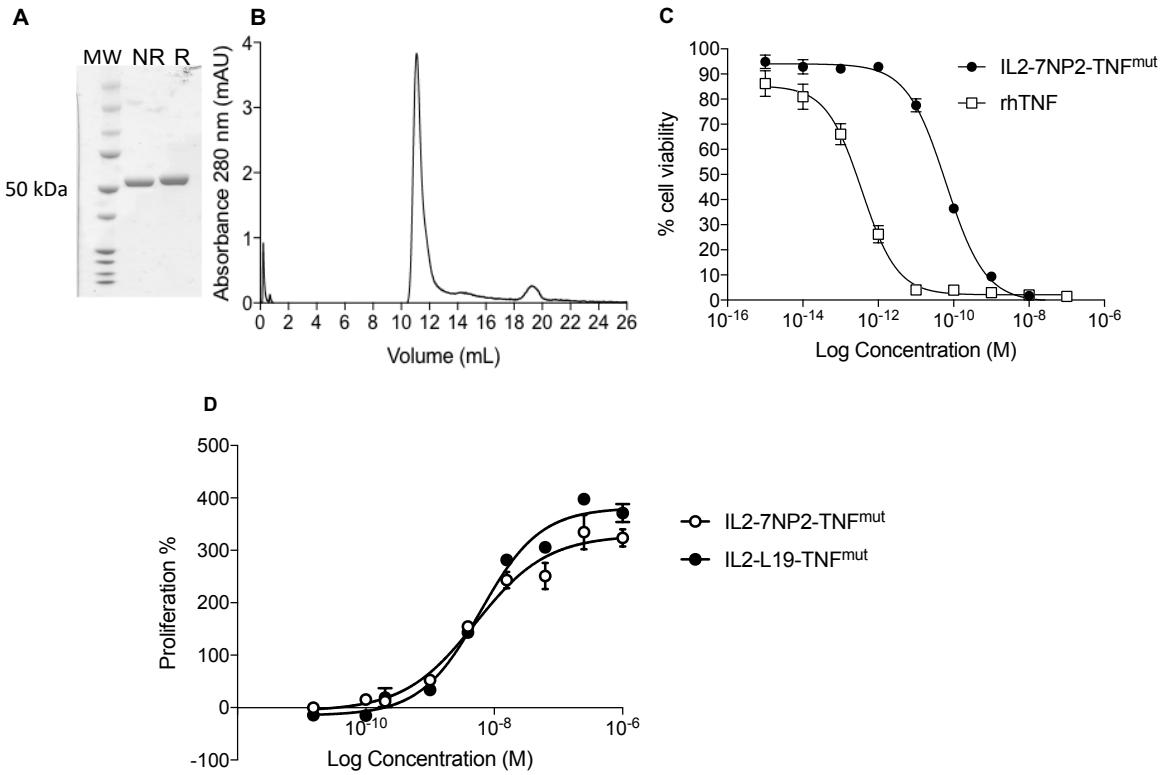

Figure S9. IL2-7NP2-TNF^{mut} characterization.

A. SDS-page, 10% gel in non-reducing (NR) and reducing (R) of purified IL2-7NP2-TNF^{mut}; B. Size exclusion chromatogram of IL2-7NP2-TNF^{mut}; C. TNF bioactivity assay on L-M fibroblast; D. IL2 bioactivity assay on CTLL-2 cells (72 h).

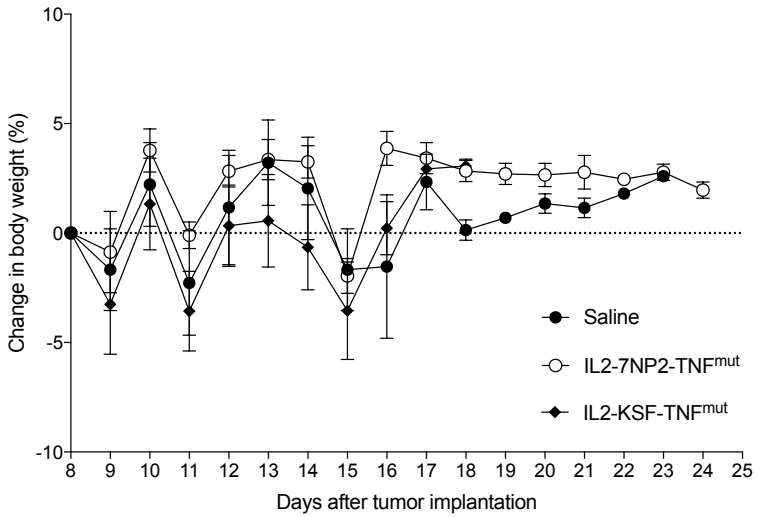

Figure S10. Body weight changes of mice treated with IL2-7NP2-TNF^{mut} in SKRC52-hFAP tumor bearing mice.

Body weight changes of mice treated with IL2-7NP2-TNF^{mut}, IL2-KSF-TNF^{mut} and saline respectively.

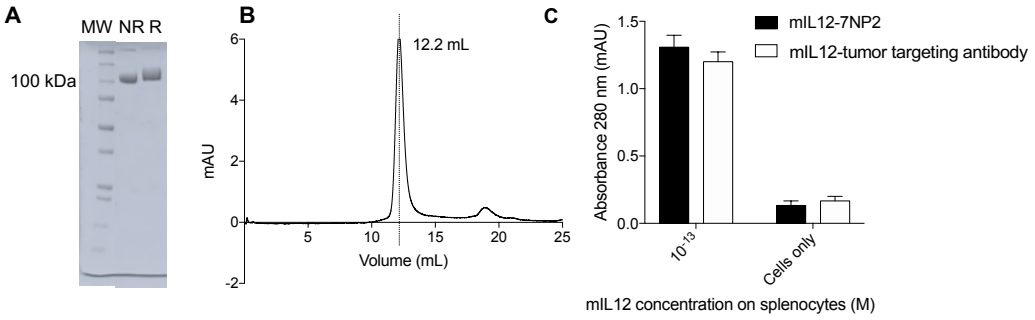

Figure S11. mIL12-7NP2 characterization.

A. SDS-page, 10% gel in non-reducing (NR) and reducing (R) condition of purified mIL12-7NP2; B. Size exclusion chromatogram of mIL12-7NP2; C. IFN-γ induction assay by mIL12-7NP2 in BALB/c splenocytes confirmed the activity of mIL12 at a concentration of 0.1 ng/mL (mIL12 general tumor targeting antibody has been used as positive control).

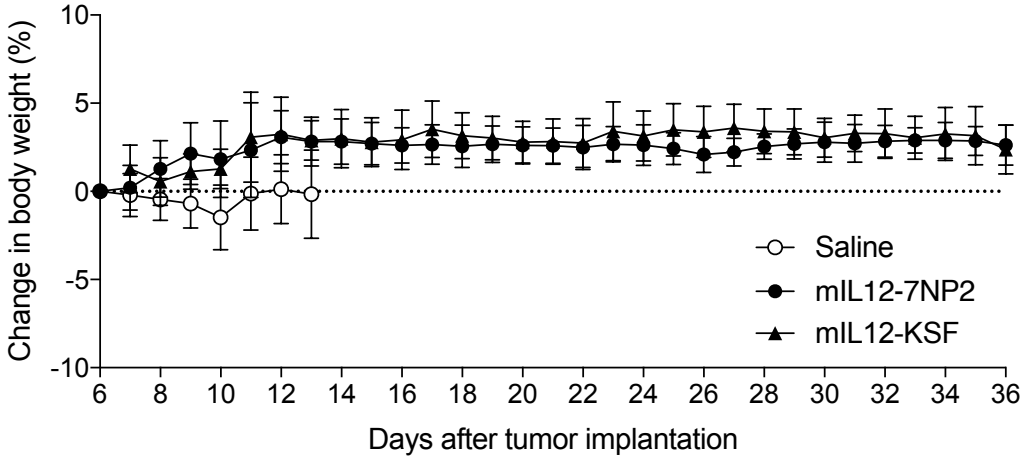

Figure S12 Body weight changes of mice treated with mIL12-7NP2 in SKRC52-hFAP tumor bearing mice.

Body weight changes of mice treated with mIL12-7NP2, mIL12-KSF and saline respectively.

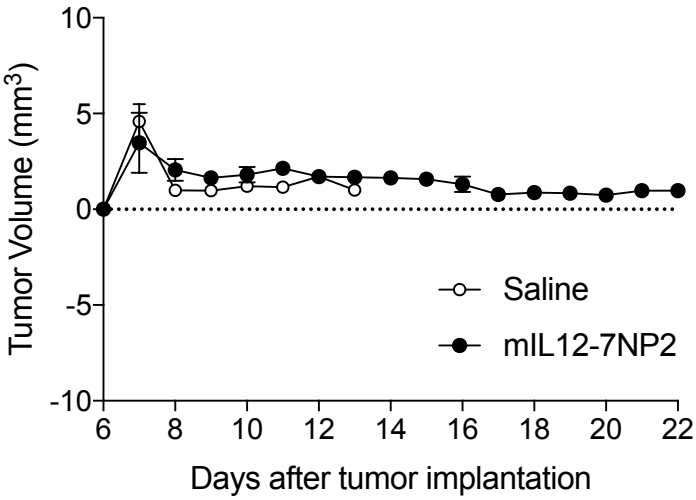

Figure S13. Body weight changes of mice treated with mIL12-7NP2 in CT26-hFAP tumor bearing mice.

Body weight changes of mice treated with mIL12-7NP2 and saline respectively.

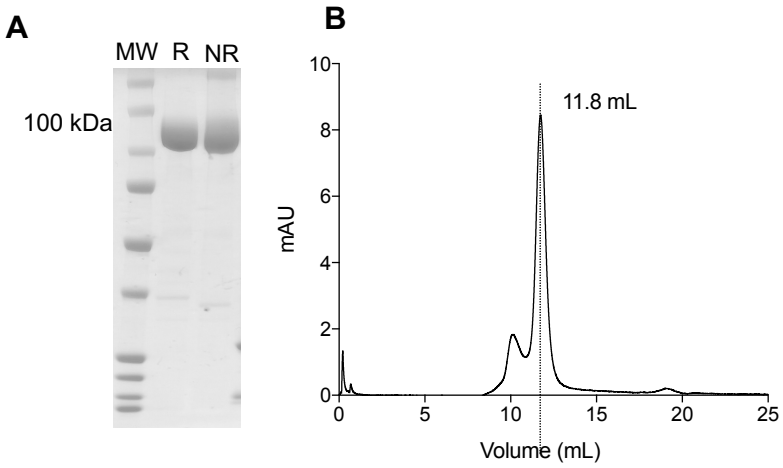

Figure S14. IL12-7NP2 characterization.

A. SDS-page, 10% gel in non-reducing (NR) and reducing (R) condition of purified IL12-7NP2; B. Size exclusion chromatogram of IL12-7NP2.

6. Conclusion and outlook

Over the last century, the understanding of cancer progression and of how the immune system discriminates a cancer cell from a healthy cell supported the development of more effective treatment. Surgery, chemotherapy, and radiotherapy have been efficacious approaches especially when the disease is localized and when used in combination. Unfortunately, these treatments encounter some disadvantages when the neoplastic lesions are not easily accessible for surgery, or they develop metastasis difficult to reach. Furthermore, chemotherapy drugs cannot distinguish between normal and malignant cells proving the limitation of this approach.

Immunotherapy revolutionized the treatment of cancer. In the last decade, the striking success of Yervoy, Nivolumab and Keytruda changed life expectancy of cancer patients convincing scientists that immunotherapy could provide benefits in the clinic[28].
Another strategy that has been explored in the past decades is the coupling of cytokines with antibodies selective for specific tumor associated antigens. Immunocytokines play an important role in fighting cancer cells, overcoming the inhibitory micro-environment created by malignancies and improving the therapeutic index of cytokines capitalizing on the targeting properties of antibody[30].

In this thesis, we have reported on the generation of human recombinant high-affinity antibodies against two tumor microenvironment-associated antigens, Tenascin C (TNC) and Fibroblast Activation Protein (FAP).

In the third chapter, we described the isolation and characterization of antibodies specific for the spliced Domain D of Tenascin C (TNC-D). TNC-D is a highly conserved glycoprotein, which comprises multiple fibronectin type 3 (FNIII) like domains. A total of eight FNIII domains are constitutionally present in the protein, whereas nine repeats (FNIII A-D) located between FNIII5-6 undergo alternative splicing giving rise to small and large isoforms of TNC. The large isoform of TNC is undetectable in adult healthy tissue while being expressed during embryogenesis[217]. However, pathological conditions such as chronic inflammation

and cancer can rapidly trigger the *de novo* synthesis of the protein[264]. TNC-D restricted expression in malignant tissue allows a selective targeting of the tumor sparing healthy organs. Therefore, and therefore makes it an ideal target for cancer therapy. In addition, the D domain is highly conserved between mouse and humans thus facilitating preclinical experiments in mouse. The isolation of antibodies selective for TNC-D started with the selection of a first parental antibody, termed L7D, from the human scFv antibody phage library "ETH-2 Gold"[284]. The selections were run with a site-specific biotinylated preparation of TNC-D: the antigen was subcloned fusing the protein to a Binding Specific Peptide (BSP) tag to carry site specific biotinylation through BirA enzyme. In this way, phage selection on streptavidin coated dynabeads were perform with a native conformation of TNC-D. To improve the affinity of L7D for the antigen (K_D: 40 nM), the antibody has been affinity matured randomizing key residues in the CDR1 of heavy and light chains. The randomization was carried using degenerated primers that introduced random mutations at V_H CDR1 positions 31, 32, 33 and V_L CDR1 positions 30, 31, 32. Phage selection against the new affinity matured library based on L7D antibody allowed the isolation of a higher affinity clone, R6N which was *in vitro* and *in vivo* further characterized. Surface plasmon resonance analysis conducted with a monomeric preparation of R6N in scFv format revealed an improvement in binding properties of the antibody with a K_D of 24 nM. Since the K_D of the antibody remains in the two digit nanomolar range, further maturation of CDR2 key residues could have improved the binding properties of the antibody.

The cross-reactivity of TNC-D between human and mouse facilitated the characterization of R6N. The antibody could recognize the antigen both on xenograft and mouse tissue slides. *Ex-vivo* biodistribution immunofluorescence-based studies allowed us to understand the targeting properties of the antibody showing that, regardless the format chosen, R6N accumulated only within the neoplastic lesion.

Since IL12 is gaining particular interest as key mediator of adaptative immune response, we decided to generate a novel immunocytokine featuring R6N antibody and IL12 as payload. The targeted delivery of IL12 represents indeed a favorable avenue to overcome the toxicities associated with this therapeutic agent[310]. The format chosen for R6N-IL12 was single-chain diabody one. This format is

particularly interesting for biotechnological and pharmaceutical development, as it consists of a single polypeptide, which can be expressed in mammalian cells efficiently. The linkers used to connect the different domains of fusion proteins can influence their structural stability, bioactivity, expression level, pharmacokinetic profiles, and their *in vivo* targeting properties[311]. R6N-IL12 was tested in immunodeficient mice bearing renal cell carcinoma tumor models showing only modest tumor growth retardation. When tested in an orthotopic glioma model in Balb/c mice, the fusion protein induced a prolonged tumor growth retardation with one complete tumor remission.

Evaluation of R6N-IL12 fusion protein in other tumor models is essential to understand the potential activity of the molecule. Combination therapy experiments with immune checkpoint inhibitors (e.g. anti-PD1) would be interesting to perform; results could be compared with well-known IL12 fusion protein, such as L19-IL12.

In the chapter 5 of this thesis, we focused on the generation of a new mAb selective for a second tumor microenvironment-associated antigen termed FAP. FAP is a serine peptidase whose expression is restricted to malignant tissue or during inflammations processes. The absence of FAP in healthy adult tissue renders this protein an attractive target for both imaging and therapeutic applications. In 2020, J. Calais defined FAP as the "next billion-dollar nuclear theranostics target" after Haberkorn and coworkers imaged more than 28 different tumor types with radiolabeled FAP ligands[248,249]. Many companies and research groups have been extensively working on the generation of antibodies or small molecules capable of targeting FAP. Neri's group has generated in 2020 a novel small ligand that binds to hFAP with affinity in the sub-nanomolar concentration range. The small molecule, termed OncoFAP, shows a rapid and homogeneous penetration within the neoplastic tissue.

Small molecules' main advantages rely on the rapid distribution and fast clearance from the bloodstream due to their small size. Fusion protein consisting of small molecules and cytokines would not take advantages of these important features. For this reason, we decided to isolate a new antibody targeting hFAP to further generate immunocytokines selective for the target. In this perspective, OncoFAP and the

new anti-FAP antibody could be used together as companion diagnostic agent and therapeutic product.

7NP2 is the antibody resulting from an affinity maturation conducted on C5 scFv, a previously discovered anti-hFAP antibody. During my project, I focused on *in vitro* affinity maturation of monoclonal antibodies. The affinity maturation procedure we decided to apply for the anti-FAP antibody started with the randomization of key residues of the CDR2, specifically of the amino acids in position 51, 52, 53 and 56 of the heavy chain and in position 51, 54 and 56 of the light chain respectively. The library contained more than $5.7*10^8$ different clones, almost covering the theoretical size. 7NP2 (K_D = 10.4 nM) was characterized by immunofluorescence and FACS analysis, confirming the binding properties of the antibody both on cells and tissues. Furthermore, 7NP2 showed a diffuse stromal staining when tested on commercial tissue microarrays of various solid malignancies, as well as on human colon cancer biopsies. The *in vivo* targeting performance of 7NP2 was evaluated in mice bearing renal cell carcinomas transduced with hFAP (SKRC52-hFAP). The antibody, both in IgG1-FITC format and as fusion protein mIL12-7NP2-FITC, could detect hFAP in the implanted tumor but not in healthy organs. The fusion protein mIL12-7NP2 was designed as mIL12-R6N in single-chain diabody format due to the encouraging preclinical results obtained with the same format also for mIL12-L19[282]. The mIL12-based immunocytokine, which retained fully activity in terms of antigen binding and cytokine activity, was potently active against SKRC52-hFAP renal cell carcinomas and CT26-hFAP colon carcinomas curing almost all the mice and inducing tumor growth retardation. 7NP2 antibody was also fused to IL2 and TNF^{mut} leading to the generation of a fusion protein similar to IL2-L19-TNF^{mut304}. The molecule showed significantly stronger anti-tumor activity in tumor xenografts expressing hFAP (SKRC52-hFAP), compared to the non-targeted product based on the KSF antibody. Our group has extensively showed that tumor targeted TNF- and IL2-based products act synergistically in fighting cancer. TNF is involved in a variety of mechanisms which induce tumor necrosis, direct killing and stimulation of anti-cancer immunity. IL2 boosts cancer specific T and NK cells which selectively kill malignant tumor cells.

To further characterize 7NP2 antibody, pharmacokinetics studies in *Cynomolgus Monkey* were conducted in order to evaluate the circulatory half-life of the IgG1(7NP2). At 0.1 mg/Kg, the product showed no sink effects at early time points and a slow clearance from bloodstream as expected for IgG1 antibodies.

Collectively, during my PhD program, I was able to isolate by phage display technology, affinity mature and characterize two monoclonal antibodies selective for tumor microenvironment-associated antigens. R6N, antibody specific for the spliced domain D of TNC, showed excellent targeting properties confirmed by immunofluorescence-based biodistribution staining and single agent activity when fused to mIL12. 7NP2, the anti-hFAP antibody, represents a promising building block for generating immunocytokines with potent anti-tumor properties. The favorable pharmacokinetic profile of the naked immunoglobulin provides a rational for future translation activities of these products.

7. References

1. Sung, H. *et al.* Global Cancer Statistics 2020: GLOBOCAN Estimates of Incidence and Mortality Worldwide for 36 Cancers in 185 Countries. *CA. Cancer J. Clin.* **71**, 209–249 (2021).
2. Zhang, J. *et al.* Germline Mutations in Predisposition Genes in Pediatric Cancer. *N. Engl. J. Med.* **373**, 2336–2346 (2015).
3. Ma, X. & Yu, H. Global burden of cancer. *Yale J. Biol. Med.* **79**, 85–94 (2006).
4. Stewart, Z. A., Westfall, M. D. & Pietenpol, J. A. Cell-cycle dysregulation and anticancer therapy. *Trends Pharmacol. Sci.* **24**, 139–145 (2003).
5. Peter, M. E. *et al.* The role of CD95 and CD95 ligand in cancer. *Cell Death Differ.* **22**, 549–559 (2015).
6. Ribatti, D. The concept of immune surveillance against tumors. The first theories. *Oncotarget* **8**, 7175–7180 (2017).
7. Dunn, G. P., Koebel, C. M. & Schreiber, R. D. Interferons, immunity and cancer immunoediting. *Nat. Rev. Immunol.* **6**, 836–848 (2006).
8. Dunn, G. P., Bruce, A. T., Ikeda, H., Old, L. J. & Schreiber, R. D. Cancer immunoediting: from immunosurveillance to tumor escape. *Nat. Immunol.* **3**, 991–998 (2002).
9. Vesely, M. D. & Schreiber, R. D. Cancer immunoediting: antigens, mechanisms, and implications to cancer immunotherapy. *Ann. N. Y. Acad. Sci.* **1284**, 1–5 (2013).
10. Hanahan, D. & Weinberg, R. A. The Hallmarks of Cancer. *Cell* **100**, 57–70 (2000).
11. Hanahan, D. & Weinberg, R. A. Hallmarks of Cancer: The Next Generation. *Cell* **144**, 646–674 (2011).
12. Tannock, I. F. Conventional cancer therapy: promise broken or promise delayed? *Lancet* **351**, SII9–SII16 (1998).
13. Baskar, R., Lee, K. A., Yeo, R. & Yeoh, K.-W. Cancer and radiation therapy: current advances and future directions. *Int. J. Med. Sci.* **9**, 193–199 (2012).
14. Chabner, B. A. & Roberts, T. G. Chemotherapy and the war on cancer. *Nat. Rev. Cancer* **5**, 65–72 (2005).
15. Farmer, P. B. Cancer Chemotherapy I: Design and Mechanism of Action of Cytotoxic Drugs BT - The Molecular Basis of Cancer. in (eds. Farmer, P.

B. & Walker, J. M.) 259–285 (Springer US, 1985). doi:10.1007/978-1-4684-7313-1_10.

16. Mayer, R. J. *et al.* Intensive Postremission Chemotherapy in Adults with Acute Myeloid Leukemia. *N. Engl. J. Med.* **331**, 896–903 (1994).
17. Younes, A. Beyond chemotherapy: new agents for targeted treatment of lymphoma. *Nat. Rev. Clin. Oncol.* **8**, 85–96 (2011).
18. Einhorn, L. H. Treatment of testicular cancer: a new and improved model. *J. Clin. Oncol.* **8**, 1777–1781 (1990).
19. Van Der Veldt, A., Smit, E. & Lammertsma, A. Positron Emission Tomography as a Method for Measuring Drug Delivery to Tumors in vivo: The Example of [11C]docetaxel . *Frontiers in Oncology* vol. 3 208 (2013).
20. DeVita, V. T. & Chu, E. A History of Cancer Chemotherapy. *Cancer Res.* **68**, 8643 LP – 8653 (2008).
21. Ehrlich, P. *Collected studies on immunity,*. (J. Wiley & Sons, 1906).
22. Rosenberg, S. A., Yang, J. C. & Restifo, N. P. Cancer immunotherapy: moving beyond current vaccines. *Nat. Med.* **10**, 909–915 (2004).
23. McCarthy, E. F. The toxins of William B. Coley and the treatment of bone and soft-tissue sarcomas. *Iowa Orthop. J.* **26**, 154–158 (2006).
24. Starnes, C. O. Coley's toxins in perspective. *Nature* **357**, 11–12 (1992).
25. Rosenberg, S. A. IL-2: The First Effective Immunotherapy for Human Cancer. *J. Immunol.* **192**, 5451–5458 (2014).
26. Couzin-Frankel, J. Cancer Immunotherapy. *Science (80-.).* **342**, 1432 LP – 1433 (2013).
27. Leach, D. R., Krummel, M. F. & Allison, J. P. Enhancement of Antitumor Immunity by CTLA-4 Blockade. *Science (80-.).* **271**, 1734 LP – 1736 (1996).
28. Sharma, P. & Allison, J. P. Immune checkpoint targeting in cancer therapy: toward combination strategies with curative potential. *Cell* **161**, 205–214 (2015).
29. Murer, P. & Neri, D. Antibody-cytokine fusion proteins: A novel class of biopharmaceuticals for the therapy of cancer and of chronic inflammation. *N. Biotechnol.* **52**, 42–53 (2019).
30. Neri, D. & Sondel, P. M. Immunocytokines for cancer treatment: Past, present and future. *Current Opinion in Immunology* vol. 40 96–102 (2016).

31. List, T. & Neri, D. Immunocytokines: A review of molecules in clinical development for cancer therapy. *Clinical Pharmacology: Advances and Applications* vol. 5 29–45 (2013).
32. Bootz, F. & Neri, D. Immunocytokines: a novel class of products for the treatment of chronic inflammation and autoimmune conditions. *Drug Discov. Today* **21**, 180–189 (2016).
33. Pasche, N. & Neri, D. Immunocytokines: A novel class of potent armed antibodies. *Drug Discovery Today* vol. 17 583–590 (2012).
34. Murphy, K., Weaver, C. & Janeway, C. *Janeway's immunobiology*. (2017).
35. Merle, N. S., Church, S. E., Fremeaux-Bacchi, V. & Roumenina, L. T. Complement System Part I – Molecular Mechanisms of Activation and Regulation . *Frontiers in Immunology* vol. 6 262 (2015).
36. Rudnick, S. I. & Adams, G. P. Affinity and avidity in antibody-based tumor targeting. *Cancer Biother. Radiopharm.* **24**, 155–161 (2009).
37. Roth, D. B. V(D)J Recombination: Mechanism, Errors, and Fidelity. *Microbiol. Spectr.* **2**, 10.1128/microbiolspec.MDNA3-0041–2014 (2014).
38. Chiu, M. L., Goulet, D. R., Teplyakov, A. & Gilliland, G. L. Antibody Structure and Function: The Basis for Engineering Therapeutics. *Antibodies (Basel, Switzerland)* **8**, 55 (2019).
39. Vidarsson, G., Dekkers, G. & Rispens, T. IgG Subclasses and Allotypes: From Structure to Effector Functions . *Frontiers in Immunology* vol. 5 520 (2014).
40. Chen, K. & Cerutti, A. The function and regulation of immunoglobulin D. *Curr. Opin. Immunol.* **23**, 345–352 (2011).
41. Woof, J. M. & Kerr, M. A. The function of immunoglobulin A in immunity. *J. Pathol.* **208**, 270–282 (2006).
42. Sutton, B. J., Davies, A. M., Bax, H. J. & Karagiannis, S. N. IgE Antibodies: From Structure to Function and Clinical Translation. *Antibodies (Basel, Switzerland)* **8**, 19 (2019).
43. Quinnell, R. J. *et al.* IgG subclass responses in a longitudinal study of canine visceral leishmaniasis. *Vet. Immunol. Immunopathol.* **91**, 161–168 (2003).
44. Brekke, O. H. & Sandlie, I. Therapeutic antibodies for human diseases at the dawn of the twenty-first century. *Nat. Rev. Drug Discov.* **2**, 52–62 (2003).
45. Carter, J. H. The immune system as a model for pattern recognition and

classification. *J. Am. Med. Inform. Assoc.* **7**, 28–41 (2000).

46. Simon, A. K., Hollander, G. A. & McMichael, A. Evolution of the immune system in humans from infancy to old age. *Proceedings. Biol. Sci.* **282**, 20143085 (2015).
47. KÖHLER, G. & MILSTEIN, C. Continuous cultures of fused cells secreting antibody of predefined specificity. *Nature* **256**, 495–497 (1975).
48. Leavy, O. The birth of monoclonal antibodies. *Nat. Immunol.* **17**, S13–S13 (2016).
49. Descotes, J. Immunotoxicity of monoclonal antibodies. *MAbs* **1**, 104–111 (2009).
50. Dekkers, G. *et al.* Affinity of human IgG subclasses to mouse Fc gamma receptors. *MAbs* **9**, 767–773 (2017).
51. Carter, P. *et al.* Humanization of an anti-p185HER2 antibody for human cancer therapy. *Proc. Natl. Acad. Sci. U. S. A.* **89**, 4285–4289 (1992).
52. He, X. *et al. Generation and characterization of a mouse/human chimeric antibody directed against extracellular matrix protein tenascin*. *Journal of Neuroimmunology* vol. 52 (1994).
53. Chames, P., Van Regenmortel, M., Weiss, E. & Baty, D. Therapeutic antibodies: successes, limitations and hopes for the future. *Br. J. Pharmacol.* **157**, 220–233 (2009).
54. Urquhart, L. Top companies and drugs by sales in 2019. *Nat. Rev. Drug Discov.* **19**, 228 (2020).
55. Winter, G. & Harris, W. J. Humanized antibodies. *Immunol. Today* **14**, 243–246 (1993).
56. Brüggemann, M., Winter, G., Waldmann, H. & Neuberger, M. S. The immunogenicity of chimeric antibodies. *J. Exp. Med.* **170**, 2153–2157 (1989).
57. Frenzel, A., Schirrmann, T. & Hust, M. Phage display-derived human antibodies in clinical development and therapy. *mAbs* vol. 8 1177–1194 (2016).
58. Jakobovits, A. Production of fully human antibodies by transgenic mice. *Curr. Opin. Biotechnol.* **6**, 561–566 (1995).
59. Brüggemann, M. *et al.* Human antibody production in transgenic animals. *Arch. Immunol. Ther. Exp. (Warsz).* **63**, 101–108 (2015).

60. Jakobovits, A., Amado, R. G., Yang, X., Roskos, L. & Schwab, G. From XenoMouse technology to panitumumab, the first fully human antibody product from transgenic mice. *Nat. Biotechnol.* **25**, 1134–1143 (2007).
61. Lonberg, N. Human antibodies from transgenic animals. *Nat. Biotechnol.* **23**, 1117–1125 (2005).
62. Smith, G. P. Filamentous fusion phage: novel expression vectors that display cloned antigens on the virion surface. *Science (80-.).* **228**, 1315 LP – 1317 (1985).
63. Lowman, H. B., Bass, S. H., Simpson, N. & Wells, J. A. Selecting high-affinity binding proteins by monovalent phage display. *Biochemistry* **30**, 10832–10838 (1991).
64. Pini, A. *et al.* Design and use of a phage display library: Antibodies with subnanomolar affinity against a marker of angiogenesis eluted from a two-dimensional gel. *J. Biol. Chem.* **273**, 21769–21776 (1998).
65. McCafferty, J., Griffiths, A. D., Winter, G. & Chiswell, D. J. Phage antibodies: filamentous phage displaying antibody variable domains. *Nature* **348**, 552–554 (1990).
66. Greg Winter, Andrew D. Griffiths, Robert E. Hawkins & Hennie R. Hoogenboom. Making Antibodies by Phage Display Technology. *Annu. Rev. Immunol* 433–55 (1994).
67. Viti, F., Nilsson, F., Demartis, S., Huber, A. & Neri, D. B. T.-M. in E. [29] Design and use of phage display libraries for the selection of antibodies and enzymes. in *Applications of Chimeric Genes and Hybrid Proteins Part A: Gene Expression and Protein Purification* vol. 326 480–505 (Academic Press, 2000).
68. Pini, A. *et al.* Design and Use of a Phage Display Library. *J. Biol. Chem.* 21769–21776 (1998).
69. Chakravarthy, B., Ménard, M., Brown, L., Atkinson, T. & Whitfield, J. Identification of protein kinase C inhibitory activity associated with a polypeptide isolated from a phage display system with homology to PCM-1, the pericentriolar material-1 protein. *Biochem. Biophys. Res. Commun.* **424**, 147–151 (2012).
70. Bulina, M. E. *et al.* Chromophore-assisted light inactivation (CALI) using the phototoxic fluorescent protein KillerRed. *Nat. Protoc.* **1**, 947–953

(2006).

71. Almagro, J. C. *et al.* Characterization of a high-affinity human antibody with a disulfide bridge in the third complementarity-determining region of the heavy chain. *J. Mol. Recognit.* **25**, 125–135 (2012).
72. Bazan, J., Całkosiñski, I. & Gamian, A. Phage displaya powerful technique for immunotherapy: 1. Introduction and potential of therapeutic applications. *Human Vaccines and Immunotherapeutics* vol. 8 1817–1828 (2012).
73. Pedersen, H. *et al.* A method for directed evolution and functional cloning of enzymes. *Proc. Natl. Acad. Sci. U. S. A.* **95**, 10523–10528 (1998).
74. Heinis, C. *et al.* Selection of catalytically active biotin ligase and trypsin mutants by phage display. *Protein Eng.* **14**, 1043–1052 (2002).
75. Bothmann, H. & Plückthun, A. Selection for a periplasmic factor improving phage display and functional periplasmic expression. *Nat. Biotechnol.* **16**, 376–380 (1998).
76. Kristensen, P. & Winter, G. Proteolytic selection for protein folding using filamentous bacteriophages. *Fold. Des.* **3**, 321–328 (1998).
77. Jespers, L., Schon, O., Famm, K. & Winter, G. Aggregation-resistant domain antibodies selected on phage by heat denaturation. *Nat. Biotechnol.* **22**, 1161–1165 (2004).
78. Parmley, S. F. & Smith, G. P. Antibody-selectable filamentous fd phage vectors: affinity purification of target genes. *Gene* **73**, 305–318 (1988).
79. Greenwood, J., Willis, A. E. & Perham, R. N. Multiple display of foreign peptides on a filamentous bacteriophage: Peptides from Plasmodium falciparum circumsporozoite protein as antigens. *J. Mol. Biol.* **220**, 821–827 (1991).
80. Iannolo, G., Minenkova, O., Petruzzelli, R. & Cesareni, G. Modifying Filamentous Phage Capsid: Limits in the Size of the Major Capsid Protein. *J. Mol. Biol.* **248**, 835–844 (1995).
81. Hoogenboom, H. R. *et al.* Multi-subunit proteins on the surface of filamentous phage: methodologies for displaying antibody (Fab) heavy and light chains. *Nucleic Acids Res.* **19**, 4133–4137 (1991).
82. Demartis, S., Tarli, L., Borsi, L., Zardi, L. & Neri, D. Selective targeting of tumour neovasculature by a radiohalogenated human antibody fragment specific for the ED-B domain of fibronectin. *Eur. J. Nucl. Med.* **28**, 534–539

(2001).

83. Kaplon, H. & Reichert, J. M. Antibodies to watch in 2019. *MAbs* **11**, 219–238 (2019).

84. Schiff, M. H. *et al.* Safety analyses of adalimumab (HUMIRA) in global clinical trials and US postmarketing surveillance of patients with rheumatoid arthritis. *Ann. Rheum. Dis.* **65**, 889–894 (2006).

85. Halpern, W. G. *et al.* Chronic Administration of Belimumab, a BLyS Antagonist, Decreases Tissue and Peripheral Blood B-Lymphocyte Populations in Cynomolgus Monkeys: Pharmacokinetic, Pharmacodynamic, and Toxicologic Effects. *Toxicol. Sci.* **91**, 586–599 (2006).

86. Group, C. R. *et al.* Ranibizumab and bevacizumab for neovascular age-related macular degeneration. *N. Engl. J. Med.* **364**, 1897–1908 (2011).

87. Silacci, M. *et al.* Design, construction, and characterization of a large synthetic human antibody phage display library. in *Proteomics* vol. 5 2340–2350 (2005).

88. Weber, M. *et al.* A highly functional synthetic phage display library containing over 40 billion human antibody clones. *PLoS One* **9**, (2014).

89. Villa, A. *et al.* A novel synthetic naïve human antibody library allows the isolation of antibodies against a new epitope of oncofetal fibronectin. *MAbs* **3**, 264–272 (2011).

90. Weide, B. *et al.* A phase II study of the L19IL2 immunocytokine in combination with dacarbazine in advanced metastatic melanoma patients. *Cancer Immunol. Immunother.* **68**, 1547–1559 (2019).

91. Schwager, K. *et al.* The antibody-mediated targeted delivery of interleukin-10 inhibits endometriosis in a syngeneic mouse model. *Hum. Reprod.* **26**, 2344–2352 (2011).

92. Danielli, R. *et al.* Intralesional administration of L19-IL2/L19-TNF in stage III or stage IVM1a melanoma patients: Results of a phase II study. *Cancer Immunol. Immunother.* **64**, 999–1009 (2015).

93. Spitaleri, G. *et al.* Phase I/II study of the tumour-targeting human monoclonal antibody–cytokine fusion protein L19-TNF in patients with advanced solid tumours. *J. Cancer Res. Clin. Oncol.* **139**, 447–455 (2013).

94. Pepper, L. R., Cho, Y. K., Boder, E. T. & Shusta, E. V. A decade of yeast surface display technology: where are we now? *Comb. Chem. High*

Throughput Screen. **11**, 127–134 (2008).

95. Lu, C. F. *et al.* Glycosyl phosphatidylinositol-dependent cross-linking of alpha-agglutinin and beta 1,6-glucan in the Saccharomyces cerevisiae cell wall. *J. Cell Biol.* **128**, 333–340 (1995).
96. Weaver-Feldhaus, J. M. *et al.* Yeast mating for combinatorial Fab library generation and surface display. *FEBS Lett.* **564**, 24–34 (2004).
97. Valldorf, B. *et al.* Antibody display technologies: selecting the cream of the crop. *Biol. Chem.* (2021) doi:doi:10.1515/hsz-2020-0377.
98. Wang, J. *et al.* Durable blockade of PD-1 signaling links preclinical efficacy of sintilimab to its clinical benefit. *MAbs* **11**, 1443–1451 (2019).
99. Ho, M. & Pastan, I. Mammalian cell display for antibody engineering. *Methods Mol. Biol.* **525**, 337–xiv (2009).
100. Zhou, C. & Shen, W. D. Mammalian Cell Surface Display of Full Length IgG BT - Antibody Engineering: Methods and Protocols, Second Edition. in (ed. Chames, P.) 293–302 (Humana Press, 2012). doi:10.1007/978-1-61779-974-7_17.
101. Robertson, N. *et al.* Development of a novel mammalian display system for selection of antibodies against membrane proteins. *J. Biol. Chem.* **295**, 18436–18448 (2020).
102. Beerli, R. R. *et al.* Isolation of human monoclonal antibodies by mammalian cell display. *Proc. Natl. Acad. Sci.* **105**, 14336 LP – 14341 (2008).
103. Lipovsek, D. & Plückthun, A. In-vitro protein evolution by ribosome display and mRNA display. *J. Immunol. Methods* **290**, 51–67 (2004).
104. Plückthun, A. Ribosome Display: A Perspective BT - Ribosome Display and Related Technologies: Methods and Protocols. in (eds. Douthwaite, J. A. & Jackson, R. H.) 3–28 (Springer New York, 2012). doi:10.1007/978-1-61779-379-0_1.
105. Li, R., Kang, G., Hu, M. & Huang, H. Ribosome Display: A Potent Display Technology used for Selecting and Evolving Specific Binders with Desired Properties. *Mol. Biotechnol.* **61**, 60–71 (2019).
106. Momenimovahed, Z. & Salehiniya, H. Epidemiological characteristics of and risk factors for breast cancer in the world. *Breast cancer (Dove Med. Press.* **11**, 151–164 (2019).
107. Carter, P. J. Potent antibody therapeutics by design. *Nat. Rev. Immunol.* **6**,

343–357 (2006).

108. Carter, P. J. & Lazar, G. A. Next generation antibody drugs: pursuit of the 'high-hanging fruit'. *Nat. Rev. Drug Discov.* **17**, 197–223 (2018).
109. Slamon, D. J. *et al.* Use of Chemotherapy plus a Monoclonal Antibody against HER2 for Metastatic Breast Cancer That Overexpresses HER2. *N. Engl. J. Med.* **344**, 783–792 (2001).
110. Humblet, Y. Cetuximab: an IgG1 monoclonal antibody for the treatment of epidermal growth factor receptor-expressing tumours. *Expert Opin. Pharmacother.* **5**, 1621–1633 (2004).
111. Wong, S.-F. Cetuximab: An epidermal growth factor receptor monoclonal antibody for the treatment of colorectal cancer. *Clin. Ther.* **27**, 684–694 (2005).
112. Polman, C. H. *et al.* A Randomized, Placebo-Controlled Trial of Natalizumab for Relapsing Multiple Sclerosis. *N. Engl. J. Med.* **354**, 899–910 (2006).
113. Dryden, G. W. Natalizumab for Moderate-to-Severe Crohn's Disease. *Gastroenterol. Hepatol. (N. Y).* **4**, 296 (2008).
114. Kiefer, J. D. & Neri, D. Immunocytokines and bispecific antibodies: two complementary strategies for the selective activation of immune cells at the tumor site. *Immunol. Rev.* **270**, 178–192 (2016).
115. June, C. H., O'Connor, R. S., Kawalekar, O. U., Ghassemi, S. & Milone, M. C. CAR T cell immunotherapy for human cancer. *Science (80-.).* **359**, 1361 LP – 1365 (2018).
116. Neri, D. Europe PMC Funders Group Antibody-cytokine fusions : versatile products for the modulation of anti-cancer immunity. **7**, 348–354 (2020).
117. Holliger, P. & Hudson, P. J. Engineered antibody fragments and the rise of single domains. *Nat. Biotechnol.* **23**, 1126–1136 (2005).
118. Borsi, L. *et al.* Selective targeting of tumoral vasculature: Comparison of different formats of an antibody (L19) to the ED-B domain of fibronectin. *Int. J. Cancer* **102**, 75–85 (2002).
119. Pasche, N. & Neri, D. Immunocytokines: a novel class of potent armed antibodies. *Drug Discov. Today* **17**, 583–590 (2012).
120. Zalevsky, J. *et al.* Enhanced antibody half-life improves in vivo activity. *Nat. Biotechnol.* **28**, 157–159 (2010).

121. Carrasquillo, J. A. *et al.* Indium-111 T101 monoclonal antibody is superior to iodine-131 T101 in imaging of cutaneous T-cell lymphoma. *J. Nucl. Med.* **28**, 281—287 (1987).
122. Seidman, J. G. & Leder, P. The arrangement and rearrangement of antibody genes. *Nature* **276**, 790–795 (1978).
123. Sievers, E. L. & Senter, P. D. Antibody-Drug Conjugates in Cancer Therapy. *Annu. Rev. Med.* **64**, 15–29 (2013).
124. Beck, A., Goetsch, L., Dumontet, C. & Corvaïa, N. Strategies and challenges for the next generation of antibody–drug conjugates. *Nat. Rev. Drug Discov.* **16**, 315–337 (2017).
125. Dal Corso, A., Gébleux, R., Murer, P., Soltermann, A. & Neri, D. A non-internalizing antibody-drug conjugate based on an anthracycline payload displays potent therapeutic activity in vivo. *J. Control. Release* **264**, 211–218 (2017).
126. Dornan, D. *et al.* Therapeutic potential of an anti-CD79b antibody–drug conjugate, anti–CD79b-vc-MMAE, for the treatment of non-Hodgkin lymphoma. *Blood* **114**, 2721–2729 (2009).
127. Lambert, J. M. & Chari, R. V. J. Ado-trastuzumab Emtansine (T-DM1): An Antibody–Drug Conjugate (ADC) for HER2-Positive Breast Cancer. *J. Med. Chem.* **57**, 6949–6964 (2014).
128. Ricart, A. D. Antibody-Drug Conjugates of Calicheamicin Derivative: Gemtuzumab Ozogamicin and Inotuzumab Ozogamicin. *Clin. Cancer Res.* **17**, 6417 LP – 6427 (2011).
129. Senter, P. D. & Sievers, E. L. The discovery and development of brentuximab vedotin for use in relapsed Hodgkin lymphoma and systemic anaplastic large cell lymphoma. *Nat. Biotechnol.* **30**, 631–637 (2012).
130. Ponziani, S. *et al.* Antibody-Drug Conjugates: The New Frontier of Chemotherapy. *Int. J. Mol. Sci.* **21**, 5510 (2020).
131. Bardia, A. *et al.* Sacituzumab Govitecan-hziy in Refractory Metastatic Triple-Negative Breast Cancer. *N. Engl. J. Med.* **380**, 741–751 (2019).
132. Lonial, S. *et al.* Belantamab mafodotin for relapsed or refractory multiple myeloma (DREAMM-2): a two-arm, randomised, open-label, phase 2 study. *Lancet Oncol.* **21**, 207–221 (2020).
133. Puvvada, S. D. *et al.* Yttrium-90-Ibritumomab Tiuxetan (Zevalin®)

Radioimmunotherapy after Cytoreduction with ESHAP Chemotherapy in Patients with Relapsed Follicular Non-Hodgkin Lymphoma: Final Results of a Phase II Study. *Oncology* **94**, 274–280 (2018).

134. Friedberg, J. W. & Fisher, R. I. Iodine-131 tositumomab (Bexxar®): radioimmunoconjugate therapy for indolent and transformed B-cell non-Hodgkin's lymphoma. *Expert Rev. Anticancer Ther.* **4**, 18–26 (2004).
135. Hess, C., Venetz, D. & Neri, D. Emerging classes of armed antibody therapeutics against cancer. *Medchemcomm* **5**, 408–431 (2014).
136. Stein, A. *et al.* Benefit-Risk Assessment of Blinatumomab in the Treatment of Relapsed/Refractory B-Cell Precursor Acute Lymphoblastic Leukemia. *Drug Saf.* **42**, 587–601 (2019).
137. Brinkmann, U. & Kontermann, R. E. The making of bispecific antibodies. *MAbs* **9**, 182–212 (2017).
138. Suresh, M. R., Cuello, A. C. & Milstein, C. Advantages of bispecific hybridomas in one-step immunocytochemistry and immunoassays. *Proc. Natl. Acad. Sci. U. S. A.* **83**, 7989–7993 (1986).
139. Spiess, C., Zhai, Q. & Carter, P. J. Alternative molecular formats and therapeutic applications for bispecific antibodies. *Mol. Immunol.* **67**, 95–106 (2015).
140. Neri, D. Antibody–cytokine fusions: Versatile products for the modulation of anticancer immunity. *Cancer Immunol. Res.* **7**, 348–354 (2019).
141. Hutmacher, C. & Neri, D. Antibody-cytokine fusion proteins: Biopharmaceuticals with immunomodulatory properties for cancer therapy. *Adv. Drug Deliv. Rev.* **141**, 67–91 (2019).
142. Rosenberg, S. A. *et al.* Observations on the Systemic Administration of Autologous Lymphokine-Activated Killer Cells and Recombinant Interleukin-2 to Patients with Metastatic Cancer. *N. Engl. J. Med.* **313**, 1485–1492 (1985).
143. Lejeune, F. J. High dose recombinant tumour necrosis factor (rTNFα) administered by isolation perfusion for advanced tumours of the limbs: a model for biochemotherapy of cancer. *Eur. J. Cancer* **31**, 1009–1016 (1995).
144. Nagata, S. *et al.* Synthesis in E. coli of a polypeptide with human leukocyte interferon activity. *Nature* **284**, 316–320 (1980).
145. Albertini, M. R. *et al.* Pilot trial of the hu14.18-IL2 immunocytokine in

patients with completely resectable recurrent stage III or stage IV melanoma. *Cancer Immunol. Immunother.* **67**, 1647–1658 (2018).

146. Hu, P. *et al.* A Chimeric Lym-1/Interleukin 2 Fusion Protein for Increasing Tumor Vascular Permeability and Enhancing Antibody Uptake. *Cancer Res.* **56**, 4998 LP – 5004 (1996).
147. Hornick, J. L. *et al.* Pretreatment with a Monoclonal Antibody/Interleukin-2 Fusion Protein Directed against DNA Enhances the Delivery of Therapeutic Molecules to Solid Tumors. *Clin. Cancer Res.* **5**, 51 LP – 60 (1999).
148. Dela Cruz, J. S., Trinh, K. R., Morrison, S. L. & Penichet, M. L. Recombinant Anti-Human HER2/neu IgG3-(GM-CSF) Fusion Protein Retains Antigen Specificity and Cytokine Function and Demonstrates Antitumor Activity. *J. Immunol.* **165**, 5112 LP – 5121 (2000).
149. Klein, C. *et al.* Cergutuzumab amunaleukin (CEA-IL2v), a CEA-targeted IL-2 variant-based immunocytokine for combination cancer immunotherapy: Overcoming limitations of aldesleukin and conventional IL-2-based immunocytokines. *Oncoimmunology* **6**, e1277306–e1277306 (2017).
150. Fallon, J. *et al. The immunocytokine NHS-IL12 as a potential cancer therapeutic*. *Oncotarget* vol. 5 www.impactjournals.com/oncotarget/ (2014).
151. Del Vecchio, M. *et al.* Interleukin-12: Biological properties and clinical application. *Clinical Cancer Research* vol. 13 4677–4685 (2007).
152. Lasek, W., Zagożdżon, R. & Jakobisiak, M. Interleukin 12: still a promising candidate for tumor immunotherapy? *Cancer Immunol. Immunother.* **63**, 419–435 (2014).
153. Trinchieri, G., Pflanz, S. & Kastelein, R. A. *Minireview The IL-12 Family of Heterodimeric Cytokines: New Players in the Regulation of T Cell Responses the heterodimer when p40 is also produced by the same cells. IL-12 is a potent inducer of interferon-(IFN-) production from T, NK, and other cell types, and it has been shown to be a potent inducer of differentiation of T helper 1 (Th1) cells. A very large number of studies in*. *Immunity* vol. 19 (2003).
154. Venetz, D., Koovely, D., Weder, B. & Neri, D. Targeted Reconstitution of Cytokine Activity upon Antigen Binding using Split Cytokine Antibody Fusion Proteins. *J. Biol. Chem.* **291**, 18139–18147 (2016).
155. Brunda, M. J. Interleukin-12. *Journal of Leukocyte Biology* vol. 55 280–288

(1994).

156. Gerosa, F. *et al.* Differential regulation of interleukin 12 and interleukin 23 production in human dendritic cells. *J. Exp. Med.* **205**, 1447–1461 (2008).

157. Otani, T. *et al.* Identification of IFN-γ-Producing Cells in IL-12/IL-18-Treated Mice. *Cell. Immunol.* **198**, 111–119 (1999).

158. Zeh, H. J., Hurd, S., Storkus, W. J. & Lotze, M. T. Interleukin-12 promotes the proliferation and cytolytic maturation of immune effectors: implications for the immunotherapy of cancer. *J. Immunother. Emphasis Tumor Immunol.* **14**, 155—161 (1993).

159. Manetti, R. *et al.* Natural killer cell stimulatory factor (interleukin 12 [IL-12]) induces T helper type 1 (Th1)-specific immune responses and inhibits the development of IL-4-producing Th cells. *J. Exp. Med.* **177**, 1199–1204 (1993).

160. Parihar, R., Dierksheide, J., Hu, Y. & Carson, W. E. IL-12 enhances the natural killer cell cytokine response to Ab-coated tumor cells. *J. Clin. Invest.* **110**, 983–992 (2002).

161. Teicher, B. A., Ara, G., Menon, K. & Schaub, R. G. In vivo studies with Interleukin-12 alone and in combination with monocyte colony-stimulating factor and/or fractionated radiation treatment. *Int. J. Cancer* **65**, 80–84 (1996).

162. Brunda, M. J. *et al.* Antitumor and antimetastatic activity of interleukin 12 against murine tumors. *J. Exp. Med.* **178**, 1223–1230 (1993).

163. Kozar, K. *et al.* Interleukin 12-based Immunotherapy Improves the Antitumor Effectiveness of a Low-Dose 5-Aza-2′-Deoxycitidine Treatment in L1210 Leukemia and B16F10 Melanoma Models in Mice. *Clin. Cancer Res.* **9**, 3124 LP – 3133 (2003).

164. Teicher, B. A., Ara, G., Buxton, D., Leonard, J. & Schaub, R. G. Optimal scheduling of interleukin 12 and chemotherapy in the murine MB-49 bladder carcinoma and B16 melanoma. *Clin. Cancer Res.* **3**, 1661 LP – 1667 (1997).

165. Nastala, C. L. *et al.* Recombinant IL-12 administration induces tumor regression in association with IFN-gamma production. *J. Immunol.* **153**, 1697 LP – 1706 (1994).

166. Gately, M. K. *et al.* Administration of recombinant IL-12 to normal mice enhances cytolytic lymphocyte activity and induces production of IFN-γ in

vivo. *Int. Immunol.* **6**, 157–167 (1994).

167. Cohen, J. IL-12 Deaths: Explanation and a Puzzle. *Science (80-.).* **270**, 908 LP – 908 (1995).
168. Xu, C. *et al.* Combination Therapy with NHS-muIL12 and Avelumab (anti-PD-L1) Enhances Antitumor Efficacy in Preclinical Cancer Models. *Clin. Cancer Res.* **23**, 5869 LP – 5880 (2017).
169. Strauss, J. *et al.* First-in-Human Phase I Trial of a Tumor-Targeted Cytokine (NHS-IL12) in Subjects with Metastatic Solid Tumors. *Clin. Cancer Res.* **25**, 99 LP – 109 (2019).
170. Pasche, N., Wulhfard, S., Pretto, F., Carugati, E. & Neri, D. The antibody-based delivery of interleukin-12 to the tumor neovasculature eradicates murine models of cancer in combination with paclitaxel. *Clin. Cancer Res.* **18**, 4092–4103 (2012).
171. Gafner, V., Trachsel, E. & Neri, D. An engineered antibody–interleukin-12 fusion protein with enhanced tumor vascular targeting properties. *Int. J. Cancer* **119**, 2205–2212 (2006).
172. Sommavilla, R. *et al.* Expression, engineering and characterization of the tumor-targeting heterodimeric immunocytokine F8-IL12. *Protein Eng. Des. Sel.* **23**, 653–661 (2010).
173. Morgan, D. A., Ruscetti, F. W. & Gallo, R. Selective in vitro growth of T lymphocytes from normal human bone marrows. *Science (80-.).* **193**, 1007 LP – 1008 (1976).
174. GILLIS, S. & SMITH, K. A. Long term culture of tumour-specific cytotoxic T cells. *Nature* **268**, 154–156 (1977).
175. Malek, T. R. The Biology of Interleukin-2. *Annu. Rev. Immunol.* **26**, 453–479 (2008).
176. Boyman, O. & Sprent, J. The role of interleukin-2 during homeostasis and activation of the immune system. *Nature Reviews Immunology* vol. 12 180–190 (2012).
177. Klapper, J. A. *et al.* High-dose interleukin-2 for the treatment of metastatic renal cell carcinoma : a retrospective analysis of response and survival in patients treated in the surgery branch at the National Cancer Institute between 1986 and 2006. *Cancer* **113**, 293–301 (2008).
178. Smith, F. O. *et al.* Treatment of metastatic melanoma using interleukin-2

alone or in conjunction with vaccines. *Clin. Cancer Res.* **14**, 5610–5618 (2008).

179. Rosenberg, S. A. *et al.* A Progress Report on the Treatment of 157 Patients with Advanced Cancer Using Lymphokine-Activated Killer Cells and Interleukin-2 or High-Dose Interleukin-2 Alone. *N. Engl. J. Med.* **316**, 889–897 (1987).
180. 32nd Annual Meeting and Pre-Conference Programs of the Society for Immunotherapy of Cancer (SITC 2017): Part One. *J. Immunother. Cancer* **5**, 86 (2017).
181. Charych, D. H. *et al.* NKTR-214, an Engineered Cytokine with Biased IL2 Receptor Binding, Increased Tumor Exposure, and Marked Efficacy in Mouse Tumor Models. *Clin. Cancer Res.* **22**, 680 LP – 690 (2016).
182. Pedretti, M. *et al.* Combination of temozolomide with immunocytokine F16-IL2 for the treatment of glioblastoma. *Br. J. Cancer* **103**, 827–836 (2010).
183. Eigentler, T. K. *et al.* A Dose-Escalation and Signal-Generating Study of the Immunocytokine L19-IL2 in Combination with Dacarbazine for the Therapy of Patients with Metastatic Melanoma. *Clin. Cancer Res.* **17**, 7732 LP – 7742 (2011).
184. Catania, C. *et al.* The tumor-targeting immunocytokine F16-IL2 in combination with doxorubicin: dose escalation in patients with advanced solid tumors and expansion into patients with metastatic breast cancer. *Cell Adh. Migr.* **9**, 14–21 (2015).
185. Hutmacher, C., Gonzalo Núñez, N., Liuzzi, A. R., Becher, B. & Neri, D. Targeted Delivery of IL2 to the Tumor Stroma Potentiates the Action of Immune Checkpoint Inhibitors by Preferential Activation of NK and CD8⁺ T Cells. *Cancer Immunol. Res.* **7**, 572 LP – 583 (2019).
186. Balkwill, F. Tumour necrosis factor and cancer. *Nat. Rev. Cancer* **9**, 361–371 (2009).
187. Carswell, E. A. *et al.* An endotoxin-induced serum factor that causes necrosis of tumors. *Proc. Natl. Acad. Sci. U. S. A.* **72**, 3666–3670 (1975).
188. van Horssen, R., ten Hagen, T. L. M. & Eggermont, A. M. M. TNF-α in Cancer Treatment: Molecular Insights, Antitumor Effects, and Clinical Utility. *Oncologist* **11**, 397–408 (2006).

189. Bradley, C. A. Prophylactic TNF blockade reduces autoimmune toxicity. *Nat. Rev. Cancer* **19**, 364 (2019).
190. Leah, E. RCT of adalimumab supports anti-TNF therapy for juvenile-onset ankylosing spondylitis. *Nat. Rev. Rheumatol.* **8**, 693 (2012).
191. Michelon, M. A. & Gottlieb, A. B. Role of golimumab, a TNF-alpha inhibitor, in the treatment of the psoriatic arthritis. *Clin. Cosmet. Investig. Dermatol.* **3**, 79–84 (2010).
192. Verhoef, C. *et al.* Isolated limb perfusion with melphalan and TNF-alpha in the treatment of extremity sarcoma. *Curr. Treat. Options Oncol.* **8**, 417–427 (2007).
193. Eggermont, A. M. *et al.* Isolated limb perfusion with tumor necrosis factor and melphalan for limb salvage in 186 patients with locally advanced soft tissue extremity sarcomas. The cumulative multicenter European experience. *Ann. Surg.* **224**, 756–765 (1996).
194. Grünhagen, D. J., de Wilt, J. H. W., Van Geel, A. N., Verhoef, C. & Eggermont, A. M. M. Isolated Limb Perfusion with TNF-α and Melphalan in Locally Advanced Soft Tissue Sarcomas of the Extremities BT - Treatment of Bone and Soft Tissue Sarcomas. in (ed. Tunn, P.-U.) 257–270 (Springer Berlin Heidelberg, 2009). doi:10.1007/978-3-540-77960-5_16.
195. De Luca, R. *et al.* A Novel Fully-Human Potency-Matched Dual Cytokine-Antibody Fusion Protein Targets Carbonic Anhydrase IX in Renal Cell Carcinomas. *Front. Oncol.* **9**, (2019).
196. Schwager, K., Hemmerle, T., Aebischer, D. & Neri, D. The Immunocytokine L19–IL2 Eradicates Cancer When Used in Combination with CTLA-4 Blockade or with L19-TNF. *J. Invest. Dermatol.* **133**, 751–758 (2013).
197. Moschetta, M. *et al.* Paclitaxel Enhances Therapeutic Efficacy of the F8-IL2 Immunocytokine to EDA-Fibronectin–Positive Metastatic Human Melanoma Xenografts. *Cancer Res.* **72**, 1814 LP – 1824 (2012).
198. Hemmerle, T. *et al.* The antibody-based targeted delivery of TNF in combination with doxorubicin eradicates sarcomas in mice and confers protective immunity. *Br. J. Cancer* **109**, 1206–1213 (2013).
199. Halin, C. *et al.* Synergistic Therapeutic Effects of a Tumor Targeting Antibody Fragment, Fused to Interleukin 12 and to Tumor Necrosis Factor

α. *Cancer Res.* **63**, 3202 LP – 3210 (2003).

200. Wigginton, J. M. *et al.* Administration of Interleukin 12 With Pulse Interleukin 2 and the Rapid and Complete Eradication of Murine Renal Carcinoma. *JNCI J. Natl. Cancer Inst.* **88**, 38–43 (1996).
201. Gillies, S. D. *et al.* Bi-functional cytokine fusion proteins for gene therapy and antibody-targeted treatment of cancer. *Cancer Immunol. Immunother.* **51**, 449–460 (2002).
202. Kalluri, R. & Zeisberg, M. Fibroblasts in cancer. *Nat. Rev. Cancer* **6**, 392–401 (2006).
203. Folkman, J. Tumor Angiogenesis: Therapeutic Implications. *N. Engl. J. Med.* **285**, 1182–1186 (1971).
204. Brocks, B. *et al. Species-Crossreactive scFv Against the Tumor Stroma Marker 'Fibroblast Activation Protein' Selected by Phage Display From an Immunized FAP / Knock-Out Mouse*. *Molecular Medicine* vol. 7 (2001).
205. Folkman, J. Angiogenesis in cancer, vascular, rheumatoid and other disease. *Nat. Med.* **1**, 27–30 (1995).
206. Wernert, N. The multiple roles of tumour stroma. *Virchows Arch.* **430**, 433–443 (1997).
207. Astrof, S. & Hynes, R. O. Fibronectins in vascular morphogenesis. *Angiogenesis* **12**, 165–175 (2009).
208. Ruoslahti, E. FIBRONECTIN AND ITS RECEPTORS. *Annu. Rev. Biochem.* **57**, 375–413 (1988).
209. McDonald, J. A. Extracellular Matrix Assembly. *Annu. Rev. Cell Biol.* **4**, 183–207 (1988).
210. Oyama, F., Hirohashi, S., Shimosato, Y., Titani, K. & Sekiguchi, K. Oncodevelopmental Regulation of the Alternative Splicing of Fibronectin Pre-Messenger RNA in Human Lung Tissues. *Cancer Res.* **50**, 1075 LP – 1078 (1990).
211. Kaczmarek, J. *et al.* Distribution of oncofetal fibronectin isoforms in normal, hyperplastic and neoplastic human breast tissues. *Int. J. Cancer* **59**, 11–16 (1994).
212. Neri, D. & Bicknell, R. Tumour vascular targeting. *Nat. Rev. Cancer* **5**, 436–446 (2005).
213. Neri, D. & Supuran, C. T. Interfering with pH regulation in tumours as a

therapeutic strategy. *Nat. Rev. Drug Discov.* **10**, 767–777 (2011).

214. Bourdon, M. A. *et al. Human Glioma-Mesenchymal Extracellular Matrix Antigen Defined by Monoclonal Antibody*. *CANCER RESEARCH* vol. 43 (1983).
215. Chiquet-Ehrismann, R., Hagios, C. & Matsumoto, K. The tenascin gene family. *Perspect. Dev. Neurobiol.* **2**, 3—7 (1994).
216. Chiquet-Ehrismann, R. & Chiquet, M. Tenascins: regulation and putative functions during pathological stress. *J. Pathol.* **200**, 488–499 (2003).
217. Midwood, K. S., Chiquet, M., Tucker, R. P. & Orend, G. Tenascin-C at a glance. *J. Cell Sci.* **129**, 4321–4327 (2016).
218. Silacci, M. *et al.* Human monoclonal antibodies to domain C of tenascin-C selectively target solid tumors in vivo. *Protein Eng. Des. Sel.* **19**, 471–478 (2006).
219. Borsi, L., Allemanni, G., Gaggero, B. & Zardi, L. Extracellular pH controls pre-mRNA alternative splicing of tenascin-C in normal, but not in malignantly transformed, cells. *Int. J. Cancer* **66**, 632–635 (1996).
220. Zagzag, D. *et al.* Tenascin expression in astrocytomas correlates with angiogenesis. *Cancer Res.* **55**, 907–914 (1995).
221. Jones, F. S. & Jones, P. L. The tenascin family of ECM glycoproteins: Structure, function, and regulation during embryonic development and tissue remodeling. *Dev. Dyn.* **218**, 235–259 (2000).
222. Hindermann, W. *et al.* Synthesis and protein distribution of the unspliced large tenascin-C isoform in oral squamous cell carcinoma. *J. Pathol.* **189**, 475—480 (1999).
223. Borsi, L. *et al.* Expression of different tenascin isoforms in normal, hyperplastic and neoplastic human breast tissues. *Int. J. Cancer* **52**, 688–692 (1992).
224. Katenkamp, K. *et al.* mRNA expression and protein distribution of the unspliced tenascin-C isoform in prostatic adenocarcinoma. *J. Pathol.* **203**, 771–779 (2004).
225. Kusagawa, H. *et al.* Expression and degeneration of tenascin-C in human lung cancers. *Br. J. Cancer* **77**, 98–102 (1998).
226. Hauptmann, S. *et al.* Extracellular matrix proteins in colorectal carcinomas. Expression of tenascin and fibronectin isoforms. *Lab. Invest.* **73**, 172–182

(1995).

227. Castellani, P., Dorcaratto, A., Siri, A., Zardi, L. & Viale, G. L. Tenascin distribution in human brain tumours. *Acta Neurochir. (Wien).* **136**, 44—50 (1995).

228. Leins, A. *et al.* Expression of tenascin-C in various human brain tumors and its relevance for survival in patients with astrocytoma. *Cancer* **98**, 2430–2439 (2003).

229. Brack, S. S., Silacci, M., Birchler, M. & Neri, D. Tumor-targeting properties of novel antibodies specific to the large isoform of tenascin-C. *Clin. Cancer Res.* **12**, 3200–3208 (2006).

230. Pezzolo, A. *et al.* Oct-4+/Tenascin C+ neuroblastoma cells serve as progenitors of tumor-derived endothelial cells. *Cell Res.* **21**, 1470–1486 (2011).

231. Oskarsson, T. *et al.* Breast cancer cells produce tenascin C as a metastatic niche component to colonize the lungs. *Nat. Med.* **17**, 867–874 (2011).

232. Orend, G., Huang, W., Olayioye, M. A., Hynes, N. E. & Chiquet-Ehrismann, R. Tenascin-C blocks cell-cycle progression of anchorage-dependent fibroblasts on fibronectin through inhibition of syndecan-4. *Oncogene* **22**, 3917–3926 (2003).

233. Balza, E. *et al.* Production and characterization of monoclonal antibodies specific for different epitopes of human tenascin. *FEBS Lett.* **332**, 39–43 (1993).

234. Siri, A. *et al.* Human tenascin: primary structure, pre-mRNA splicing patterns and localization of the epitopes recognized by two monoclonal antibodies. *Nucleic Acids Res.* **19**, 525–531 (1991).

235. Riva, P. *et al.* Treatment of intracranial human glioblastoma by direct intratumoral administration of 131I-labelled anti-tenascin monoclonal antibody BC-2. *Int. J. Cancer* **51**, 7–13 (1992).

236. Riva Pietro, A. A. F. G. et al. Local Treatment of Malignant Gliomas by Direct Infusion of Specific MonoclonalAntibodies Labeled with 131I: Comparison of the Results Obtained inRecurrent and Newly Diagnosed Tumors. *Cancer Reaserch* **55**, 5952–5956 (1995).

237. Paganelli, G. *et al.* Pre-targeted immunodetection in glioma patients: tumour localization and single-photon emission tomography imaging of

[99mTc]PnAO-biotin. *Eur. J. Nucl. Med.* **21**, 314–321 (1994).

238. Bigner, D. D. *et al. Iodine-131-Labeled Antitenascin Monoclonal Antibody 81C6 Treatment of Patients With Recurrent Malignant Gliomas: Phase I Trial Results*. *J Clin Oncol* vol. 16 (1998).
239. Rizzieri, D. A. *et al.* Phase 1 trial study of 131I-labeled chimeric 81C6 monoclonal antibody for the treatment of patients with non-Hodgkin lymphoma. *Blood* **104**, 642–648 (2004).
240. Petronzelli, F. *et al.* Improved tumor targeting by combined use of two antitenascin antibodies. in *Clinical Cancer Research* vol. 11 (2005).
241. Goldstein, L. A. & Chen, W.-T. Identification of an Alternatively Spliced Seprase mRNA That Encodes a Novel Intracellular Isoform *. *J. Biol. Chem.* **275**, 2554–2559 (2000).
242. Garin-Chesa, P., Oldt, L. J. & Rettigt, W. J. *Cell surface glycoprotein of reactive stromal fibroblasts as a potential antibody target in human epithelial cancers (tumor mesenchyme/colon cancer/breast cancer/tenascin/wound healing)*. *Proc. Natl. Acad. Sci. USA* vol. 87 (1990).
243. Rettig, W. J. *et al. Differential Expression of Cell Surface Antigens and Glial Fibrillary Acidic Protein in Human Astrocytoma Subsets1*. (1986).
244. Rettig, W. J. *et al.* Cell-surface glycoproteins of human sarcomas: differential expression in normal and malignant tissues and cultured cells. *Proc. Natl. Acad. Sci. U. S. A.* **85**, 3110–3114 (1988).
245. Aertgeerts, K. *et al.* Structural and Kinetic Analysis of the Substrate Specificity of Human Fibroblast Activation Protein α * . *J. Biol. Chem.* **280**, 19441–19444 (2005).
246. Huang, Y. *et al.* Fibroblast activation protein-α promotes tumor growth and invasion of breast cancer cells through non-enzymatic functions. *Clin. Exp. Metastasis* **28**, 567–579 (2011).
247. Park, J. E. *et al. Fibroblast Activation Protein, a Dual Specificity Serine Protease Expressed in Reactive Human Tumor Stromal Fibroblasts*. http://www.jbc.org (1999).
248. Calais, J. FAP: The next billion dollar nuclear theranostics target? *J. Nucl. Med.* **61**, 163–165 (2020).
249. Kratochwil, C. *et al.* 68Ga-FAPI PET/CT: Tracer uptake in 28 different kinds of cancer. *J. Nucl. Med.* **60**, 801–805 (2019).

250. Puré, E. & Blomberg, R. Pro-tumorigenic roles of fibroblast activation protein in cancer: back to the basics. *Oncogene* **37**, 4343–4357 (2018).
251. Fischer, E. *et al.* Radioimmunotherapy of fibroblast activation protein positive tumors by rapidly internalizing antibodies. *Clin. Cancer Res.* **18**, 6208–6218 (2012).
252. Claus, C. *et al.* Tumor-targeted 4-1BB agonists for combination with T cell bispecific antibodies as off-the-shelf therapy. *Sci. Transl. Med.* **11**, eaav5989 (2019).
253. Waldhauer, I. *et al.* Simlukafusp alfa (FAP-IL2v) immunocytokine is a versatile combination partner for cancer immunotherapy. *MAbs* **13**, (2021).
254. Link, A. *et al.* Abstract 3752: Preclinical pharmacology of MP0310: A 4-1BB/FAP bispecific DARPin drug candidate promoting tumor-restricted T-cell costimulation. *Cancer Res.* **78**, 3752 LP – 3752 (2018).
255. Millul, J. *et al.* An ultra-high-affinity small organic ligand of fibroblast activation protein for tumor-targeting applications. *Proc. Natl. Acad. Sci. U. S. A.* **118**, 1–10 (2021).
256. Walsh, G. Biopharmaceutical benchmarks 2018. *Nat. Biotechnol.* **36**, 1136–1145 (2018).
257. Kaplon, H. & Reichert, J. M. Antibodies to watch in 2019. *MAbs* **11**, 219–238 (2019).
258. Scott, A. M., Wolchok, J. D. & Old, L. J. Antibody therapy of cancer. *Nat. Rev. Cancer* **12**, 278–287 (2012).
259. Lane, D. M. *et al.* Radioimmunotherapy of metastatic colorectal tumours with iodine-131-labelled antibody to carcinoembryonic antigen: phase I/II study with comparative biodistribution of intact and F(ab')2 antibodies. *Br. J. Cancer* **70**, 521–525 (1994).
260. Dan, N. *et al.* Antibody-Drug Conjugates for Cancer Therapy: Chemistry to Clinical Implications. *Pharmaceuticals (Basel).* **11**, 32 (2018).
261. Nilsson, F., Kosmehl, H., Zardi, L. & Neri, D. Targeted Delivery of Tissue Factor to the ED-B Domain of Fibronectin, a Marker of Angiogenesis, Mediates the Infarction of Solid Tumors in Mice. *Cancer Res.* **61**, 711 LP – 716 (2001).
262. Zigler, M., Shir, A. & Levitzki, A. Targeted cancer immunotherapy. *Curr. Opin. Pharmacol.* **13**, 504—510 (2013).

263. Villa, A. *et al.* A high-affinity human monoclonal antibody specific to the alternatively spliced EDA domain of fibronectin efficiently targets tumor neo-vasculature in vivo. *Int. J. Cancer* **122**, 2405–2413 (2008).
264. Tucker, R. P. & Chiquet-Ehrismann, R. Tenascin-C: Its functions as an integrin ligand. *International Journal of Biochemistry and Cell Biology* vol. 65 165–168 (2015).
265. Dobbertin, A. *et al.* Analysis of combinatorial variability reveals selective accumulation of the fibronectin type III domains B and D of tenascin-C in injured brain. *Exp. Neurol.* **225**, 60–73 (2010).
266. Giblin, S. P. & Midwood, K. S. Tenascin-C: Form versus function. *Cell Adhesion and Migration* vol. 9 48–82 (2015).
267. Chiquet-Ehrismann, R. *Tenaseins, a growing family of extraeellular matrix proteins*.
268. Reardon, D. A. *et al.* A pilot study: 131I-Antitenascin monoclonal antibody 81c6 to deliver a 44-Gy resection cavity boost. *Neuro. Oncol.* **10**, 182–189 (2008).
269. Rizzieri, D. A. *et al.* Phase 1 trial study of 131I-labeled chimeric 81C6 monoclonal antibody for the treatment of patients with non-Hodgkin lymphoma. *Blood* **104**, 642–648 (2004).
270. De Santis, R. *et al.* Novel antitenascin antibody with increased tumour localisation for Pretargeted Antibody-Guided RadioimmunoTherapy (PAGRITR). *Br. J. Cancer* **88**, 996–1003 (2003).
271. Rami, A., Behdani, M., Yardehnavi, N., Habibi-Anbouhi, M. & Kazemi-Lomedasht, F. An overview on application of phage display technique in immunological studies. *Asian Pacific Journal of Tropical Biomedicine* vol. 7 599–602 (2017).
272. Alfaleh, M. A. *et al.* Phage Display Derived Monoclonal Antibodies: From Bench to Bedside. *Frontiers in Immunology* vol. 11 (2020).
273. Winter, G., Griffiths, A. D., Hawkins, R. E. & Hoogenboom, H. R. Making Antibodies by Phage Display Technology. *Annu. Rev. Immunol.* **12**, 433–455 (1994).
274. Huston, J. S. *et al. Protein engineering of antibody binding sites: Recovery of specific activity in an anti-digoxin single-chain Fv analogue produced in Escherichia coli*. *Proc. Natl. Acad. Sci. USA* vol. 85 (1988).

275. Dwyer, G. *et al. Cloning and expression of murine IL-12*. http://www.jimmunol.org/content/148/11/3433 (2018).
276. Weiss, T., Weller, M., Guckenberger, M., Sentman, C. L. & Roth, P. NKG2D-based CAR T cells and radiotherapy exert synergistic efficacy in glioblastoma. *Cancer Res.* **78**, 1031–1043 (2018).
277. Weber, M. *et al.* A highly functional synthetic phage display library containing over 40 billion human antibody clones. *PLoS One* **9**, e100000–e100000 (2014).
278. Fairhead, M. & Howarth, M. Site-specific biotinylation of purified proteins using BirA. *Methods Mol. Biol.* **1266**, 171–184 (2015).
279. Beckett, D., Kovaleva, E. & Schatz, P. J. A minimal peptide substrate in biotin holoenzyme synthetase-catalyzed biotinylation. *Protein Sci.* 921–929 (1999).
280. Pasche, N. *et al.* Cloning and characterization of novel tumor-targeting immunocytokines based on murine IL7. *J. Biotechnol.* **154**, 84–92 (2011).
281. Gébleux, R., Stringhini, M., Casanova, R., Soltermann, A. & Neri, D. Non-internalizing antibody–drug conjugates display potent anti-cancer activity upon proteolytic release of monomethyl auristatin E in the subendothelial extracellular matrix. *Int. J. Cancer* **140**, 1670–1679 (2017).
282. Puca, E. *et al.* The antibody-based delivery of interleukin-12 to solid tumors boosts NK and CD8+ T cell activity and synergizes with immune checkpoint inhibitors. *Int. J. Cancer* **146**, 2518–2530 (2020).
283. Weiss, T. *et al.* NKG2D-Dependent antitumor effects of chemotherapy and radiotherapy against glioblastoma. *Clin. Cancer Res.* **24**, 882–895 (2018).
284. Silacci, M. *et al.* Design, construction, and characterization of a large synthetic human antibody phage display library. *Proteomics* **5**, 2340–2350 (2005).
285. Thoring, L., Dondapati, S. K., Stech, M., Wüstenhagen, D. A. & Kubick, S. High-yield production of 'difficult-to-express' proteins in a continuous exchange cell-free system based on CHO cell lysates. *Sci. Rep.* **7**, (2017).
286. Weller, M. *et al.* European Association for Neuro-Oncology (EANO) guideline on the diagnosis and treatment of adult astrocytic and oligodendroglial gliomas. *The Lancet Oncology* vol. 18 e315–e329 (2017).
287. Jin, M.-Z. & Jin, W.-L. The updated landscape of tumor microenvironment

and drug repurposing. *Signal Transduct. Target. Ther.* **5**, 166 (2020).

288. Sahai, E. *et al.* A framework for advancing our understanding of cancer-associated fibroblasts. *Nat. Rev. Cancer* **20**, 174–186 (2020).
289. Micke, P. & Ostman, A. Tumour-stroma interaction: cancer-associated fibroblasts as novel targets in anti-cancer therapy? *Lung Cancer* **45**, 163–175 (2004).
290. Paulsson, J. & Micke, P. Prognostic relevance of cancer-associated fibroblasts in human cancer. *Seminars in Cancer Biology* vol. 25 61–68 (2014).
291. Olumi, A. F. *et al. Carcinoma-associated Fibroblasts Direct Tumor Progression of Initiated Human Prostatic Epithelium 1*. Cancer research vol. 59 (1999).
292. Bhome, R. *et al.* Exosomal microRNAs derived from colorectal cancer-associated fibroblasts: role in driving cancer progression. *Aging (Albany. NY).* **9**, 2666–2694 (2017).
293. Busek, P., Mateu, R., Zubal, M., Kotackova, L. & Sedo, A. *Targeting fibroblast activation protein in cancer-Prospects and caveats*. *Frontiers In Bioscience* vol. 23 (1933).
294. Tuxhorn, J. A., Ayala, G. E. & Rowley, D. R. Reactive stroma in prostate cancer progression. *J. Urol.* **166**, 2472–2483 (2001).
295. Liu, R., Li, H., Liu, L., Yu, J. & Ren, X. Fibroblast activation protein: A potential therapeutic target in cancer. *Cancer Biology and Therapy* vol. 13 123–129 (2012).
296. Lindner, T. *et al.* Targeting of activated fibroblasts for imaging and therapy. *EJNMMI Radiopharm. Chem.* **4**, 16 (2019).
297. Busek, P. *et al.* Increased tissue and circulating levels of dipeptidyl peptidase-IV enzymatic activity in patients with pancreatic ductal adenocarcinoma. *Pancreatology* **16**, 829–838 (2016).
298. Liao, Y., Xing, S., Xu, B., Liu, W. & Zhang, G. Evaluation of the circulating level of fibroblast activation protein α for diagnosis of esophageal squamous cell carcinoma. *Oncotarget* **8**, 30050–30062 (2017).
299. Scott, A. M. *et al. A Phase I Dose-Escalation Study of Sibrotuzumab in Patients with Advanced or Metastatic Fibroblast Activation Protein-positive Cancer 1*. (2003).

300. Clark, J., Vagenas, P., Panesar, M. & Cope, A. P. What does tumour necrosis factor excess do to the immune system long term? *Ann. Rheum. Dis.* **64**, iv70 LP-iv76 (2005).
301. Trinchieri, G. Interleukin-12: A Proinflammatory Cytokine with Immunoregulatory Functions that Bridge Innate Resistance and Antigen-Specific Adaptive Immunity. *Annu. Rev. Immunol.* **13**, 251–276 (1995).
302. Hemmerle, T., Hess, C., Venetz, D. & Neri, D. Tumor targeting properties of antibody fusion proteins based on different members of the murine tumor necrosis superfamily. *J. Biotechnol.* **172**, 73–76 (2014).
303. De Luca, R. *et al.* Potency-matched dual cytokine–antibody fusion proteins for cancer therapy. *Mol. Cancer Ther.* **16**, 2442–2451 (2017).
304. De Luca, R. *et al.* Potency-matched Dual Cytokine–Antibody Fusion Proteins for Cancer Therapy. *Mol. Cancer Ther.* **16**, 2442 LP – 2451 (2017).
305. Pellegrino, C. *et al.* Impact of Ligand Size and Conjugation Chemistry on the Performance of Universal Chimeric Antigen Receptor T-Cells for Tumor Killing. *Bioconjug. Chem.* **31**, 1775–1783 (2020).
306. Mock, J., Pellegrino, C. & Neri, D. A universal reporter cell line for bioactivity evaluation of engineered cytokine products. *Sci. Rep.* **10**, 3234 (2020).
307. Mehta, A. K., Gracias, D. T. & Croft, M. TNF activity and T cells. *Cytokine* **101**, 14–18 (2018).
308. Huyghe, L. *et al.* Safe eradication of large established tumors using neovasculature-targeted tumor necrosis factor-based therapies. *EMBO Mol. Med.* **12**, e11223 (2020).
309. Halin, C. *et al.* Enhancement of the antitumor activity of interleukin-12 by targeted delivery to neovasculature. *Nat. Biotechnol.* **20**, 264–269 (2002).
310. Atkins, M. B. *et al.* Phase I evaluation of intravenous recombinant human interleukin 12 in patients with advanced malignancies. *Clin. Cancer Res.* **3**, 409 LP – 417 (1997).
311. Chen, X., Zaro, J. L. & Shen, W.-C. Fusion protein linkers: property, design and functionality. *Adv. Drug Deliv. Rev.* **65**, 1357–1369 (2013).

Acknowledgments

Vorrei esprimere la mia sincera gratitudine al Prof. Dott. Dario Neri per avermi dato la possibilità di svolgere il mio dottorato presso Philochem, lavorando su progetti stimolanti. Sarò sempre grata per gli insegnamenti, scientifici e non, che mi ha dato durante questi anni. Sono inoltre molto felice di poter proseguire il mio percorso lavorativo in un nuovo ruolo a Philochem e sono certa continuerò a imparare da lui.

Ringrazio il Prof. Dott. Guido Grandi per essere stato il mio relatore durante questi anni di dottorato. Anche se ci siamo visti non di frequente, sono onorata di poter aver avuto lui come supervisore.

Un ringraziamento speciale va al Dott. Roberto De Luca. Sono entrata in laboratorio che quasi non sapevo cosa fosse una PCR e grazie a lui ora esco con un dottorato (e tante proteine clonate). Grazie a Roby per essere sempre stato disponibile, per tutti gli insegnamenti, per la fruttuosa collaborazione che siamo riusciti ad avere.

Un sentito ringraziamento alla Prof.ssa Dott.ssa Marina Lotti e al Prof. Dott. Daniele Sblattero per aver valutato la mia tesi ed essere stati componenti chiave del comitato di dottorato.

Grazie di cuore al Dott. Mattia Matasci per la sua costante presenza. Infinite grazie alla Dott.ssa Alessandra Villa per avermi trasmesso grinta e determinazione, grazie per le tante librerie elettroporate e per il suo prezioso aiuto.

Un grazie agli ultimi componenti del gruppo Neri in ETH per la loro disponibilità durante i primi due anni di dottorato. Un grazie in particolare al Dott. Marco Catalano per tutte le masse corse, i caffè dell'LTK e la pazienza con la mia testa dura.

Un ringraziamento di cuore a tutto il gruppo Philochem. In particolare Fred, Anne, Lottie, Louis, Dott. Baptiste Gouyou, Abdullah, Aureliano, Andrea, Luca e Eleonora per essere sempre stati disponibili e aver risolto non pochi grattacapi scientifici. Grazie alle mie nuove colleghe Dott.ssa Teresa Hemmerle, Dott.ssa

Jacqueline Mock e Dott.ssa Andrea Ommer e al Dott. Giuliano Elia per avermi accolto a braccia aperte nella nuova posizione e nel nuovo ufficio. Grazie alla mia studentessa Virginie De Woelmont per l'aiuto in laboratorio negli ultimi mesi di lavoro. Un sentito grazie a Adrian per aver sempre rallegrato le mie giornate e a Jacopo, per i calcoli a mente, le discussioni scientifiche, per la sua sensibilità così bella.

A quello che è diventato il "Friendly groupe" la mia profonda riconoscenza. Ha e sta rendendo Zurigo una casa e non un posto di passaggio, divendendo il gruppo di amici che avevo sempre desiderato. Un immenso grazie al Dott. Christian Pellegrino e al Dott. Gabriele Bassi, i miei salvatori: grazie perché da un dito tagliato è nata una bellissima amicizia. Grazie al Dott. Emanuele Puca per l'appoggio, l'incoraggiamento, la costante disponibilità. Grazie al Dott. Samuele Cazzamalli perchè il suo supporto e la sua amicizia sono davvero preziose. Vi voglio bene amici.

Non sarebbero stati tre anni di dottorato così intensi senza i colleghi dell'ufficio più rumoroso di Philochem. Grazie al Dott. Tiziano Ongaro, per avermi insegnato ad essere ancora più attenta ai dettagli e per la sua dolcezza, così rara. Grazie a Cesare: in pochissimo tempo è diventato uno dei miei punti di riferimento e spero lo sarà per un bel po'. Grazie al compagno di avventure per eccellenza, Corbi: che dire, sono stati tre anni pazzeschi avendolo come fratellone. Grazie per avermi fatto capire i clonaggi, grazie per le risate, il supporto, le nostre litigate, i pomeriggi in cell culture e i viaggi in macchina cantando (mancherai come l'aria qui a Zurigo, vedi di farti vedere spesso). Infine grazie alla guapita Sheila: grazie perché non è stata un'amica come tutte le altre. Ha aperto il mio cuore, mi ha permesso di stare al suo fianco, è stata un'ancora di salvezza in uno dei momenti più duri della mia vita. Grazie per il nostro essere chiassose, per avermi insegnato ad essere forte, per il suo esserci, a prescindere.
Grazie ragazzi, perché non siete mai stati semplici colleghi. Avete avverato uno dei più grandi desideri si possano pensare: l'andare a lavoro e trovare i propri amici.

Senza le mie radici non sarei arrivata fin qui. Grazie alle amiche di una vita, Marta e Franci, per riuscire a farmi sentire a casa, sempre. Grazie per la vostra presenza e

per avermi fatto concludere un altro traguardo con voi. La mia profonda gratitudine va alla mia famiglia, per il sostegno e per non avermi mai fatto pesare la distanza o le settimane troppe impegnate. Il mio infinito grazie a mamma e papà, senza i quali non sarei arrivata qui. Grazie per il vostro amore incondizionato.

Infine, grazie a Richi. Non sarei mai giunta alla fine di questo percorso senza di lui e probabilmente non sarei nemmeno partita. Grazie per non avermi mai lasciato sola, per la lucidità che mi sta trasmettendo, per avermi sempre stimolato a fare il mio massimo, per esserci stato in ogni singolo momento di questo dottorato (anche con Illustrator). Grazie per essere diventato la mia famiglia e il mio futuro.